

LIBRARY
Michigan State
University

This is to certify that the

dissertation entitled

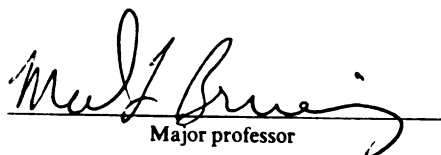
Fundamental Study of the Ion Permeability of Ultrathin,
Layered Polyelectrolyte Films

presented by

Jeremy James Harris

has been accepted towards fulfillment
of the requirements for

Ph.D degree in CHEMISTRY


Major professor

Date 08/17/01

PLACE IN RETURN BOX to remove this checkout from your record.
 TO AVOID FINES return on or before date due.
 MAY BE RECALLED with earlier due date if requested.

DATE DUE	DATE DUE	DATE DUE
09 01 02 NOV 10 2002		
AUG 30 2003		
08 21 03		

Fundamental Study of the Ion Permeability of Ultrathin, Layered Polyelectrolyte Films

By

Jeremy James Harris

AN ABSTRACT OF A DISSERTATION

**Submitted to
Michigan State University
in partial fulfillment of the requirements
for the degree of**

DOCTOR OF PHILOSOPHY

Department of Chemistry

2001

Professor Merlin L. Bruening

ABSTRACT

FUNDAMENTAL STUDY OF THE ION PERMEABILITY OF ULTRATHIN, LAYERED POLYELECTROLYTE FILMS

By

Jeremy James Harris

Layered polyelectrolyte films are attractive as coatings and membranes because of their ease of synthesis and versatility. The feasibility of utilizing these films, however, will depend on their permeability and stability under relevant conditions. Cyclic voltammetry and electrochemical impedance spectroscopy studies presented in this thesis show that the permeability of poly(allylamine hydrochloride) (PAH)/poly(styrene sulfonate) (PSS) coatings depends on the number of bilayers in the film, deposition conditions, and solution pH. Unfortunately, even the most passivating films are relatively permeable and unstable at high pH. To overcome this problem we employ PAH/poly(acrylic acid) (PAA) films which, when heated, form a nylon-like coating that dramatically decreases film permeability while increasing stability.

Ultrathin films such as layered polyelectrolytes are attractive membrane materials because they potentially offer both high flux and high selectivity. Synthesis of such membranes is challenging, however, as it requires defect-free deposition of a film at the surface of a porous support. Scanning electron microscopy shows that adsorption of layered polyelectrolyte films on porous alumina supports naturally results in a defect-free membrane. Ion transport through these membranes is primarily controlled by Donnan

interactions between the ions and the fixed charge present in the film, which results in high selectivity between anions of different valence.

Layered polyelectrolyte films offer several means for controlling ion-flux through these membranes. Since Donnan interactions at the film/solution interface greatly affect ion-transport, capping the films with an additional anionic polyelectrolyte layer enhances the monovalent/divalent anion selectivity of these membranes. While selectivity depends on membrane surface charge, the flux through these membranes is affected by film composition. PAH/PAA membranes show similar selectivities as PAH/PSS membranes but with only 70% of the ion flux. To enhance selectivity while maintaining flux, composite membranes were constructed that utilize the high flux of PAH/PSS membranes along with the blocking effects of PAH/PAA membranes. Membranes composed of 5 PSS/PAH bilayers capped with 2.5-bilayers of PAA/PAH show $\text{Cl}^-/\text{SO}_4^{2-}$ selectivity as high as 350. Utilization of charge, membrane composition, and cross-linking provide for specific tailoring of membrane properties.

Utilization of polyelectrolyte membranes for water purification will require a pressure gradient to achieve sufficient water flux. When used as nanofiltration elements, PSS/PAH membranes show Ca^{2+} rejections of 90+% along with very high water flux. Cross-linking and fluorination of polyelectrolyte membranes further increases Na^+ and SO_4^{2-} rejections, with respect to PSS/PAH membranes, while maintaining an appreciable flux. Na^+ and SO_4^{2-} rejection values for composite membranes are >60 and >90%, respectively, for both 50 and 1000 ppm solutions. Thus, polyelectrolyte membranes not only offer easy means for membrane modification, but may provide solutions to current problems in membrane separations.

To Mom, Dad, & Shannon

ACKNOWLEDGEMENTS

“Even when on the right track, you’ll get run over if you just sit there.”

First, I would like to thank my advisor, Professor Merlin Bruening. You showed me how to be an insightful scientist and one heck of a proofreader. Thank you for taking a chance and allowing me to join your group. I have really enjoyed my four years at MSU. Finally, how could I forget those “competitive” golf matches we engaged in during the last four years and I do believe that I hold the edge.

Next, I would like to thank my family; Mom, Dad, Julie, Jessica, Grandma and Grandpa, for all of their support and love in everything that I have pursued in my life. Much thanks to my in-laws, Jim and Sheryl, for your support and ever-flowing advice. Mom & Dad, thanks for giving me the chance (\$\$) to further my education at Wooster and thank you for the support while at MSU even though you didn’t quite understand what I was doing. Did you ever think I would be where I am at today?

Shannon, my wife and my best friend, thank you for your love and support and paying half the rent. It has been a blessing to have you by my side during this journey and I look forward to many more. I have often told you that you are the reason I am where I am today. Thanks.

Finally... The many friends that have been passengers with me on this four-year trip whether you wanted to be or not. In no particular order; Dale, Wendy, Karen, Bob, Kristi, Shannon, Art, Shawn, Pat, Kirk, Todd, Barb, Bill & Julie. Last but not least the Bruening group, past and present; Dan, Wenxi, Keith, KP, Sandra, Anagi, Bo, Skanth, Milind, and Jinhua. Thanks for the many “stimulating” conversations about chemistry

and life. This work was partially supported by the Department of Energy Office of Basic Energy Sciences, the National Science Foundation (CE-9816108), and the Center for Fundamental Research at Michigan State University.

TABLE OF CONTENTS

List of Tables	viii
List of Figures	ix
List of Abbreviations	xiii
Chapter 1: Introduction and Background	1
I. Development of Thin Films	1
II. History and Development of Layered Polyelectrolyte Films	3
III. Ion-Permeability of Layered Polyelectrolyte Films	6
IV. Use of Layered Polyelectrolyte Films as Ion-Separation Membranes	9
V. Use of Layered Polyelectrolyte Films as Nanofiltration Membranes	12
VI. References	15
Chapter 2: Electrochemical and in Situ Ellipsometric Investigation of the Permeability and Stability of Layered Polyelectrolyte Films	21
I. Introduction	21
II. Experimental	22
A. Chemicals and Solutions	22
B. Techniques	24
III. Results and Discussion	27
A. Characterization of Polyelectrolyte Films	27
B. Film Swelling	30
C. Investigation of Film Permeability to $\text{Fe}(\text{CN})_6^{3-/4-}$	33
D. Investigation of Film Permeability to $\text{Ru}(\text{NH}_3)_6^{2+/3+}$	41
E. Permeability as a Function of Time	45
F. Permeability as a Function of the Number of Bilayers	46
F. Effect of Supporting Electrolyte on the Permeability of Polyelectrolyte Films	48
G. Comparing Permeabilities of PAH/PAA and PAH/PSS Multilayer Films	50
IV. Conclusions	51
V. References	53
Chapter 3: Synthesis of Passivating, Nylon-Like Coatings through Cross-linking of Ultrathin Polyelectrolyte Films	56
I. Introduction	56
II. Experimental	57
III. Results and Discussion	58
IV. References	68

Chapter 4: Layered Polyelectrolyte Films as Selective, Ultrathin Membranes for Anion Separations	69
I. Introduction	69
II. Experimental	70
A. Materials	70
B. Transport Studies	71
III. Results and Discussion	73
IV. Conclusions	88
V. References	89
 Chapter 5: Development of Polyelectrolyte Films as Nanofiltration Membranes	 92
I. Introduction	92
II. Experimental	93
A. Chemicals	93
B. Polyelectrolyte Deposition and Derivatization on Porous Alumina Supports	94
C. Nanofiltration	95
III. Results and Discussion	98
A. Nanofiltration Performance of PSS/PAH Membranes	98
B. Modeling of Ion Transport Through Polyelectrolyte Membranes	102
C. Performance of Composite and Derivatized Polyelectrolyte Membranes	105
IV. Conclusions	105
V. References	108
 Chapter 6: Conclusions and Future Work	 110
I. Stability and Ion-Permeability of Layered Polyelectrolyte Films Deposited on Solid Supports	110
II. Polyelectrolyte Films as Anion-Separation Membranes	111
III. Characterization of Nanofiltration Membranes Made from Layered Polyelectrolyte Films	111
IV. Future Work	112
 Appendix A: Derivatization of Distribution Coefficient	 114

LIST OF TABLES

Table 2.1	Average peak currents ($\mu\text{A}/\text{cm}^2$) from cyclic voltammograms ($\text{Fe}(\text{CN})_6^{3-}$) measured at PAH/PSS coated gold electrodes in different buffered solutions.	34
Table 2.2	Average R_{ct} values ($\Omega\text{-cm}^2$) from impedance plots ($\text{Fe}(\text{CN})_6^{3-/4-}$) of PAH/PSS coated gold electrodes in different buffered solutions.	40
Table 2.3	Average peak currents ($\mu\text{A}/\text{cm}^2$) from cyclic voltammograms ($\text{Ru}(\text{NH}_3)_6^{3+}$) at PAH/PSS coated gold electrodes in different buffered solutions.	42
Table 2.4	Average R_{ct} values ($\Omega\text{-cm}^2$) from impedance plots ($\text{Ru}(\text{NH}_3)_6^{2+/3+}$) of PAH/PSS coated gold electrodes in different buffered solutions.	44
Table 4.1	Anion flux values ($\text{moles cm}^{-2} \text{ s}^{-1}$) through bare alumina and alumina substrates coated with between 1-5.5- or 10-bilayers of PAH/PSS.	80
Table 5.1	Rejection and flux values (listed in parentheses) in $\text{m}^3 \text{ m}^{-2} \text{ d}^{-1}$ for various polyelectrolyte films used as nanofiltration membranes. Rejection values listed represent % decrease in permeate ion concentration relative to the feed concentration in the collected permeate. The fluorinated film was heated at 180 °C for 2 hrs. The salt solutions were NaCl, Na_2SO_4 , and CaCl_2 .	99
Table 5.2	Flux and rejection values for several commercially available nanofiltration membranes and PSS/PAH membranes. Feed solutions were NaCl, MgSO_4 , and CaCl_2 .	101
Table 5.3	Theoretical values for the concentration of fixed charge (M) in polyelectrolyte membranes calculated using Equation 5.2 and rejection values in Table 5.1.	104

LIST OF FIGURES

Figure 1.1	Schematic diagram of the “Dip n’Rinse” procedure for the deposition of a polyelectrolyte film on a gold electrode coated with a monolayer of carboxylates. In the actual structure of these films, polycations and polyanions are intermingled.	4
Figure 2.1	Ellipsometric thickness (squares) and FTIR-ERS absorbances at 1037 cm^{-1} (circles) for multilayered PAH/PSS films made in the presence of supporting salt. The standard deviation for the absorbance values for each bilayer is ~2%. The standard deviations for the ellipsometric thickness values are <0.3 nm.	28
Figure 2.2	FTIR-ERS spectra of PAH/PSS films (made with supporting electrolyte) composed of 1-5 bilayers.	29
Figure 2.3	FTIR-ERS spectrum of a 9-bilayer PAH/PAA film (made with no supporting electrolyte) deposited on a gold electrode.	31
Figure 2.4	In situ ellipsometric thickness (circles) and cyclic voltammetry ($5\text{ mM Fe(CN)}_6^{3-}$) peak current values (squares) as a function of immersion time for a 10-bilayer PAH/PSS film (made with supporting salt) in pH 3.2- (A), 6.3 (B), and 10-buffered solutions (C).	32
Figure 2.5	CVs ($5\text{ mM Fe(CN)}_6^{3-}$) at a gold electrode coated with a five-bilayer PAH/PSS film (made with supporting electrolyte). CVs were measured in solutions buffered at pH 3.2 (A: dash), pH 6.3 (A: solid line), pH 10 (B: circles), and pH 3.2 after immersion in pH 10 (B: squares).	36
Figure 2.6	Randles’ circuit used to fit impedance data where R_{ct} = charge transfer resistance, R_s = solution resistance, C_{dl} = double-layer capacitance, and Z_w = Warburg element.	38
Figure 2.7	Impedance data ($\text{Fe(CN)}_6^{3-/4-}$) for a gold electrode coated with a five-bilayer PAH/PSS film (made with supporting electrolyte). Plots were obtained in solutions buffered at pH 3.2 (A), 6.3 (B), 10 (C), and 3.2 after immersion in pH 10 (D). Solid circles represent experimental data and open circles show fits obtained with a Randles’ equivalent circuit.	39
Figure 2.8	(A) CVs ($5\text{ mM Ru(NH}_3)_6^{3+}$) of a gold electrode coated with a five-bilayer PAH/PSS film (made with supporting electrolyte). CVs shown were measured in solutions buffered at pH 10 (circles) and pH 3.2 after immersion in pH 10 (squares). (B) Impedance data ($5\text{ mM Ru(NH}_3)_6^{2+/3+}$) for a gold electrode coated with a five-bilayer PAH/PSS film (made with	

	supporting electrolyte). Plots were obtained after immersion in pH 10-buffered solutions (circles) and after reimmersion in pH 3.2-buffered solutions (squares).	43
Figure 2.9	CVs ($5 \text{ mM Fe(CN)}_6^{3-}$) of a gold electrode coated with a layer of MPA (dashed line) or with a 1- (solid line), 2- (diamonds), 3- (circles), 4- (squares), or 5-bilayer (diamonds) PAH/PSS film. CVs were measured in solutions buffered at pH 6.3 and films were made from solutions containing supporting electrolyte.	47
Figure 2.10	CVs ($5 \text{ mM Fe(CN)}_6^{3-}$, pH 6.3) of gold electrodes coated with a 20-bilayer PAH/PSS film prepared with no supporting electrolyte (circles, thickness of 16 nm), a 5-bilayer PAH/PAA film prepared with supporting electrolyte (dashes, thickness of 44 nm), a 9-bilayer PAH/PAA prepared with no supporting electrolyte (diamonds, thickness of 15 nm), or a 4-bilayer PAH/PSS film prepared with supporting electrolyte (solid line with x markers, thickness of 15 nm).	49
Figure 3.1	Schematic representation of cross-linking between PAA and PAH chains. The actual structure of these films is likely highly intermingled not discrete layers as shown in this representation.	59
Figure 3.2	FTIR-ERS spectra of 9-bilayer PAH/PAA films before heating (A), after heating at 130 °C (B), or after heating at 215 °C (C).	60
Figure 3.3	XPS spectra of the N_{1s} region of a 9-bilayer PAH/PAA film before (A) and after heating for 2 hours at 215 °C (B). Binding energy is referenced to the C_{1s} peak for hydrocarbons (284.6 eV).	62
Figure 3.4	Cyclic voltammograms ($0.005 \text{ M Fe(CN)}_6^{3-}$ in $0.025 \text{ Na}_2\text{HPO}_4$, $0.025 \text{ NaH}_2\text{PO}_4$, $1 \text{ M Na}_2\text{SO}_4$, pH 6.3) at gold electrodes coated with 9-bilayers of PAH/PAA before (3A, dashed line), after heating a film at 130 °C for 2 hours (3A, solid line and 3B, dashed line), or after heating a film at 215 °C (3B and C, solid lines). Scan rate of 0.1 V/s and electrode area of 0.1 cm^2 . The electrode was immersed in the solution for 2 minutes prior to data acquisition.	63
Figure 3.5	Impedance plots ($0.005 \text{ M Fe(CN)}_6^{3-/4-}$ in $0.025 \text{ Na}_2\text{HPO}_4$, $0.025 \text{ NaH}_2\text{PO}_4$, $1 \text{ M Na}_2\text{SO}_4$, pH 6.3) for gold electrodes coated with 9-bilayer PAH/PAA films before heating (A), after heating at 130 °C (B), or after heating at 215 °C (C). Scale bars apply to both x- and y-axes. Frequency range $1\text{-}10^5 \text{ Hz}$. Sinusoidal voltage: 5 mV about E° . The electrode was immersed in solution for 5 minutes prior to data acquisition.	65
Figure 3.6	Modified Randles' equivalent circuit used to model impedance data from gold electrodes modified with cross-linked PAH/PAA films.	66

Figure 4.1	Dialysis cell used to measure ion-permeability of polyelectrolyte membranes: conductivity meter (A), electric stirrer (B), conductivity electrode (C), receiving phase (D), source phase (E), membrane (F), and magnetic stir bar (G).	72
Figure 4.2	FESEM images of the filtrate side of a porous alumina substrate (A), and alumina substrates coated with 2 (B), 4 (C), or 5 PAH/PSS bilayers (D). The circles in image C are likely defects in the film structure. Samples were coated with ~5 nm Au for imaging.	74
Figure 4.3	FESEM images of the permeate side of a bare alumina substrate before film deposition (A), after restricting deposition to the filtrate side (B), or following complete alumina immersion in polyelectrolyte solutions (C).	76
Figure 4.4	Cross-sectional FESEM images of the filtrate side of a bare alumina substrate (A) and an alumina substrate coated with 5-bilayers of PAH/PAA (B). Film thickness \cong 40 nm.	77
Figure 4.5	Cross-sectional FESEM image showing the lack of polyelectrolyte deposition in the inner pores of an alumina substrate where the filtrate side is coated with a 10-bilayer PAH/PSS film.	78
Figure 4.6	Plot of normalized receiving-phase conductivity (K_2SO_4) as a function of time when the source phase was separated from the receiving phase by a bare alumina substrate (open squares), or a 1- (diamonds), 2- (squares), 3- (triangles), 4- (inverted triangles), 5- (circles), or 10-bilayer (X's) PAH/PSS film.	81
Figure 4.7	Plot of normalized receiving-phase conductivity as a function of time when the source phase was separated from the receiving phase by a 5-bilayer PAH/PSS film. Different symbols represent different salts: KCl (triangles), KNO_3 (squares), K_2SO_4 (diamonds), $K_2Ni(CN)_4$ (circles), and $K_3Fe(CN)_6$ (inverted triangles).	82
Figure 4.8	FESEM images of the top of an alumina substrate coated with either a 4.5-bilayer PAA/PAH film heated at 115 C (A) or a 5-bilayer PSS/PAH film coated with 1.5-bilayers of PAA/PAH (B). Samples were coated with 5 nm Au for imaging.	87
Figure 5.1	Experimental setup for nanofiltration experiments: Ar tank (1), stainless steel feed tank (2), centrifugal pump (3), prefilter (4), flowmeter (5), pressure gauges (6), membrane cells (7), and graduated cylinders (8). System pressure was 70 psi and flowrate was 18 mL/min.	96

Figure 5.2 Schematic diagram of the nanofiltration membrane cell. (A) shows how the cell is placed together: inlet/outlet ports (1&2), threads (3), rubber o-ring (4), alumina membrane (5), porous stainless steel frit (6), cap that frit fits in and presses the membrane tight against O-ring (7), and threaded bottom part of cell that top part screws into (8). The cell is assembled in the direction of the arrow. (B) shows a bottom view of the upper portion of cell: recessed inlet/outlet channels (1&2) and o-ring (3). 97

Figure 5.3 Reaction scheme for derivatization of composite membranes with 1H-1H-perfluorooctylamine (PFOA). In step 1 the acid groups of PAA are converted to a mixed anhydride. In step 2, the amine group of PFOA reacts with the anhydride resulting in attachment of PFOA to the composite film through an amide linkage. 107

LIST OF ABBREVIATIONS

C_{dl}	double-layer capacitance
C_A^{mem}	concentration of species A in membrane phase
C_A^{sol}	concentration of species A in solution phase
CV	cyclic voltammogram
ΔE_p	$ E_{pa} - E_{pc} $ in CV
$E^{\circ'}$	equilibrium potential of couple
FTIR-ERS	Fourier transform infrared – external reflectance spectroscopy
Hz	Hertz
i_p	peak current
MPA	mercaptopropionic acid
Ω	ohms
PAH	poly(allylamine hydrochloride)
PSS	poly(styrene sulfonate)
PAA	poly(acrylic acid)
R_{ct}	charge transfer resistance
R_s	solution resistance
s	second
T	temperature
V	volt
z_A	valence of ion A
z_B	valence of ion B
z_X	valence of fixed charge in membrane
Z_w	Warburg impedance

CHAPTER 1

Introduction and Background

I. Development of Thin Films

Controlled surface modification with ultrathin, organic films began with the work of Langmuir and Blodgett in the 1930's.^{1,2} Since then, there have been many advances in this area of research with each discovery having its own unique benefits and limitations.³⁻⁶ One of the latest techniques for the modification of surfaces is the use of layered polyelectrolyte films.⁶ Advantages of this deposition technique include an increase in the types of substrates used for coating, increased film stability, and a wider variety of film constituents. This thesis presents an investigation of the ion permeability of layered polyelectrolyte films and their use as ion-separation membranes.

Deposition of films using the Langmuir-Blodgett (LB) technique first showed that organic molecules could be deposited onto a solid support with a high degree of order.^{1,2} The deposition of LB films begins with compression of a monolayer of amphiphilic molecules on a liquid surface (typically water) in a Langmuir trough. The amphiphiles orient themselves so that the hydrophilic end of the molecule is in contact with the aqueous phase. Film deposition occurs as a substrate is lowered, perpendicular to the liquid surface, into the trough. This results in deposition of one layer of molecules. Subsequent layers are deposited by repeated immersions in the Langmuir trough. Although LB films are highly ordered, they are limited to low thicknesses, and the weak van der Waals forces holding the film together provide little stability.⁷ Another disadvantage relates to the required amphiphilic nature of the absorbed molecules, which restricts film composition severely.

In the early 1980's, the development of self-assembled monolayers (SAMs) provided a new and convenient method to construct modified surfaces.^{8,9} The majority of SAMs are alkanethiols, which rely on the formation of the M-S (M=Au, Cu, Fe, Ag) bonds for adhesion between the substrate and adsorbate. SAMs offer greater convenience for film deposition relative to LB films because the substrate is simply immersed in a solution containing the self-assembling molecule. Although SAMs provide a simple method for film deposition, they lack any means for stable formation of multilayered films, and the M-S bond stability becomes an issue at high temperatures.^{10,11}

The limitations imposed by SAMs and LB films elicited the development of new procedures for thin film deposition that provide greater film stability while maintaining control over film structure and composition. The introduction of layered polyelectrolyte films by Decher and coworkers provided the ability to create thin films with well-defined control over film thickness and composition.¹² Multiple electrostatic interactions between the individual polyelectrolyte layers provide the basis for film formation and stability. The synthesis of these films, which involves alternating immersions of a substrate in solutions containing polycations and polyanions, is simple and does not require organic solvents or expensive instrumentation. An additional advantage of layered polyelectrolyte films is their ability to deposit on a wide variety of substrates. Both LB films and SAMs require smooth surfaces for defect-free film deposition. With polyelectrolyte films, one only needs a charged surface to begin deposition, because adsorption of these films tends to cover defects.¹³ This furthers the possible applications of layered polyelectrolyte films.

II. History and Development of Layered Polyelectrolyte Films

Iler was the first to show the premise for depositing films based on electrostatic interactions with his work on multilayered, charged colloidal particles.¹⁴ Decher and Hong then extended this idea to the sequential adsorption of alternating layers of charged polymers.^{6,12} Decher's technique provided remarkable nanoscale control of film thickness and composition. Additionally, the only prerequisite for inclusion of a material in the film is that the moiety be charged, and this greatly increases the possibilities for film structure and composition. The variety of films made by the alternating polyelectrolyte deposition (APD) technique is illustrated by the use of DNA,¹⁵ redox-active polymers,^{16,17} charged viruses,¹⁸ semiconductor particles,^{19,20} conducting polymers,²¹ and inorganic sheets,^{13,19,22-25} in the formation of layered polyelectrolyte films. The type of substrate used in the APD process also varies widely and includes examples such as SiO₂,^{26,27} quartz,^{12,28} glass,^{29,30} Au modified with a charged monolayer,³¹ charged colloids,³²⁻³⁴ and polymers.³⁵⁻³⁹ This wide range in film composition has led to extensive research concerning the structure and application of polyelectrolyte films.

Synthesis of layered polyelectrolyte films is a simple "Dip n' Rinse" (Figure 1.1) procedure, which begins with immersion of a charged substrate into a solution containing an oppositely charged polyelectrolyte. A film forms due to electrostatic interactions between the substrate and polyelectrolyte. This process is driven by entropy, which increases due to the displacement of counter-ions from the surface by the adsorbing polyelectrolyte chain. Rinsing of the substrate with water and immersion in a second

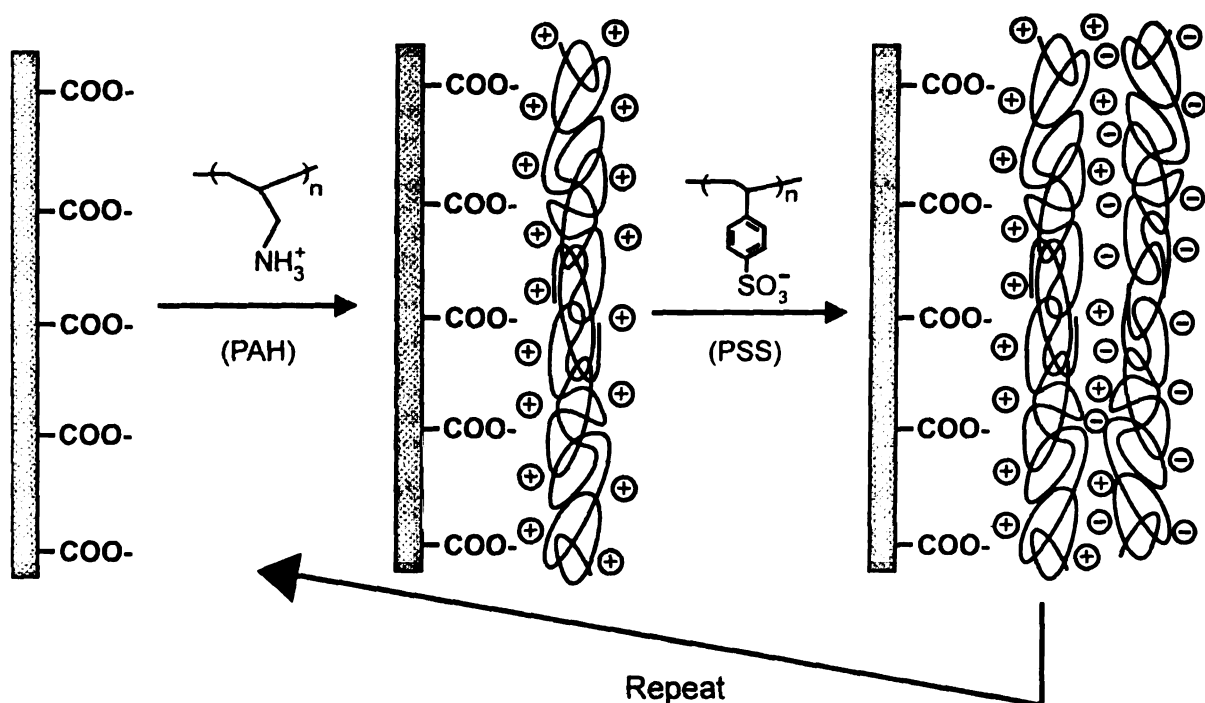


Figure 1.1: Schematic diagram of the "Dip n' Rinse" procedure for the deposition of a polyelectrolyte film on a gold electrode coated with a monolayer of carboxylates. In the actual structure of these films polycations and polyanions are intermingled.

solution containing an oppositely charged polyelectrolyte yields another layer on the surface. Repetition of this process produces multilayer films whose thickness depends on the number of polyelectrolyte depositions,^{12,40,41} pH of the deposition solutions,⁴² and the supporting salt concentration in the polyelectrolyte solutions.^{31,41,43}

Several groups examined the growth and structure of polyelectrolyte films using techniques such as small angle X-ray scattering,⁴⁴ X-ray and neutron reflectometry,⁴⁴⁻⁴⁹ UV/VIS spectroscopy,^{27,30,50} scanning electron microscopy,⁵¹ atomic force microscopy,^{22,24,51} X-ray photoelectron spectroscopy,^{26,36} time-of-flight secondary ion mass spectrometry,^{37,52} radiolabelling,^{53,54} quartz crystal microbalance gravimetry,⁵⁵⁻⁵⁷ and optical ellipsometry.^{24,47} The prevailing theory on polyelectrolyte film structure is that the individual layers are highly intermingled with surrounding layers.^{46,48,53}

Schlenoff and coworkers used electrochemical techniques to investigate electron-transfer through polyelectrolyte films containing redox-active layers.^{16,58} These studies showed a large degree of intermingling between individual polyelectrolyte layers, which resulted in electron transfer between electro-active layer-pairs, even when separated by four non-conducting layer-pairs.

Due to the high degree of entanglement between polyelectrolyte layers, there appears to be one-to-one charge compensation between polyanion and polycation layers. Several studies detected no counter ions in the bulk of polyelectrolyte films, supporting the theory of one-to-one charge compensation.^{46,48,53} Schlenoff and coworkers used radiolabeled ions to show that charge compensation is >99% intrinsic within the bulk of poly(diallyldimethylammonium)/PSS films, while at the surface there exists ~45% charge excess with respect to the total layer charge.⁵³ The excess charge at the surface is due to

the formation of loops and trains, which extend into the solution.⁵⁹ The interface-induced nonstoichiometry caused by the formation of loops and trains at the film surface provides the driving force for subsequent layer adsorption.⁵⁹ Charge screening by supporting electrolyte controls the degree of extrinsic charge; therefore, greater film thicknesses result from increased salt concentrations in the deposition solutions.

After determining the nature of polyelectrolyte film structure, research began focusing on possible applications of layered polyelectrolyte films. These films are relevant to sensing,^{28,57,60,61} separations,^{38,39,62-64} and electronics^{17,20,21,58} applications because of their simple layer-by-layer synthesis and wide tunability. Additionally, these films can naturally cover defects¹³ and coat substrates with unusual geometries. The feasibility of applying these films will depend on their permeability and stability under relevant conditions. Some applications, (e.g., sensing) require highly permeable films, while others (e.g., anti-corrosion coatings) necessitate impermeable films. While there is much information on the growth and structure of polyelectrolyte films in the “dry” state,^{6,30,31,40,42,44,46,49,51,65,66} there is less understanding of the structure of films exposed to solvent.^{29,55,56,67} Our interest in using polyelectrolyte films for ion-separation applications requires an understanding of solvated film properties.

III. Ion-Permeability of Layered Polyelectrolyte Films

Several groups performed fundamental studies of ion-transport through polyelectrolyte films. Möhwald and von Klitzing examined the transport of neutral quenchers (to within 14 nm of the substrate) in polyelectrolyte films using time-dependent fluorescence.^{29,68} These studies suggest two regions of differing

polyelectrolyte film structure as indicated by a change in the diffusion coefficients of the quencher probes. The outer layers of the film are bound more loosely than the film bulk, which probably has a higher degree of entanglement with neighboring layers. This gives rise to decreases in the effective diffusion coefficients of the quencher probes in the film interior. A second conclusion from these studies was that film structure depends strongly on the concentration of supporting electrolyte in the polymer deposition solutions. Films made without supporting electrolyte show drastic increases in film permeability as compared to those made with supporting electrolyte due to the smaller degree of layer interpenetration and smaller layer thicknesses.

Lindholm-Sethson and coworkers investigated the ion-permeability of layered PAH/PSS films using electrochemical techniques.⁶⁹ They examined the change in film permeability to redox probes as a function of the number of bilayers in the film and the individual bilayer thicknesses. Two types of films were used: thick and thin multilayer films with bilayer thicknesses of 12 and 2 nm, respectively. Film thickness was controlled by varying the amount of H₂SO₄ in both the PAH and PSS solutions. The cyclic voltammetry of thin polyelectrolyte films in this recent study shows trends similar to those in this thesis. Fe(CN)₆⁴⁻ permeability decreased with the addition of each polyelectrolyte bilayer until after the addition of 8-bilayers, the CV response was primarily due to capacitive current. When Os(bipy)₃³⁺ was used as a redox couple, the film showed no inhibition of cation flux until the deposition of 5-bilayers. Deposition of further layers greatly decreased flux. In the thick bilayer system, a thin film CV response was observed indicating adsorption of the redox-active molecule in the film. As

expected, the amount of ion adsorption increased with the addition of each polyelectrolyte bilayer.

In Chapter 2 of this thesis, we examine the permeability of two different types of layered polyelectrolyte films as a function of solution pH, number of bilayers, and film composition using electrochemical techniques. This study differs from Möhwald and von Klitzing's work as we describe the film permeability through the entire structure to the substrate surface (They limited their tests to ~14 nm from the substrate surface). The results presented here complement those of Lindholm-Sethson but, in addition, we examine film permeability under various solution conditions and as a function of the film structure. Our initial studies focus on layered poly(allylamine hydrochloride)/poly(styrenesulfonate) (PAH/PSS) and PAH/poly(acrylic acid) (PAH/PAA) films in pH 3.2-, pH 6.3-, and pH 10-buffered solutions. Cyclic voltammetry indicates that solvent-swollen film structure and permeability are highly dependent on solution pH. Electrochemical impedance spectroscopy shows that multilayer PAH/PSS films block gold electrodes and that passivation varies with the number of polyelectrolyte bilayers, solution pH, and the concentration of salt used in film deposition. In contrast, PAH/PAA films are highly permeable even after deposition of films as thick as 44 nm.

Although PAH/PAA films are highly permeable, the presence of carboxylate and amine groups provides a convenient means to covalently cross-link these films and make them highly blocking. Chapter 3 of this thesis discusses the permeability of such cross-linked, nylon-like films and illustrates their increased stability over a wide pH range. Fourier transform infrared external reflection spectroscopy (FTIR-ERS) and X-ray photoelectron spectroscopy (XPS) confirm the conversion of carboxylate and ammonium

groups into amide bonds while electrochemical impedance spectroscopy shows that 11-13 nm-thick cross-linked films have resistances as high as $10^5 \Omega\text{-cm}^2$.

IV. Use of Layered Polyelectrolyte Films as Ion-Separation Membranes

Anion separation membranes have a long and rich history in many industrial fields. Applications include salt production from seawater,⁷⁰⁻⁷² acid and dye recovery from brine solutions,^{62,73-75} separation of organic acids during food processing,⁷⁶ sensors,^{77,78} and separation of pollutants from groundwater.⁷⁹⁻⁸¹ The majority of anion separation processes include polymer membranes used in conjunction with electrodialysis. The properties (e.g. hydrophilicity^{70,72,82-84} and degree of cross-linking^{71,76}) of the polymer membrane dictate flux and selectivity. Although polymer membranes are extensively used, there are several drawbacks such as low porosity and large membrane thicknesses^{73,75,81,84-86} (50-500 μm), which are due to manufacturing limitations. In an attempt to enhance separations by these membranes, a polyelectrolyte layer is deposited on anion-exchange membranes. In some cases, enhanced performance is observed with this type of modification.^{63,87,88}

The inherent disadvantages of thick membranes may be overcome with the development of an ultrathin polymer skin on a highly porous support material. Layered polyelectrolyte films deposited on porous alumina supports may provide a versatile means for investigating such ion-separation membranes. Several groups recently reported the use of polyelectrolyte films to modify porous polymer substrates for gas separation.^{35,38,39,64} In some cases, these studies show selectivity enhancements with polyelectrolyte films containing between 10 and 200 layers. A recent study showed the

applicability of polyelectrolyte films for the separation of monovalent and divalent ions.⁸⁹ However, none of these reports address the issue of whether film deposition occurs at the membrane surface or within the pores. Determining the structure of polyelectrolyte films deposited on porous substrates and the factors controlling transport of mono-, di-, and trivalent anions of varying size through multilayered, ultrathin polyelectrolyte films represents the second objective of this thesis.

Deposition of an ultrathin film on a porous support is a challenging endeavor, as one must coat the substrate without depositing material in the pores of the support. Porous alumina was chosen as the support material for these studies due to its high pore density and well-defined porous structure. In addition, the regular support structure allows for convenient field emission scanning electron microscope (FESEM) studies to determine film coverage and whether deposition occurs within the pores. Utilizing the simple ADP procedure, polyelectrolyte films were deposited on porous alumina supports. FESEM images show that as few as five-bilayers (<25 nm) of polyelectrolyte effectively cover the surface without filling of underlying pores.

Dialysis measurements with these membranes show that Donnan exclusion is the primary selection mechanism in ion transport. Selectivity values for $\text{Cl}^-/\text{SO}_4^{2-}$ and $\text{Cl}^-/\text{Fe}(\text{CN})_6^{3-}$ transport were 6 and 500, respectively, for a 4.5-bilayer PSS/PAH membrane. PAA/PAH membranes show similar selectivity values along with a 70% decrease in overall ion flux. To increase selectivity, composite membranes were developed to utilize the high Cl^- transport of PSS/PAH films and the high SO_4^{2-} rejection and cross-linkability of PAA/PAH membranes. These composite membranes contain a thin layer of PAA/PAH deposited on a PSS/PAH precursor film and show a wide range of selectivity

values depending on the number of PAA/PAH layers and cross-linking temperatures. Such films can form ultrathin barriers that allow high flux along with selective transport of anions, where anion charge and size determine selectivity.

Krasemann and Tieke recently reported ion-permeation results for layered polyelectrolyte films deposited on a polymeric support material.⁸⁹ In this study, the effect of bilayer thickness and charge density on ion transport was determined by varying the pH and the supporting electrolyte concentration in the polymer deposition solutions. With PAH/PSS films deposited from solutions containing supporting electrolyte, the Na^+ flux steadily decreased with deposition of up to 30 bilayers but then was constant with further bilayer depositions. Mg^{2+} flux decreased at a higher rate than Na^+ flux and continued decreases were observed for films with up to 90 bilayers, resulting in $\text{Na}^+/\text{Mg}^{2+}$ selectivity values of between 30 and 112. Anion selectivity values (Cl^- over SO_4^{2-}) of between 17 and 45 were observed with similar films made in the presence of supporting electrolyte. Films deposited with no supporting electrolyte showed similar trends with respect to decreases in flux with increasing numbers of bilayers, but fluxes were generally higher and selectivity lower for these films.

In addition to studying transport as a function of bilayer thickness and number of bilayers, Krasemann and Tieke also investigated the effect of polyelectrolyte charge density on ion transport through polyelectrolyte films. One way to alter charge density in these films is through the incorporation of polyelectrolytes with differing charge densities. As expected, the ion flux decreased and in some cases ion selectivity increased as the charge density increased. A second method of changing the film charge density is by varying the pH of deposition solutions. For films deposited at low pH values where

the majority of the amine groups of PAH are protonated, there is decreased cation flux due to the increased charge repulsion between the film and cation.

Krasemann and Tieke attribute high selectivities to a bipolar membrane transport mechanism where the ion encounters repulsion at each layer of oppositely charged polyelectrolyte. They cite several reasons for their explanation. When supporting electrolyte is present, the polyelectrolyte deposits in a globular form as opposed to a rod-like structure. This globular form may not allow for the complete interpenetration of the polyelectrolyte and therefore may result in a higher degree of free charge in the film. This results in lower ion flux due to the increased Donnan repulsion produced by the electrostatic interactions between the ion in solution and free charge in the film. However, our studies see a maximum $\text{Cl}^-/\text{SO}_4^{2-}$ selectivity of 6 with the deposition of 5-bilayers of PSS/PAH with no further increase in selectivity with deposition of an additional 5-bilayers. Moreover, simulations by Lebedev and coworkers show that a multi-bipolar structure will not enhance selectivity.⁹⁰ Our studies suggest that the outer layer charge is the dominant factor in controlling flux as opposed to the multiple bilayer structure suggested by Krasseman and Tieke. We suspect that in Krasemann and Tiekess study they did not initially form an ultrathin film that fully covered the substrate. Selectivity enhancement with increasing numbers of layers in the film is also suggestive of a multi-bipolar membrane structure. Tieke suggests that selectivity would increase with the number of bipolar interfaces encountered.

V. Use of Layered Polyelectrolyte Films as Nanofiltration Membranes

Although diffusion dialysis measurements provide an initial assessment of film permeability, this technique is not a practical method for large-scale ion separations. Such separations generally require electrodialysis or reverse osmosis (RO) membranes. RO processes utilize a pressure differential across the membrane along with partitioning in the separation of solutes.^{91,92} Traditionally, RO has been subdivided into 3 categories; high-pressure RO, low-pressure RO, and nanofiltration, which is often referred to as “soft” RO (operating pressures of <200 psi). Size exclusion and charge in the membrane both play a role in the rejection properties of nanofiltration membranes. Typical applications include residential and industrial water softening along with filtration of various organic constituents (e.g. humic substances, pesticides, and insecticides).^{74,93-96}

There are a limited number of materials currently being used in membrane separations. RO and nanofiltration membranes are typically constructed from linear and cross-linked polyamides and polyetherurea polymers.^{91,92,97-100} The majority of these membrane systems consist of a thick, highly porous support material coated with a thin “skin”, which provides selectivity and determines membrane flux. Challenges currently facing nanofiltration membranes are fouling, Cl₂ resistance, and increasing salt rejections while maintaining high fluxes at low operating pressures. Present research on membranes has focused on developing thinner composite layers, chemical derivatization of commercial membranes, and developing new membrane materials related to polyamide and cellulosic materials. Childs and coworkers have deviated from the notion of “thinner is better” and have been modifying membranes with pore filling polyelectrolytes to enhance membrane performance.^{63,88,101} Layered polyelectrolyte

films offer the possibility of creating ultrathin membranes as well as the ability to easily derivatize membranes for increased salt rejection or introduction of anti-fouling properties.

In the final chapter of this thesis, PSS/PAH films deposited on porous alumina supports are tested under nanofiltration conditions. The high degree of charge in these membranes provides moderate and high ion rejections for monovalent and divalent species, respectively. In addition, high permeate fluxes are maintained with the high level of ion rejections. Trends from the diffusion dialysis results, such as changes in rejection with changes in the outer layer charge, are observed in the nanofiltration results. The high rejections and permeate flux values compare very well with commercially available nanofiltration membranes.

VI. References

- 1) Langmuir, I. *J. Am. Chem. Soc.* **1917**, *39*, 1848-1852.
- 2) Blodgett, K. B. *J. Am. Chem. Soc.* **1935**, *57*, 1007-1010.
- 3) Swalen, J. D.; Allara, D. L.; Andrade, J. D.; Chandross, E. A.; Garodd, S.; Israelachvili, J.; McCarthy, T. J.; Murray, R.; Pease, R. F.; Rabolt, J. F.; Wynne, K. J.; Yu, H. *Langmuir* **1987**, *3*, 932-950.
- 4) Ulman, A. *Introduction to Thin Organic Films: From Langmuir-Blodgett to Self-Assembly*; Academic Press: Boston, 1991.
- 5) Ulman, A. *Chem. Rev.* **1996**, *96*, 1533-1554.
- 6) Decher, G. *Science* **1997**, *277*, 1232-1237.
- 7) Embs, F.; Funhoff, D.; Laschewsky, A.; Licht, U.; Ohst, H.; Prass, W.; Ringsdorf, H.; Wegner, G.; Wehrmann, R. *Adv. Mater.* **1991**, *3*, 25-30.
- 8) Allara, D. L.; Nuzzo, R. G. *Langmuir* **1985**, *1*, 45-52.
- 9) Nuzzo, R. G.; Dubois, L. H. *Chem. Rev.* **1996**, *96*, 1533-1554.
- 10) Schlenoff, J. B.; Li, M.; Ly, H. *J. Am. Chem. Soc.* **1995**, *117*, 12528-12536.
- 11) Nuzzo, R. G.; Fusco, F. A.; Allara, D. L. *J. Am. Chem. Soc.* **1987**, *109*, 2358-2368.
- 12) Decher, G.; Hong, J.-D.; Schmitt, J. *Thin Solid Films* **1992**, 831-835.
- 13) Kleinfeld, E. R.; Ferguson, G. S. *Chem. Mater.* **1996**, *8*, 1575-1578.
- 14) Iler, R. K. *J. Coll. Int. Sci* **1966**, *21*, 569-594.
- 15) Lvov, Y.; Decher, G.; Sukhorukov, G. *Macromolecules* **1993**, *26*, 5396-5399.
- 16) Laurent, D.; Schlenoff, J. B. *Langmuir* **1997**, *13*, 1552-1557.
- 17) Wu, A.; Yoo, D.; Lee, J.-K.; Rubner, M. F. *J. Am. Chem. Soc.* **1999**, *121*, 4883-4891.
- 18) Lvov, Y.; Haas, H.; Decher, G.; Möhwald, H. *Langmuir* **1994**, *10*, 4232-4236.
- 19) Cassagneau, T.; Mallouk, T. E.; Fendler, J. H. *J. Am. Chem. Soc.* **1998**, *120*, 7848-7859.

- 20) Kotov, N. A.; Dékány, I.; Fendler, J. H. *J. Phys. Chem.* **1995**, *99*, 13065-13069.
- 21) Fou, A. C.; Rubner, M. F. *Macromolecules* **1995**, *28*, 7115-7120.
- 22) Kerimo, J.; Adams, D. M.; Barbara, P. F.; Kaschak, D. M.; Mallouk, T. E. *J. Phys. Chem. B* **1998**, *102*, 9451-9460.
- 23) Kim, H.-N.; Keller, S. W.; Mallouk, T. E. *Chem. Mater.* **1997**, *9*, 1414-1421.
- 24) Fang, M.; Kaschak, D. M.; Sutorik, A. C.; Mallouk, T. E. *J. Am. Chem. Soc.* **1997**, *119*, 12184-12191.
- 25) Kleinfeld, E. R.; Ferguson, G. S. *Science* **1994**, *265*, 370-373.
- 26) Sukhishvili, S. A.; Granick, S. *J. Chem. Phys.* **1998**, *109*, 6861-6868.
- 27) Lvov, Y.; Ariga, K.; Ichinose, I.; Kunitake, T. *J. Am. Chem. Soc.* **1995**, *117*, 6117-6123.
- 28) Yang, X.; Johnson, S.; Shi, J.; Holesinger, T.; Swanson, B. *Sensors and Actuators B* **1997**, *45*, 87-92.
- 29) Klitzing, R. v.; Möhwald, H. *Macromolecules* **1996**, *29*, 6901-6906.
- 30) Ferreira, M.; Rubner, M. F. *Macromolecules* **1995**, *28*, 7107-7114.
- 31) Caruso, F.; Niikura, K.; Furlong, D. N.; Okahata, Y. *Langmuir* **1997**, *13*, 3422-3426.
- 32) Caruso, F.; Lichtenfeld, H.; Giersig, M.; Möhwald, H. *J. Am. Chem. Soc.* **1998**, *120*, 8523-8524.
- 33) Caruso, F.; Caruso, R. A.; Möhwald, H. *Science* **1998**, *282*, 1111-1114.
- 34) Donath, E.; Sukhorukov, G. B.; Caruso, F.; Davis, S. A.; Möhwald, H. *Angew. Chem. Int. Ed.* **1998**, *37*, 2202-2205.
- 35) Kotov, N. A.; Magonov, S.; Tropsha, E. *Chem. Mater.* **1998**, *10*, 886-895.
- 36) Chen, W.; McCarthy, T. J. *Macromolecules* **1997**, *30*, 78-86.
- 37) Delcorte, A.; Bertrand, P.; Wischeroff, E.; Laschewsky, A. *Langmuir* **1997**, *13*, 5125-5136.
- 38) Ackern, F. v.; Krasemann, L.; Tieke, B. *Thin Solid Films* **1998**, *327-329*, 762-766.

- 39) Leväsalmi, J.-M.; McCarthy, T. J. *Macromolecules* **1997**, *30*, 1752-1757.
- 40) Hoogeveen, N. G.; Cohen Stuart, M. A.; Fleer, G. J. *Langmuir* **1996**, *12*, 3675-3681.
- 41) Dubas, S. T.; Schlenoff, J. B. *Macromolecules* **1999**, *32*, 8153-8160.
- 42) Yoo, D.; Shiratori, S. S.; Rubner, M. F. *Macromolecules* **1998**, *31*, 4309-4318.
- 43) Harris, J. J.; Bruening, M. L. *Langmuir* **2000**, *16*, 2006-2013.
- 44) Lvov, Y.; Decher, G.; Haas, H.; Möhwald, H.; Kalachev, A. *Physica B* **1994**, *198*, 89-91.
- 45) Sukhorukov, G. B.; Schmitt, J.; Decher, G. *Ber. Bunsenges. Phys. Chem.* **1996**, *100*, 948-953.
- 46) Schmitt, J.; Grunewald, T.; Decher, G.; Pershan, P. S.; Kjaer, K.; Losche, M. *Macromolecules* **1993**, *26*, 7058-7063.
- 47) Tronin, A.; Lvov, Y.; Nicolini, C. *Colloid Polym. Sci.* **1994**, *272*, 1317-1321.
- 48) Lösche, M.; Schmitt, J.; Decher, G.; Bouwman, W. G.; Kjaer, K. *Macromolecules* **1998**, *31*, 8893-8906.
- 49) Decher, G.; Lvov, Y.; Schmitt, J. *Thin Solid Films* **1994**, *244*, 772-777.
- 50) Sukhorukov, G. B.; Möhwald, H.; Decher, G.; Lvov, Y. M. *Thin Solid Films* **1996**, 220-223.
- 51) Caruso, F.; Furlong, D. N.; Ariga, K.; Ichinose, I.; Kunitake, T. *Langmuir* **1998**, *14*, 4559-4565.
- 52) Delcorte, A.; Bertrand, P.; Arys, X.; Jonas, A.; Wischeroff, E.; Mayer, B.; Laschewsky, A. *Surf. Sci.* **1996**, *366*, 149-165.
- 53) Schlenoff, J. B.; Ly, H.; Li, M. *J. Am. Chem. Soc.* **1998**, *120*, 7626-7634.
- 54) Schlenoff, J. B.; Li, M. *Ber. Bunsenges. Phys. Chem* **1996**, *100*, 943-947.
- 55) Lvov, Y.; Ariga, K.; Onda, M.; Ichinose, I.; Kunitake, T. *Colloid Surf. A* **1999**, *146*, 337-346.
- 56) Xu, H.; Schlenoff, J. B. *Langmuir* **1994**, *10*, 241-245.
- 57) Caruso, F.; Niikura, K.; Furlong, D. N.; Okahata, Y. *Langmuir* **1997**, *13*, 3427-3433.

- 58) Schlenoff, J. B.; Laurent, D.; Ly, H.; Stepp, J. *Adv. Mater.* **1998**, *10*, 347-349.
- 59) Lowack, K.; Helm, C. A. *Macromolecules* **1998**, *31*, 823-833.
- 60) Montrel, M. M.; Sukhorukov, G. B.; Petrov, A. I.; Shabarchina, L. I.; Sukhorukov, B. I. *Sensors and Actuators B* **1997**, *42*, 225-231.
- 61) Lowy, D. A.; Finklea, H. O. *Electrochimica Acta* **1997**, *42*, 1325-1335.
- 62) Nam, S. Y.; Lee, Y. M. *J. Membr. Sci.* **1997**, 161-171.
- 63) Mika, A. M.; Childs, R. F.; Dickson, J. M.; McCarry, B. E.; Gagnon, D. R. *J. Membr. Sci.* **1997**, 81-92.
- 64) Stroeve, P.; Vasquez, V.; Coelho, M. A. N.; Rabolt, J. F. *Thin Solid Films* **1996**, 708-712.
- 65) Lvov, Y.; Decher, G.; Möhwald, H. *Langmuir* **1993**, *9*, 481-486.
- 66) Decher, G.; Eckle, M.; Schmitt, J.; Struth, B. *Colloid & Interface Sci.* **1998**, *3*, 32-39.
- 67) Shubin, V.; Linse, P. *J. Phys. Chem.* **1995**, *99*, 1285-1291.
- 68) Klitzing, R. v.; Möhwald, H. *Thin Solid Films* **1996**, 352-356.
- 69) Han, S.; Lindholm-Sethson, B. *Electrochimica Acta* **1999**, *45*, 845-853.
- 70) Saracco, G.; Zanetti, M. C. *Ind. Eng. Chem. Res.* **1994**, *33*, 96-101.
- 71) Sata, T. *J. Membr. Sci.* **1994**, *93*, 117-135.
- 72) Sata, T.; Yamaguchi, T.; Kawamura, K.; Matsusaki, K. *J. Chem. Soc., Faraday Trans.* **1997**, *93*, 457-462.
- 73) Moon, P. J.; Parulekar, S. J.; Tsai, S. *J. Membr. Sci.* **1998**, *141*, 75-89.
- 74) Xu, X.; Spencer, G. *Desalination* **1997**, *114*, 129-137.
- 75) Stachera, D. M.; Childs, R. F.; Mika, A. M.; Dickson, J. M. *J. Membr. Sci.* **1998**, *148*, 199-127.
- 76) Gudernatsch, W.; Krumbholz, C. H.; Strathmann, H. *Desalination* **1990**, *79*, 249-260.
- 77) Toniolo, R.; Comisso, N.; Bontempelli, G.; Schiavon, G.; Sitran, S. *Electroanalysis* **1998**, *10*, 942-947.

- 78) Ugo, P.; Moretto, L. M.; Mazzocchin, G. A.; Guerriero, P.; Martin, C. R. *Electroanalysis* **1998**, *10*, 1168-1173.
- 79) Hell, F.; Lahnsteiner, J.; Frischherz, H.; Baumgartner, G. *Desalination* **1998**, *117*, 173-180.
- 80) Fryxell, G. E.; Liu, J.; Hauser, T. A.; Nie, Z.; Ferris, K. F.; Mattigod, S.; Gong, M.; Hallen, R. T. *Chem. Mater.* **1999**, *11*, 2148-2154.
- 81) Sata, T.; Yamaguchi, T.; Matsusaki, K. *J. Chem. Soc., Chem Comm.* **1995**, 1153-1154.
- 82) Sata, T.; Yamaguchi, T.; Matsusaki, K. *J. Phys. Chem.* **1995**, *99*, 12875-12882.
- 83) Sata, T.; Tagami, Y.; Matsusaki, K. *J. Phys. Chem. B* **1998**, *102*, 8473-8479.
- 84) Sata, T.; Mine, K.; Higa, M. *J. Membr. Sci.* **1998**, *141*, 137-144.
- 85) Zeng, X.; Ruckenstein, E. *J. Membr. Sci.* **1998**, *148*, 195-205.
- 86) Narebska, A.; Warszawski, A. *Sep. Sci. Technol.* **1992**, *27*, 703-715.
- 87) Mika, A. M.; Childs, R. F.; Dickson, J. M. *J. Membr. Sci.* **1999**, *153*, 45-56.
- 88) Childs, R. F.; Mika, A. M.; Pandey, A. K.; McCrory, C.; Mouton, S.; Dickson, J. M. *Sep. Pur. Tech.* **2001**, *22-23*, 507-517.
- 89) Krasemann, L.; Tieke, B. *Langmuir* **2000**, *16*, 287-290.
- 90) Lebedev, K.; Ramirez, P.; Mafé, S.; Pellicer, J. *Langmuir* **2000**, *16*, 9941-9943.
- 91) Bhattacharyya, D.; Williams, M. E. *Membrane Handbook*; Bhattacharyya, D.; Williams, M. E., Ed.; Van Nostrand Reinhold: New York, 1992, pp 263-280.
- 92) Brandt, D. C.; Leitner, G. F.; Leitner, W. E. *Reverse Osmosis*; Brandt, D. C.; Leitner, G. F.; Leitner, W. E., Ed.; Van Nostrand Reinhold: New York, 1993, pp 1-8.
- 93) Bohdziewicz, J.; Bodzek, M.; Wasik, E. *Desalination* **1999**, *121*.
- 94) Berg, P.; Hagmeyer, G.; Gimbel, R. *Desalination* **1997**, *113*, 205-208.
- 95) Hofman, J. A. M. H.; Beerendonk, E. F.; Folmer, H. C.; Kruithof, J. C. *Desalination* **1997**, *113*, 209-214.

- 96) Rautenbach, R.; Linn, T.; Eilers, L. *J. Membr. Sci.* **2000**, *174*, 231-241.
- 97) Childress, A. E.; Elimelech, M. *Environ. Sci. Technol.* **2000**, *34*, 3710-3716.
- 98) Kim, K. J.; Chowdhury, G.; Matsuura, T. *J. Membr. Sci.* **2000**, *179*, 43-52.
- 99) Kim, C. K.; Kim, J. H.; Roh, I. J.; Kim, J. J. *J. Membr. Sci.* **2000**, *165*, 189-199.
- 100) Košutic, K.; Kaštelan-Kunst, L.; Kunst, B. *J. Membr. Sci.* **2000**, *168*, 101-108.
- 101) Mika, A. M.; Childs, R. F.; Dickson, J. M. *Desalination* **1999**, *121*, 149-158.

CHAPTER 2

Electrochemical and in situ Ellipsometric Investigation of the Permeability and Stability of Layered Polyelectrolyte Films

I. Introduction

Layered polyelectrolyte films¹ are attractive for sensing,²⁻⁵ separations,⁶⁻¹¹ anti-corrosion,¹² and electronics¹³⁻¹⁶ applications because of their ease of synthesis and wide variability. The feasibility of using these films will depend on their permeability and stability under relevant conditions. Some applications, (e.g., sensing) require highly permeable films, while others (e.g., anti-corrosion coatings) necessitate impermeable films. While there is much information on the growth and structure of polyelectrolyte films in the “dry” state,^{1,5,17-28} there is less understanding of the structure of films exposed to solvent.²⁹⁻³⁵ Our interest in using polyelectrolyte films for ion-separation applications requires an understanding of solvated film properties.

Utilization of layered polyelectrolyte films as sensor or ion-separation materials will depend critically on their stability and ion-permeability in aqueous solution. To elucidate solvated film properties, electrochemical and in situ ellipsometric studies were used to determine the permeability and stability of layered poly(allylamine hydrochloride)/poly(styrenesulfonate) (PAH/PSS) and PAH/poly(acrylic acid) (PAA) films. The permeability of these layered polyelectrolyte films to $\text{Fe}(\text{CN})_6^{3-}$ and $\text{Ru}(\text{NH}_3)_6^{3+}$ depends on solution pH, the number of bilayers in the film, whether supporting electrolyte is present during film deposition, and the nature of constituent polycations and polyanions. Cyclic voltammetry and impedance spectroscopy show that film permeability is similar in pH 3.2- and pH 6.3-buffered solutions but increases

dramatically in alkaline solutions. In situ ellipsometry helps to explain these results. Upon immersion in pH 3.2- and 6.3-buffered solutions, the thickness of PAH/PSS films increases by 40%, but swelling is constant over time. At pH 10, these films initially swell by 40% but then continue to swell for several minutes before delaminating. The onset of increased swelling corresponds with dramatic increases in film permeability.

Both peak current (cyclic voltammetry) and charge transfer resistance (ac impedance) depend on the number of polyelectrolyte bilayers and deposition conditions. The structure of the first two bilayers is more porous than that of later bilayers. Adding supporting electrolyte to deposition solutions results in thicker bilayers and changes film permeability. For PAH/PSS films, the use of supporting electrolyte during film formation results in a much less permeable film (comparing films of similar thickness). In the case of PAH/PAA films, however, the use of supporting salt results in highly permeable films (even with thicknesses as high as 44 nm). Thus, proper choice of constituent polyelectrolytes and deposition conditions permits control over the permeability of layered polyelectrolyte films.

II. Experimental

A. Chemicals and Solutions

Poly(allylamine) hydrochloride ($M_w=50-65,000$), sodium poly(styrenesulfonate) ($M_w \cong 70,000$), and 3-mercaptopropionic acid were used as received from Aldrich. Hexaammineruthenium(III) chloride and hexaammineruthenium(II) chloride were used as received from either Aldrich or Alfa Aesar. Poly(acrylic acid) (25% by wt. in water; $M_w \cong 90,000$) was used as received from Acros. Solutions for electrochemical studies

contained 1.0 M Na_2SO_4 and were buffered with the following salts: 0.2 M CH_3COOH + 0.0036 M CH_3COONa (pH = 3.2), 0.025 M NaH_2PO_4 + 0.025 M Na_2HPO_4 (pH = 6.3), and 0.025 M Na_2CO_3 + 0.025 M NaHCO_3 (pH = 10). Solutions for cyclic voltammetry contained 0.005 M $\text{K}_3\text{Fe}(\text{CN})_6$ or 0.005 M $\text{Ru}(\text{NH}_3)_6\text{Cl}_3$, and solutions for impedance measurements contained equimolar (0.005 M) $\text{K}_3\text{Fe}(\text{CN})_6/\text{K}_4\text{Fe}(\text{CN})_6$ or $\text{Ru}(\text{NH}_3)_6\text{Cl}_3/\text{Ru}(\text{NH}_3)_6\text{Cl}_2$ in the above mentioned buffers. $\text{Ru}(\text{NH}_3)_6^{2+}$ undergoes oxidation to $\text{Ru}(\text{NH}_3)_6^{3+}$ so quantitative electrolysis was performed until the open circuit potential reached the formal redox potential of the couple (as determined from cyclic voltammetry).

PSS deposition solutions (15 mL total volume, pH 2.3) contained 55 mg of polymer and 1.5 mL of 0.01 M HCl. Solutions for preparing films in the presence of supporting electrolyte also contained 0.5 M MnCl_2 .^{17,21} PAH deposition solutions (15 mL total volume, pH 2.1) for PAH/PSS films contained 28 mg polymer and 1.5 mL of 0.01 M HCl. Deposition solutions were made following literature procedures.¹⁷ For depositions in the presence of supporting electrolyte, PAH solutions contained 0.5 M NaBr (PAH/PSS films) or 0.5 M NaCl (PAH/PAA films). The presence of MnCl_2 causes the precipitation of PAA at pH values of ~ 5 so we chose to use NaCl as the supporting electrolyte for PAH/PAA deposition. PAA solutions were prepared by diluting 1.5 mL of stock PAA solution (25% by wt.) to a final volume of 250 mL. Deposition solutions for PAH/PAA films made with supporting salt (0.5 M NaCl) were adjusted to pH 4.5 with NaOH or HCl. Deposition solutions for PAH/PAA films made without supporting salt were adjusted to pH 5.6 (PAA) and 5.1 (PAH). The higher pH yields thinner films with fewer loops and trains because of electrostatic repulsion between the monomer units.

Deposition times were five minutes for PAH and two minutes for PAA and PSS except for PAH/PAA films made without supporting electrolyte. A five minute immersion for both PAH and PAA was used for these films.

Adjusting the pH of polymer solutions is challenging, as polyelectrolytes tend to adsorb to the pH electrode. Before pH adjustment the pH electrode was immersed in 0.1 M HCl followed by 0.1 M NaOH for ~1 min with water rinses following each immersion. The polyelectrolyte solution is stirred constantly during the pH adjustment and 0.1 M HCl or 0.1 M NaOH was added dropwise. Following the addition of HCl or NaOH, the pH electrode was immersed in the stirred solution until the reading stabilized. The electrode was removed and stored in water between measurements. If the reading did not stabilize or if adjustments took longer than ~15 min the electrode was rinsed again in HCl and NaOH.

Gold slides (electron-beam evaporation of 200 nm of Au on 20 nm Ti on Si(100) wafers) were UV/O₃ cleaned for 15 minutes and immediately immersed in an ethanolic solution containing 0.002 M mercaptopropionic acid (MPA) for 30 minutes. Slides were then rinsed with ethanol followed by Millipore water (18 M Ω -cm). To prepare one polyelectrolyte bilayer, the MPA-coated slide was first immersed in PAH and then rinsed under a continuous stream of water for one minute. Following deposition of PAH, the slide was immersed in a solution of either PSS or PAA followed by a one minute rinse. Additional bilayers were prepared similarly. Slides were dried with nitrogen only after the desired number of bilayers were deposited.

B. Techniques

Electrochemical measurements were made using a standard three-electrode cell containing a Ag/AgCl (3 M KCl) reference electrode and a platinum wire counter electrode. The working electrode was a gold slide sealed in a plastic o-ring holder with an exposed area of 0.1 cm². A CH-Instruments 604 Electrochemical Analyzer was used to perform the impedance and cyclic voltammetry measurements. A scan rate of 0.1 V/sec was used for all cyclic voltammograms. Impedance measurements were taken at frequencies ranging from 0.1 to 10⁵ Hz using a 5 mV sinusoidal voltage centered around $E^{0'}$ of Fe(CN)₆^{3-/4-} or Ru(NH₃)₆^{2+/3+}. Solutions containing Ru(NH₃)₆^{2+/3+} were purged with nitrogen for five minutes prior to measurement, and the cell was kept under flowing nitrogen for the duration of the experiment.

On each electrode, voltammetric and then impedance data were collected at several pH values in the following order: pH 3.2, 6.3, 10, and pH 3.2 after immersion in pH 10. Cyclic voltammetry (Fe(CN)₆³⁻ and Ru(NH₃)₆³⁺) indicates that peak currents for electrodes coated with 3-, 4-, and 5-bilayers of PAH/PSS are stable after a 20-minute immersion in each of the buffered solutions. A 20-minute immersion was thus used prior to both voltammetry and impedance measurements. A two-minute immersion was adequate for PAH/PAA films and 1-, 2-, and 20-bilayer PAH/PSS films as these films are highly permeable. Between cyclic voltammetry and impedance experiments, the electrode was rinsed with water. Charge transfer resistance (R_{ct}) values (Table 2 & 4) were obtained by fitting impedance data with a Randles' circuit using complex non-linear squares regression (LEVM 7.0 by J. Ross McDonald, distributed by Solartron).

(

w

re

in

d

P

a

C

fr

b

a

in

c

w

p

re

b

p

m

(t

re

Ellipsometric measurements were obtained with a rotating analyzer ellipsometer (Model M-44; J.A. Woollam) using WVASE32 software. Substrate parameters (n & k) were measured after absorption of MPA. This insures that any changes in substrate reflectivity due to Au-S bonds will not affect subsequent measurements. The angle of incidence was 75° for all experiments. The thickness values for PAH/PSS films were determined using 44 wavelengths between 414.0 and 736.1 nm. Refractive indices of PAH/PSS films containing between 1- and 5-bilayers (made with supporting salt) were assumed to be the same as those determined for a 10-bilayer film using ellipsometry. Over this wavelength region, the refractive indices for a 10-bilayer PAH/PSS film ranged from 1.53-1.66. A refractive index of 1.5 was assumed for films containing 20 PAH/PSS bilayers (no supporting electrolyte) or 9 PAH/PAA bilayers (no supporting electrolyte), as these films are not sufficiently thick for refractive index determination. Refractive index and thickness values for PAH/PAA films (made with supporting salt) were calculated simultaneously from the experimental Ψ and Δ values between the wavelengths of 465.8 and 548.8 nm (n values ranged from 1.56-1.60). This region produced the best graphical fit, but calculation of the thickness over the entire wavelength region changes the thickness by < 1.0 nm.

In situ ellipsometry was performed on 10-bilayer PAH/PSS films in each of the buffered solutions using a home-built plastic cell with glass windows. The cell was first placed on the sample stage without windows and the stage height was adjusted for maximum intensity and flatness. The addition of the cell windows creates two reflections (from the front and rear windows). To align the windows, they were adjusted so that both reflections overlap the incident beam ensuring that the windows are perpendicular to the

be

fo

ch

w

w

el

38

th

II

.4

de

thi

bi

rep

up

thi

wi

no

ma

Pa

beam (within 0.1°). The effect of the windows on measurements of dry films is $<0.25^\circ$ for both Ψ and Δ . This possible error in Ψ and Δ , due to the windows, results in a $\sim 1\%$ change in the calculated film thickness (~ 0.5 nm) as compared to measurements made without the cell. Buffered solutions were then poured into the cell and measurements were recorded as a function of time until a stable thickness was observed. In situ ellipsometry was performed on four different 10-bilayer PAH/PSS films (dry thickness of 38 ± 2 nm). The standard deviation of the swollen thickness in the four samples was less than 5 nm in each buffered solution (pH 3.2, 6.3, and 3.2 after pH 10).

III. Results and Discussion

A. Characterization of Polyelectrolyte Films

Consistent with previous studies,^{17,20,26,36,37} ellipsometry of "dry" films demonstrates uniform, stepwise growth of PAH/PSS coatings as seen in Figure 2.1. The thickness increase after the addition of each bilayer (with the exception of the initial bilayer, which was 2.4 ± 0.3 nm thick) was 3.8 ± 0.3 nm, which agrees with previous reports.^{17,26,36,37} PAH/PSS films made with no supporting salt also exhibit linear growth up to 20-bilayers. A 20-bilayer PAH/PSS film has a thickness of 16 ± 2 nm. The thickness of PAH/PAA films made in the presence of supporting salt increases linearly with the number of bilayers,²⁰ but growth of these films in the absence of salt yields nonlinear growth.¹² The average thickness of a 5-bilayer PAH/PAA film made with supporting electrolyte is 44 ± 2 nm, while the thickness of a 9-bilayer PAH/PAA film made without salt is 15 ± 1 nm.

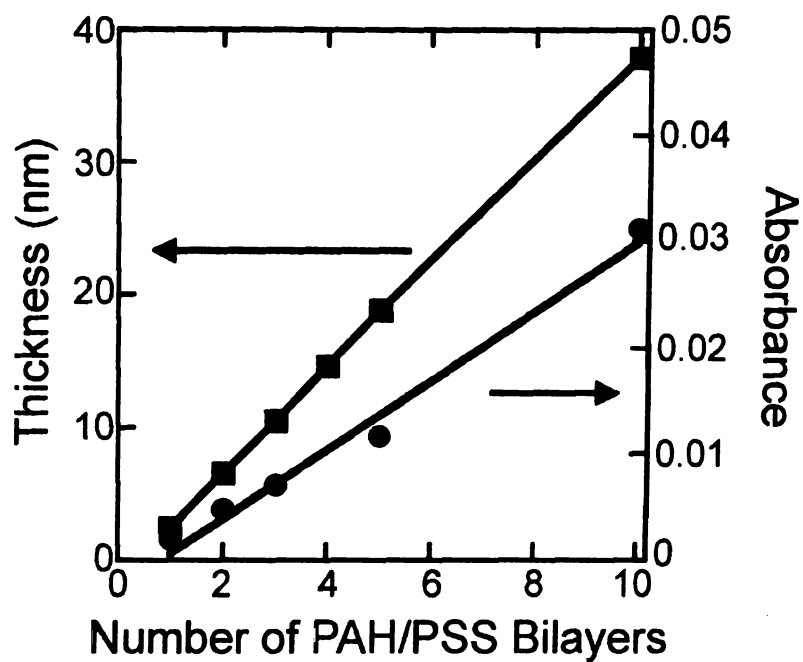


Figure 2.1: Ellipsometric thickness (squares) and FTIR-ERS absorbances at 1037 cm^{-1} (circles) for multilayered PAH/PSS films made in the presence of supporting salt. The standard deviation for the absorbance values for each bilayer is $\sim 2\%$. The standard deviations for the ellipsometric thickness values are $< 0.3\text{ nm}$.

gr

co

h

P:

de

At

bil

pe

2.2

po

B

in

bil

con

um

film

tra

and

by

FTIR external reflection spectroscopy (FTIR-ERS) also confirms the stepwise growth of PAH/PSS films. Figure 2.2 shows the FTIR-ERS spectra of PAH/PSS films containing up to 5-bilayers. The sulfonate absorbances, 1220, 1175, 1036, and 1005 cm^{-1} , dominate the spectrum of PAH/PSS films, which agrees with previous spectra of PAH/PSS/Immunoglobulin G films.¹⁹ Symmetric and anti-symmetric $-\text{NH}_3^+$ deformations are visible between 1625-1560 cm^{-1} and 1550-1505 cm^{-1} , respectively.³⁸ Absorbance values increase approximately linearly (Figure 2.1) with the number of bilayers, which supports the ellipsometric data. The protonated and deprotonated acid peaks, 1706 and 1575 cm^{-1} , respectively, dominate the spectra of PAH/PAA films (Figure 2.3) and again increases in absorbance values occur with the addition of each bilayer of polyelectrolyte.

B. Film Swelling

In situ ellipsometry allows one to investigate the swelling of polyelectrolyte films in water. Upon immersion in pH 3.2- and 6.3-buffered solutions, the thickness of a 10-bilayer PAH/PSS film increases ~40% due to absorption of water. Swelling remains constant during the ten minutes of immersion (± 1 nm) as seen in Figure 2.4A&B. After immersion in pH 3.2 and 6.3 buffers, refractive index values (450.5 nm) for the PAH/PSS film decrease by ~4% (1.60 to 1.54). This decrease is consistent with a final volume fraction of between 30 and 40% water ($n=1.33$). The percent swelling of films at pH 3.2 and 6.3 is reasonable as a previous study indicates that the volume of PAH/PSS films at 100% humidity is $\geq 40\%$ water.²⁷ Upon immersion in a pH 10-buffered solution, the film

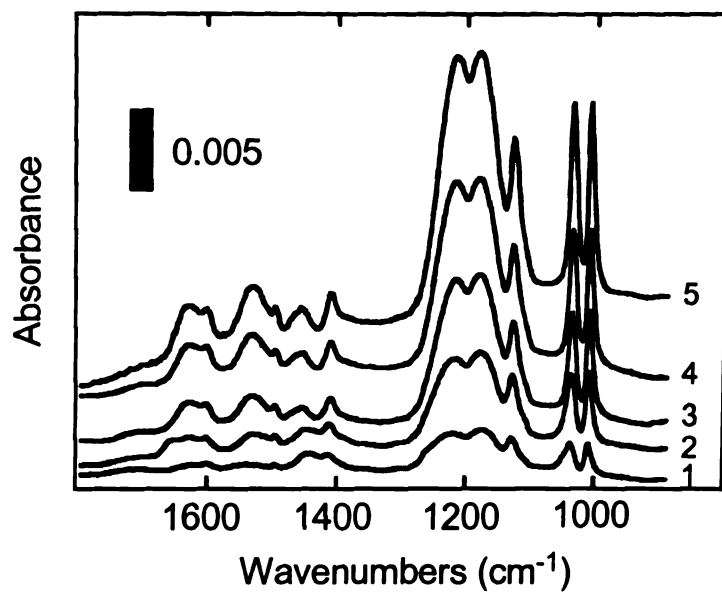


Figure 2.2: FTIR-ERS spectra of PAH/PSS films (made with supporting salt) composed of 1-5 bilayers.

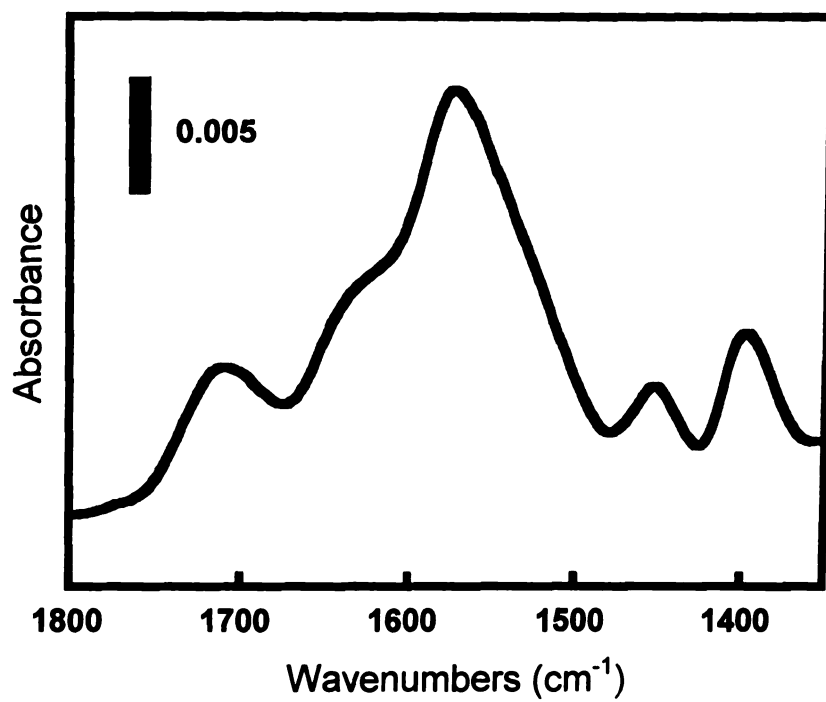


Figure 2.3: FTIR-ERS spectrum of a 9-bilayer PAH/PAA film (made with no supporting electrolyte) deposited on a gold electrode.

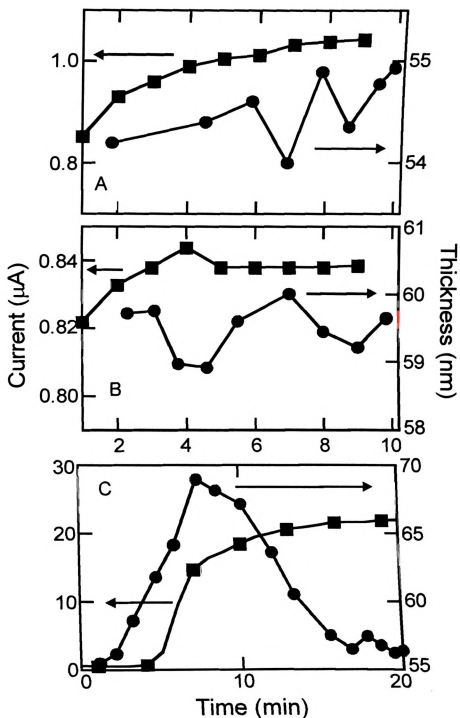


Figure 2.4: In situ ellipsometric thickness (circles) and cyclic voltammetry (5 mM $\text{Fe}(\text{CN})_6^{3-}$) peak current values (squares) as a function of immersion time for a 10-bilayer PAH/PSS film (made with supporting salt) in pH 3.2- (A), 6.3- (B), and 10-buffered solutions (C).

swells as in lower pH buffers, but continues to swell for approximately seven additional minutes (Figure 2.4C). Over the following ten minutes, the film thickness returns to approximately its original value. A subsequent immersion in a pH 3.2-buffered solution results in a reduced amount of stable swelling (20% increase from dry thickness).

The additional swelling at pH 10 is probably due to deprotonation of the amine groups of PAH. At pH 10, this deprotonation causes a charge imbalance to develop in the film. To compensate the remaining negative charges, the film must absorb Na^+ from solution³⁰ and probably some additional water. The subsequent decrease in thickness at high pH is likely due to delamination of the film and this is suggested by ex situ experiments. Immersion of a PAH/PSS film (made with supporting salt) into a pH 10-buffered solution, rinsing, and measurement of a “dry” thickness indicate that up to 30% of the film is lost due to delamination during the rinsing and drying process. Re-immersion in pH 3.2-buffered solutions and subsequent rinsing results in the same “dry” thickness as that after immersion in pH 10-buffered solutions. Although in situ and ex situ experiments show some delamination, both studies indicate that a significant portion of the film remains on the substrate after immersion in a pH 10-buffered solution. This is probably due to the high degree of overlap and intermingling of the polymer layers.^{25,27} The film instability shown by in situ ellipsometry suggests, however, that PAH/PSS films will probably not be useful for sensing or separation applications in alkaline solutions.

C.

de

pr

st

co

ve

va

pt

bu

in

pi

in

Th

el

el

fr

pe

ra

at

in

m

m

C. Investigation of Film Permeability to $\text{Fe}(\text{CN})_6^{3-/4-}$

The effectiveness of polyelectrolyte films as ion-separation membranes will depend on their ability to selectively inhibit transport of specific ions. Electrochemistry provides an initial assessment of film permeability and serves as a sensitive probe of structural changes in PAH/PSS films. Cyclic voltammetry affords qualitative comparisons of the passivating abilities of different films based on peak currents and voltammogram shape. Peak currents (i_p) in cyclic voltammograms (CVs) of $\text{Fe}(\text{CN})_6^{3-}$ vary with pH as given in Table 2.1. There is little difference between CVs in pH 3.2 and pH 6.3 solutions. However, in the case of 4- and 5-bilayer films immersed in pH 10-buffered solutions, i_p increases ~50-fold with respect to values at pH 3.2 and 6.3. The increase in peak current values at high pH may be due to an increase in the number of pinholes to the substrate (increased swelling) as well as film delamination. A second immersion in pH 3.2 buffer yields nearly the same value of i_p as in basic solution. The shape of CVs (Figure 2.5) also helps in understanding the processes occurring at the electrode-film interface. At pH 3.2 and 6.3, CVs of a 5-bilayer film-coated electrode are broad and plateau-shaped (Figure 2.5A), suggesting current originating from an array of microelectrodes (pinholes)^{39,40} or slow diffusion through the polyelectrolyte film.⁴¹ At pH 10, CVs show larger peak currents along with a quasi-reversible voltammogram ($\Delta E_p = 180 \pm 25$ mV) (Figure 2.5B). This change in CV shape at pH 10 points to a transition to semi-infinite linear diffusion.⁴⁰ At pH 3.2 after immersion in pH 10, the CVs show an even more reversible response ($\Delta E_p = 100 \pm 8$ mV). Although i_p values at pH 10 and pH 3.2 after immersion in pH 10 are similar in magnitude (Table 2.1), the decrease in peak splitting (ΔE_p) suggests variation in film

Table 2.1: Average peak currents ($\mu\text{A}/\text{cm}^2$) from cyclic voltammograms ($\text{Fe}(\text{CN})_6^{3-}$) measured at PAH/PSS coated gold electrodes in different buffered solutions

PAH/PSS Bilayers (n)	pH 3.2	pH 6.3	pH 10	pH 3.2 after pH 10
5	9 ± 1	7 ± 1	400 ± 60	400 ± 60
4	10 ± 1	9 ± 1	550 ± 40	470 ± 130
3	20 ± 1	20 ± 1	600 ± 10	660 ± 50
2	480 ± 200	440 ± 170	500 ± 70	720 ± 50
1	700 ± 40	670 ± 50	670 ± 70	830 ± 140
MPA monolayer	890 ± 30	770 ± 30	848 ± 30	890 ± 40

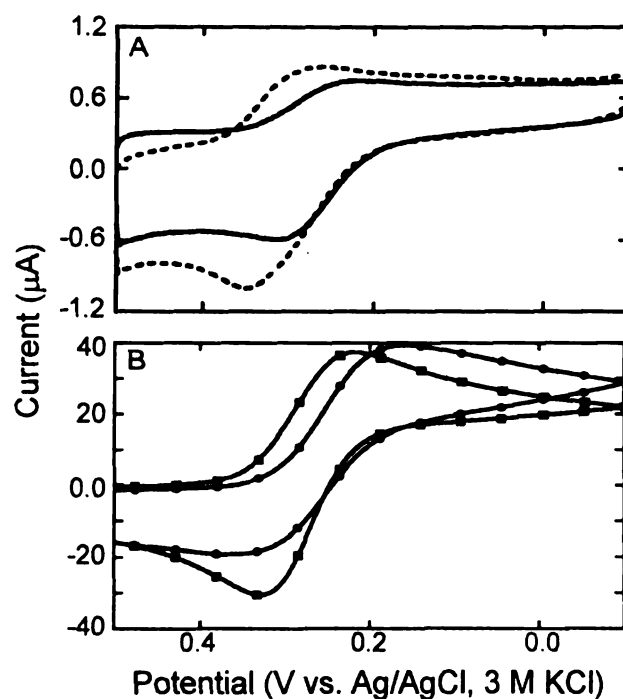


Figure 2.5: CVs ($5 \text{ mM Fe(CN)}_6^{3-}$) at a gold electrode coated with a 5-bilayer PAH/PSS film (made with supporting electrolyte). CVs were measured in solutions buffered at pH 3.2 (A:dash), pH 6.3 (A:solid line), pH 10 (B:circles), and pH 3.2 after immersion in pH 10 (B:squares).

stru

affa

volt

cun

ind

san

tho

tota

191

offi

imp

emp

inte

blo

fin

val

is f

ele

tha

by

dec

structure or charge. The comparable i_p values with the increased reversibility at pH 3.2 after immersion in pH 10 is somewhat surprising. Typically, a more reversible voltammogram indicates better access to the electrode, which should result in higher peak currents. It is possible that after a second immersion in pH 3.2 buffer there are large individual defect areas of semi-infinite diffusion leading to decreased ΔE_p values. At the same time, however, there may be fewer defects, and hence i_p values could be similar to those observed in voltammograms at pH 10. Impedance data (below) suggest that the total active area of the electrode is greater at pH 10 than at pH 3.2 after immersion in pH 10 buffer.

Impedance spectroscopy is a complementary technique to cyclic voltammetry that often allows quantitative determination of kinetic and diffusion parameters.^{42,43} Impedance methods are also attractive because of the small sinusoidal potentials that are employed, as opposed to the wide potential window used in cyclic voltammetry. To interpret impedance data, we used the Randles' circuit shown in Figure 2.6. For highly blocking films ($R_{ct} \sim 10^4 \Omega\text{-cm}^2$) we also used a modified Randles' circuit that contains film capacitance and resistance elements.⁴⁴ Both models yield similar (within 20%) R_{ct} values for the highly resistive systems. The circuit element of most interest to this work is R_{ct} because it often relates directly to the accessibility of the underlying gold electrode.^{42,45} Figure 2.7 illustrates the fits obtained with a Randles' equivalent circuit to the experimental impedance data in each of the buffered solutions

Impedance data for a 5-bilayer PAH/PSS film (Table 2.2) confirm the trends shown by cyclic voltammetry. Increases in peak current values should be accompanied by decreases in charge transfer resistance values. The difference between R_{ct} values for a

Fig
res
ele

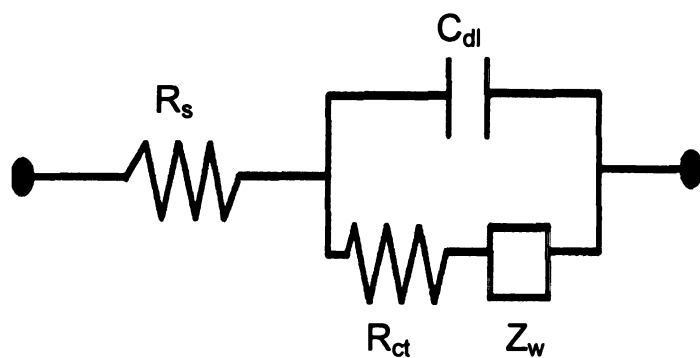


Figure 2.6: Randles' circuit used to fit impedance data where R_{ct} = charge transfer resistance, R_s = solution resistance, C_{dl} = double-layer capacitance, and Z_w = Warburg element.

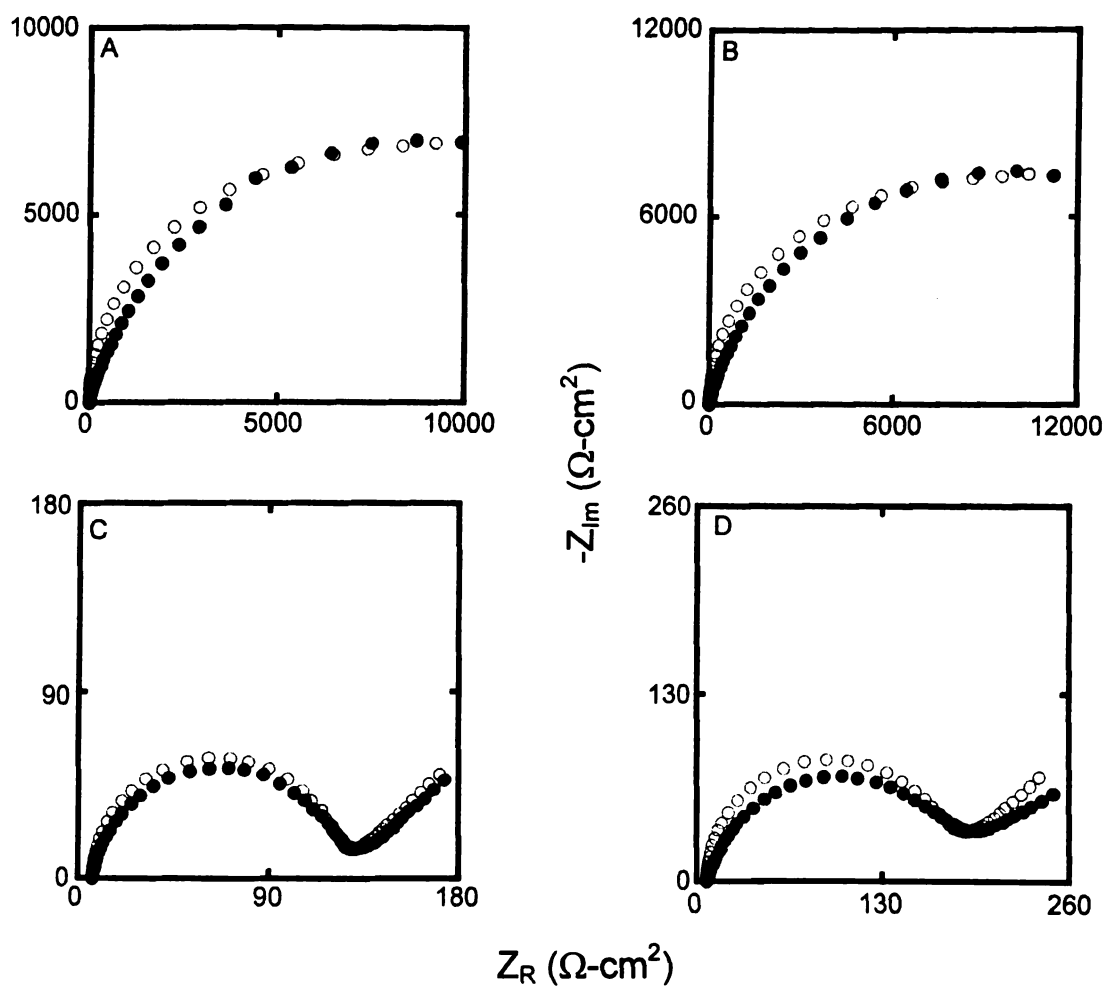


Figure 2.7: Impedance data ($\text{Fe}(\text{CN})_6^{3-/4-}$) for a gold electrode coated with a 5-bilayer PAH/PSS film (made with supporting electrolyte). Plots were obtained in solutions buffered at pH 3.2 (A), 6.3 (B), 10 (C), and 3.2 after immersion in pH 10 (D). Solid circles represent experimental data and open circles show fits obtained with a Randles' equivalent circuit.

Table 2.
coated g

Table 2.2: Average R_{ct} values ($\Omega\text{-cm}^2$) from impedance plots ($\text{Fe(CN)}_6^{3-/4-}$) of PAH/PSS coated gold electrodes in different buffered solutions.

PAH/PSS Bilayers (n)	pH 3.2	pH 6.3	pH 10	pH 3.2 After pH 10
5	12000 ± 3000	13000 ± 2000	100 ± 20	170 ± 70
4	10000 ± 1000	9000 ± 1000	50 ± 10	80 ± 50
3	5000 ± 350	4000 ± 300	40 ± 2	70 ± 30
2	10 ± 3	20 ± 10	20 ± 10	10 ± 4
1	2 ± 1	7 ± 2	6 ± 3	2 ± 1

5-bilayer film ($\text{Fe}(\text{CN})_6^{3-/4-}$) measured in pH 3.2- and 6.3-buffered solutions is less than 10%. Cyclic voltammetry indicates a dramatic increase in film permeability at pH 10 and pH 3.2 after immersion in pH 10, which is supported by the impedance data. For electrodes coated with 5-bilayers, R_{ct} decreases by 120-fold in pH 10 solutions and by 70-fold in pH 3.2 solutions after immersion in pH 10 buffered solutions (both with respect to initial measurements at pH 3.2). Lower R_{ct} values at pH 10 than at pH 3.2 after immersion in pH 10 suggest a larger active electrode area at pH 10.

Impedance plots for 5-bilayer films in pH 3.2- and pH 6.3-buffered solutions (Figure 2.7A&B) show only a quarter circle with no visible Warburg line, indicating complete kinetic control of the electron transfer process.⁴² The complex impedance plots for 5-bilayer films in pH 10 and pH 3.2 after immersion in pH 10 (Figure 2.7C&D) are characterized by the appearance of small, nearly complete semicircles in the high frequency domain and a straight line at low frequencies. The response at low frequencies is indicative of facile kinetics⁴³ and greater access to the underlying electrode.

D. Investigation of Film Permeability to $\text{Ru}(\text{NH}_3)_6^{2+/3+}$

As with $\text{Fe}(\text{CN})_6^{3-}$, the permeability of PAH/PSS films to $\text{Ru}(\text{NH}_3)_6^{3+}$ increases in alkaline solutions (Table 2.3). However, the trend in the shape of CVs at pH 10 and pH 3.2 after immersion in pH 10 is different for $\text{Ru}(\text{NH}_3)_6^{3+}$ than for $\text{Fe}(\text{CN})_6^{3-}$. For $\text{Ru}(\text{NH}_3)_6^{3+}$ the voltammogram is more reversible at pH 10 as seen in Figure 2.8A. The difference between the two couples is likely due to their charge. At pH 3.2, $\text{Ru}(\text{NH}_3)_6^{3+}$ may experience some repulsion from ammonium groups in the film. Impedance data acquired with $\text{Ru}(\text{NH}_3)_6^{2+/3+}$ (Table 2.4) are consistent with the trends in the cyclic

Table 2.3: Average peak currents ($\mu\text{A}/\text{cm}^2$) from cyclic voltammograms ($\text{Ru}(\text{NH}_3)_6^{3+}$) at PAH/PSS coated gold electrodes in different buffered solutions.

PAH/PSS Bilayers (n)	pH 3.2	pH 6.3	pH 10	pH 3.2 after pH 10
5	170 ± 100	80 ± 40	730 ± 70	470 ± 150
4	240 ± 30	180 ± 20	790 ± 20	640 ± 50
3	280 ± 40	180 ± 30	700 ± 40	600 ± 100
2	640 ± 40	600 ± 90	590 ± 50	580 ± 160
1	700 ± 20	720 ± 40	650 ± 40	730 ± 160
MPA monolayer	880 ± 20	860 ± 20	790 ± 40	800 ± 40

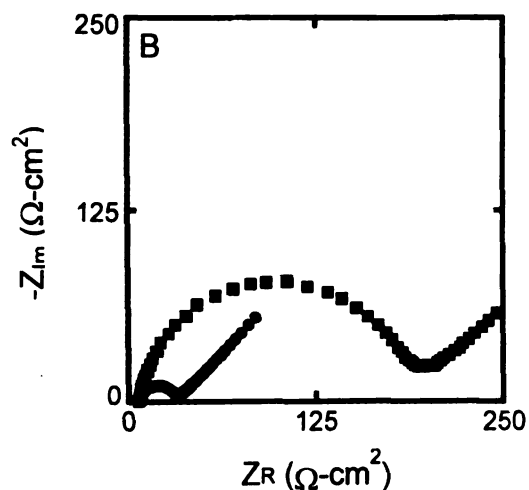
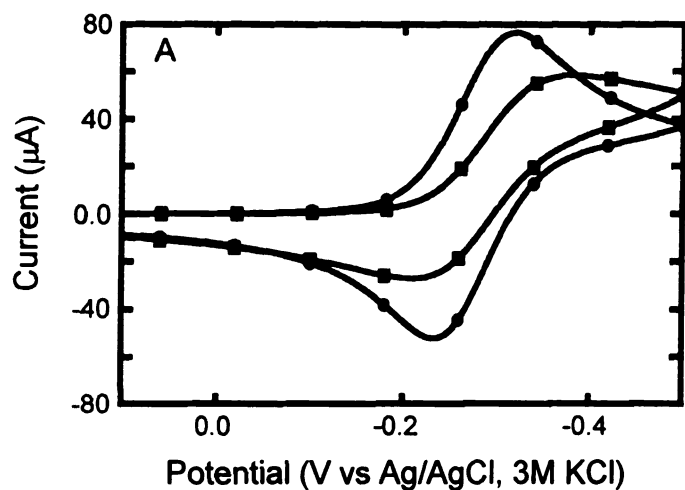


Figure 2.8: (A) CVs ($5 \text{ mM Ru(NH}_3)_6^{3+}$) of a gold electrode coated with a 5-bilayer PAH/PSS film (made with supporting electrolyte). CVs shown were measured in solutions buffered at pH 10 (circles) and pH 3.2 after immersion in pH 10 (squares). (B) Impedance data ($5 \text{ mM Ru(NH}_3)_6^{2+/3+}$) for a gold electrode coated with a 5-bilayer PAH/PSS film (made with supporting electrolyte). Plots were obtained after immersion in pH 10-buffered solutions (circles) and after reimmersion in pH 3.2-buffered solutions (squares).

Table 2.4: Average R_{ct} values ($\Omega\text{-cm}^2$) from impedance plots ($\text{Ru}(\text{NH}_3)_6^{2+/3+}$) of PAH/PSS coated gold electrodes in different buffered solutions.

PAH/PSS Bilayers	pH 3.2	pH 6.3	pH 10	pH 3.2 after pH 10
5	740 ± 400	800 ± 400	20 ± 10	170 ± 80
4	300 ± 30	360 ± 20	10 ± 1	80 ± 50
3	180 ± 100	220 ± 40	10 ± 2	120 ± 30
2	9 ± 6	20 ± 25	5 ± 2	50 ± 10
1		No discernible R_{ct}		

vol

Th

kin

sol

val

Fe

ele

E.

lik

ho

tin

6.

a t

DC

m

el

st

st

el

V

voltammetry data, which indicate the highest permeability (lowest R_{ct} values) at pH 10. The domination of the Warburg line at pH 10 (Figure 2.8B), which is indicative of facile kinetics (mass transfer control), is also consistent with higher permeabilities in basic solutions. The increase in R_{ct} at pH 3.2 after immersion in pH 10 compared to R_{ct} values at pH 10 shows that a portion of the film remains on the electrode surface. Both $Fe(CN)_6^{3-/4-}$ and $Ru(NH_3)_6^{2+/3+}$ impedance data suggest a decrease in the active area of the electrode after reimmersion in acidic solutions.

E. Permeability as a Function of Time

Film swelling observed with in situ ellipsometry indicates that permeability will likely depend on immersion time in alkaline solutions. Thus, we decided to investigate how cyclic voltammetry varies with time. Figure 2.4 shows how peak currents vary with time when an electrode coated with a 10-bilayer PAH/PSS film is immersed in pH 3.2-, 6.3-, and 10-buffered solutions. Immersions in pH 3.2- and 6.3-buffered solutions, show a minimal increase in i_p with time, as seen in Figure 2.4A&B and over this period there is no change from the plateau-shaped voltammogram.

Immersion in a pH 10-buffered solution do not show steady i_p values. A 20-minute immersion in pH 10-buffered solution results in a 30-fold increase in i_p for an electrode coated with a 10-bilayer PAH/PSS film. For the first four minutes, the CVs are stable with only an ~20% increase in i_p . Subsequently, i_p rapidly increases and begins to stabilize after 10 minutes. Swelling of PAH/PSS films, as determined by in situ ellipsometry, occurs on the same time scale as increases in i_p as seen in Figure 2.4C. Voltammograms for a 10 bilayer-coated electrode in pH 10-buffered solution change

fro

(pl

ch

inc

to

F.

re:

w)

vo

th

qu

pl

el

va

hc

(T

o

b

A

o

from those characteristic of a microelectrode system or slow diffusion through the film (plateau peaks) to those of a quasireversible system during a 20-minute immersion. The changes in voltammogram shape (plateau to quasireversible) and the increases in i_p indicate that the film is undergoing pH-induced structural changes creating greater access to the underlying electrode.

F. Permeability as a Function of the Number of Bilayers

Increasing the number of bilayers in the film should increase charge transfer resistance and decrease peak current values because pathways to the electrode surface will become fewer and longer. This is indeed the trend we generally observe using cyclic voltammetry. The most drastic changes in electrode blocking occur upon introduction of the third bilayer as seen in Figure 2.9. For one- and two-bilayer films, CVs contain a quasireversible response while CVs of electrodes coated with a three-bilayer film show plateau-shaped voltammograms at low pH values. Peak currents (Fe(CN)_6^{3-}) at electrodes covered with a one- or two-bilayer film are 85% and 55%, respectively, of i_p values for a MPA-modified gold electrode at low pH. The presence of a third bilayer, however, results in an ~40-fold reduction in peak current at low and moderate pH values (Table 1).

Impedance spectroscopy also shows the dependence of permeability on the number of polyelectrolyte bilayers on the surface. For electrodes coated with one- and two-bilayer films, the Warburg diffusion element dominates the complex impedance plots. Addition of a third bilayer results in complete kinetic control as seen by the appearance of only a semicircle in the complex impedance plot at low pH values. There is a >200

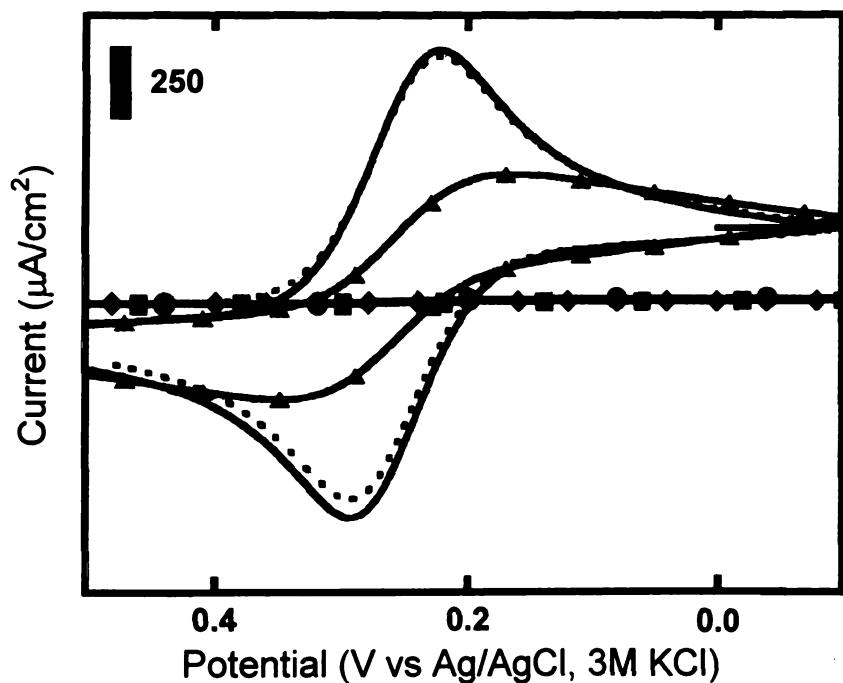


Figure 2.9: CVs (5 mM $\text{Fe}(\text{CN})_6^{3-}$) of a gold electrode coated with a layer of MPA (dashed line) or with a 1- (solid line), 2- (triangles), 3- (circles), 4- (squares), or 5-bilayer (diamonds) PSS/PAH film. CVs were measured in solutions buffered at pH 6.3 and films were made from solutions containing supporting electrolyte.

fold increase in charge transfer resistance between a two and three bilayer film as opposed to the small increase in R_{ct} values between one and two bilayer films (Table 2.2: low and moderate pH). Electrochemical data with $\text{Ru}(\text{NH}_3)_6^{2+/3+}$ (Table 2.3&2.4) also show similar changes in permeability with an increasing number of polyelectrolyte layers.

The nonlinear decrease in permeability with the number of bilayers suggests a different structure in the first two bilayers than in the rest of the film. Previous studies indicate that the first few polyelectrolyte bilayers have a different thickness than later bilayers.^{23,28} With each subsequent bilayer, the charge is multiplied until stepwise growth is achieved. This agrees with the electrochemical data, which suggest that there is greater access to the underlying gold electrode within the first two bilayers. These data show that separations applications will likely require several polyelectrolyte bilayers to be effective.

F. Effect of Supporting Electrolyte on the Permeability of Polyelectrolyte Films

The addition of supporting salt to deposition solutions changes the structure and thickness of polyelectrolyte films by screening the ionic charges and allowing for the formation of loops and trains.^{32,46} Polyelectrolytes in solutions without supporting salt assume a linear structure, as there is a large amount of charge-charge repulsion between monomer units.^{46,47} For separation and anti-corrosion applications it is important to understand how bilayer structure affects transport properties of the film. Voltammetric and impedance measurements ($\text{Fe}(\text{CN})_6^{3-/4-}$) indicate that PAH/PSS films made from solutions containing no supporting salt are much more permeable than films made with

supporting salt as seen in Figure 2.10. A 20-bilayer PAH/PSS film prepared without salt (thickness = 16 nm) is much more permeable than a four-bilayer PAH/PSS film prepared with salt (thickness = 15 nm). An electrode coated with a 20-bilayer PAH/PSS film shows an 80-fold higher i_p value and a 1500-fold lower R_{ct} value than an electrode coated with a four-bilayer film made with salt (pH 6.3). Voltammetric and impedance measurements do not indicate that solution pH changes the permeability of 20-bilayer PAH/PSS films. However, small changes in i_p are difficult to detect when values are nearly as high as those of a bare gold electrode. The thin, flat PAH/PSS bilayers prepared without salt offer a vastly more open film structure than films containing a large number of loops and trains.

G. Comparing Permeabilities of PAH/PAA and PAH/PSS Multilayer Films

PAH/PAA films made with no supporting electrolyte are similar in permeability to PAH/PSS films prepared without salt. Peak current values ($\text{Fe}(\text{CN})_6^{3-}$ in pH 6.3-buffered solutions) for electrodes coated with PAH/PAA films (nine-bilayers; ~15 nm) are $470 \pm 110 \mu\text{A}/\text{cm}^2$ compared to $710 \pm 70 \mu\text{A}/\text{cm}^2$ for an electrode coated with a 20-bilayer PAH/PSS film (thickness = 16 nm). CVs of a PAH/PAA-coated electrode show a nearly reversible response ($\Delta E_p \sim 80\text{mV}$) similar to that observed for PAH/PSS films made with no supporting salt (Figure 2.10). The somewhat lower i_p value for PAH/PAA films may be due to the larger bilayer thickness¹² and more intermingling of the polymer layers.

Interestingly, fabrication of PAH/PAA films in the presence of supporting salt does not yield the same decrease in permeability seen with PAH/PSS films. The permeability of PAH/PAA films increases with the formation of loops and trains in the polymer

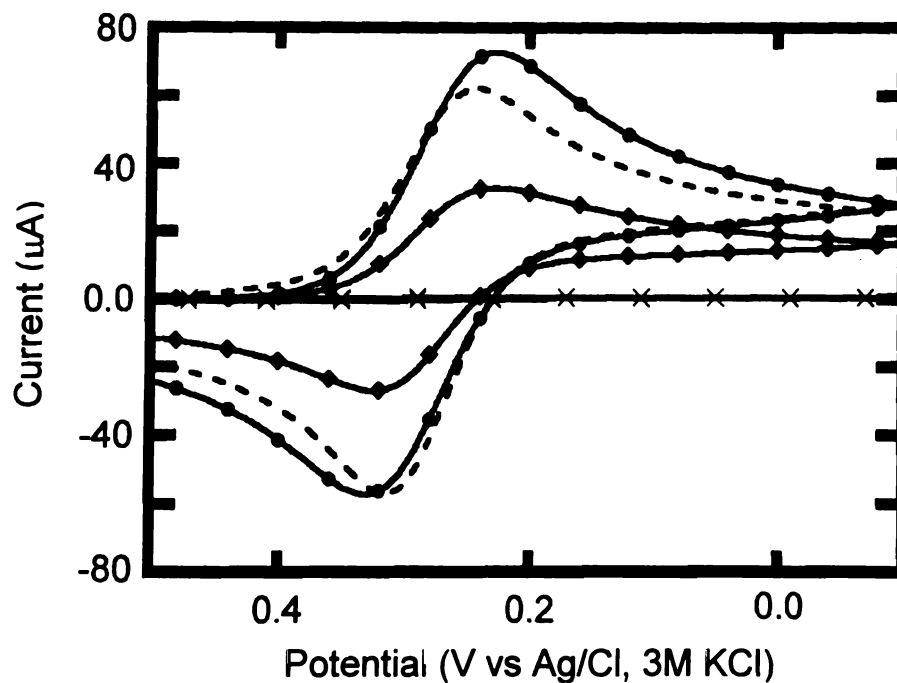


Figure 2.10: CVs (5 mM $\text{Fe}(\text{CN})_6^{3-}$, pH 6.3) of gold electrodes coated with a 20-bilayer PAH/PSS film prepared with no supporting electrolyte (circles, thickness of 16 nm), a 5-bilayer PAH/PAA film prepared with supporting electrolyte (dashes, thickness of 44 nm), a 9-bilayer PAH/PAA prepared with no supporting electrolyte (diamonds, thickness of 15 nm), or a 4-bilayer PAH/PSS film prepared with supporting electrolyte (solid line with x markers, thickness of 15 nm).

coating. This may be due to the fact that PAA does not contain bulky pendant groups. An electrode coated with a 5-bilayer PAH/PAA film made with supporting salt (thickness of 44 nm) has an average i_p value of $690 \pm 80 \mu\text{A}/\text{cm}^2$ at pH 6.3. This is a 50% increase from the i_p value (pH 6.3) for a nine-bilayer PAH/PAA film made with no supporting electrolyte (thickness of 15 nm). Impedance measurements of PAH/PAA films (made with or without the addition of supporting salt) and PAH/PSS films (made without supporting salt) also indicate high permeabilities as the impedance plots only contain the Warburg element. Apparently, the addition of supporting salt to PAH/PAA films makes for a more open and loose structure as seen by the increase in i_p values.

IV. Conclusions

The permeability of polyelectrolyte films varies widely with the number of bilayers in the film, ambient pH, and deposition conditions. Permeability of PAH/PSS films made with supporting salt decreases nonlinearly with the number of bilayers because the structure of the initial layers is different from that of outer layers. Film permeability is relatively independent of solution pH at low and moderate values but increases drastically in basic solutions. In situ ellipsometric studies indicate that PAH/PSS films swell in water by ~40% at low and moderate pH values. At high pH, the film swells further and then begins to delaminate. This additional swelling accounts for higher permeabilities in basic solution. Addition of supporting salt during film deposition dramatically alters the structure of PAH/PSS films. The formation of loops and trains in PAH/PSS films due to the presence of supporting electrolyte probably yields the large decrease in film permeability.

The permeability of PAH/PAA films prepared in the presence of supporting salt is much greater than that of PAH/PSS films. Apparently, the formation of loops and trains in 5-bilayer PAH/PAA films does not have the same effect as in PAH/PSS films. This observation is likely due to differences in size and hydrophobicity of the pendant groups of PAA and PSS. Chapter 3 examines the ion-separation properties of polyelectrolyte films deposited on permeable substrates.

V. References

- 1) Decher, G. *Science* **1997**, 277, 1232-1237.
- 2) Lowy, D. A.; Finklea, H. O. *Electrochimica Acta* **1997**, 42, 1325-1335.
- 3) Montrel, M. M.; Sukhorukov, G. B.; Petrov, A. I.; Shabarchina, L. I.; Sukhorukov, B. I. *Sensors and Actuators B* **1997**, 42, 225-231.
- 4) Yang, X.; Johnson, S.; Shi, J.; Holesinger, T.; Swanson, B. *Sensors and Actuators B* **1997**, 45, 87-92.
- 5) Caruso, F.; Niikura, K.; Furlong, D. N.; Okahata, Y. *Langmuir* **1997**, 13, 3427-3433.
- 6) Mika, A. M.; Childs, R. F.; Dickson, J. M.; McCarry, B. E.; Gagnon, D. R. *J. Membr. Sci.* **1997**, 81-92.
- 7) Nam, S. Y.; Lee, Y. M. *J. Membr. Sci.* **1997**, 161-171.
- 8) Leväsalmi, J.-M.; McCarthy, T. J. *Macromolecules* **1997**, 30, 1752-1757.
- 9) Ackern, F. v.; Krasemann, L.; Tieke, B. *Thin Solid Films* **1998**, 327-329, 762-766.
- 10) Stroeve, P.; Vasquez, V.; Coelho, M. A. N.; Rabolt, J. F. *Thin Solid Films* **1996**, 708-712.
- 11) Krasemann, L.; Tieke, B. *Langmuir* **2000**, 16, 287-290.
- 12) Harris, J. J.; DeRose, P. M.; Bruening, M. L. *J. Am. Chem. Soc.* **1999**, 121, 1978-1979.
- 13) Kotov, N. A.; Dékány, I.; Fendler, J. H. *J. Phys. Chem.* **1995**, 99, 13065-13069.
- 14) Fou, A. C.; Rubner, M. F. *Macromolecules* **1995**, 28, 7115-7120.
- 15) Schlenoff, J. B.; Laurent, D.; Ly, H.; Stepp, J. *Adv. Mater.* **1998**, 10, 347-349.
- 16) Wu, A.; Yoo, D.; Lee, J.-K.; Rubner, M. F. *J. Am. Chem. Soc.* **1999**, 121, 4883-4891.
- 17) Caruso, F.; Niikura, K.; Furlong, D. N.; Okahata, Y. *Langmuir* **1997**, 13, 3422-3426.
- 18) Ferreira, M.; Rubner, M. F. *Macromolecules* **1995**, 28, 7107-7114.

- 19) Caruso, F.; Furlong, D. N.; Ariga, K.; Ichinose, I.; Kunitake, T. *Langmuir* **1998**, *14*, 4559-4565.
- 20) Yoo, D.; Shiratori, S. S.; Rubner, M. F. *Macromolecules* **1998**, *31*, 4309-4318.
- 21) Lvov, Y.; Ariga, K.; Ichinose, I.; Kunitake, T. *J. Am. Chem. Soc.* **1995**, *117*, 6117-6123.
- 22) Decher, G.; Hong, J.-D.; Schmitt, J. *Thin Solid Films* **1992**, 831-835.
- 23) Decher, G.; Lvov, Y.; Schmitt, J. *Thin Solid Films* **1994**, *244*, 772-777.
- 24) Lvov, Y.; Decher, G.; Möhwald, H. *Langmuir* **1993**, *9*, 481-486.
- 25) Schmitt, J.; Grunewald, T.; Decher, G.; Pershan, P. S.; Kjaer, K.; Losche, M. *Macromolecules* **1993**, *26*, 7058-7063.
- 26) Tronin, A.; Lvov, Y.; Nicolini, C. *Colloid Polym. Sci.* **1994**, *272*, 1317-1321.
- 27) Lösche, M.; Schmitt, J.; Decher, G.; Bouwman, W. G.; Kjaer, K. *Macromolecules* **1998**, *31*, 8893-8906.
- 28) Hoogeveen, N. G.; Cohen Stuart, M. A.; Fleer, G. J. *Langmuir* **1996**, *12*, 3675-3681.
- 29) Schlenoff, J. B.; Li, M. *Ber. Bunsenges. Phys. Chem* **1996**, *100*, 943-947.
- 30) Schlenoff, J. B.; Ly, H.; Li, M. *J. Am. Chem. Soc.* **1998**, *120*, 7626-7634.
- 31) Xu, H.; Schlenoff, J. B. *Langmuir* **1994**, *10*, 241-245.
- 32) Shubin, V.; Linse, P. *J. Phys. Chem.* **1995**, *99*, 1285-1291.
- 33) Lvov, Y.; Ariga, K.; Onda, M.; Ichinose, I.; Kunitake, T. *Colloid Surf. A* **1999**, *146*, 337-346.
- 34) Klitzing, R. v.; Möhwald, H. *Thin Solid Films* **1996**, 352-356.
- 35) Klitzing, R. v.; Möhwald, H. *Macromolecules* **1996**, *29*, 6901-6906.
- 36) Lvov, Y.; Decher, G.; Haas, H.; Möhwald, H.; Kalachev, A. *Physica B* **1994**, *198*, 89-91.
- 37) Lvov, Y.; Decher, G.; Sukhorukov, G. *Macromolecules* **1993**, *26*, 5396-5399.

- 38) Lin-Vien, D.; Colthup, N. B.; Fateley, W. G.; Grasselli, J. G. *The Handbook of Infrared and Raman Characteristic Frequencies of Organic Molecules*; Academic Press: New York, 1991.
- 39) Menon, V. P.; Martin, C. R. *Anal. Chem.* **1995**, *67*, 1920-1928.
- 40) Chailapakul, O.; Crooks, R. M. *Langmuir* **1995**, *11*, 1329-1340.
- 41) Savéant, J.-M. *J. Electroanal. Chem.* **1991**, *302*, 91-101.
- 42) Sabatani, E.; Rubinstein, I. *J. Phys. Chem.* **1987**, *91*, 6663-6669.
- 43) Bard, A. J.; Faulkner, L. R. *Electrochemical Methods: Fundamentals and Applications*; John Wiley & Sons: New York, 1980.
- 44) Zhao, M.; Bruening, M. L.; Zhou, Y. F.; Bergbreiter, D. E.; Crooks, R. M. *Isr. J. Chem.* **1997**, *37*, 277-286.
- 45) Sabatani, E.; Cohen-Boulakia, J.; Bruening, M. L.; Rubinstein, I. *Langmuir* **1993**, *9*.
- 46) Steeg, H. G. M. v. d.; Stuart, M. A. C.; Keizer, A. d.; Bijsterbosch, B. H. *Langmuir* **1992**, *8*, 2538-2546.
- 47) Dobrynin, A. V.; Rubinstein, M. *Macromolecules* **1999**, *32*, 915-922.

S

L

P

st

d

P

d

a

h

f

f

a

n

h

a

d

s

CHAPTER 3

Synthesis of Passivating, Nylon-Like Coatings through Cross-linking of Ultrathin Polyelectrolyte Films

I. Introduction

Although deposition of PAH/PSS films provides a convenient means for passivating gold electrodes, these films are still too permeable to be used for practical substrate protection. One reason for the permeability of PAH/PSS films is the high degree of swelling observed in these films as seen in Chapter 2. Another drawback of the PAH/PSS system is its instability in alkaline solutions, which results from the deprotonation of amine groups of PAH. One possible means for improving the stability and passivation characteristics of polyelectrolyte films is to replace the ionic interactions holding the film together with stronger covalent linkages.

This chapter describes the heat-induced formation of covalent cross-links from the formation of amide bonds between the carboxylate and ammonium groups of PAH/PAA films.¹ Unlike many layered polyelectrolyte films, these cross-linked, nylon-like films are stable over a wide pH range and highly impermeable. This stabilization strategy resembles that used by other groups when forming layered polymer films with covalent linkages.²⁻⁴ However, post-deposition cross-linking of polyelectrolytes preserves the advantages inherent in the APD process (e.g., no need for organic solvents and a convenient deposition procedure).

II. Experimental

To synthesize PAH/PAA films on gold, we first form a monolayer of mercaptopropionic acid (MPA) by immersing a gold-coated silicon wafer (Si(100) wafers coated with 20 nm Ti and 200 nm of Au by electron beam evaporation) in 1.5 mM MPA in ethanol for 30 minutes. (Use of MPA, rather than a longer molecule such as mercaptoundecanoic acid, avoids possible blocking of the electrode by the monolayer.) Upon deprotonation, the monolayer provides a negatively charged surface. Immersion of the MPA-modified gold slide in a PAH solution (0.02 M with respect to the repeating unit, pH adjusted to 5.1 with NaOH) for 5 minutes yields a layer of positively charged polymer on the substrate. Subsequent immersion in a PAA solution (0.01 M with respect to the repeating unit, pH adjusted to between 5.6 and 5.7 with NaOH) for 5 minutes results in deposition of the first negatively charged layer. Supporting electrolyte was not used in the deposition of these ultrathin PAH/PAA films. Repetition of this procedure allows synthesis of films with a large number of polyelectrolyte layers. We rinsed samples with Milli-Q water (18 M Ω -cm) for one minute after the deposition of each layer, and we dried with N₂ only after deposition of the desired number of layers.

Procedures for the electrochemical and ellipsometric characterizations of cross-linked PAH/PAA were the same as described in Chapter 1 for PAH/PSS films. The peak current values from the cyclic voltammograms was determined as the current value at the standard reduction potential of Fe(CN)₆³⁻ (~260 mV). Baselines were sometimes difficult to draw for CV's with films heated at 215 °C due to the low faradaic current. XPS data was collected on a PHI 540 Small Spot X-ray Photoelectron Spectrometer by Dr. Per Askeland. The N_{1s} region of a 9-bilayer PAH/PAA film before and after heating for 2 hours at 215 °C was used to determine presence of amide cross-links. Binding energy is

referenced to the C_{1s} peak for hydrocarbons (284.6 eV). XPS (survey spectra) was unable to detect the inclusion of either Na⁺ or Cl⁻ ions into the polyelectrolyte film.

III. Results and Discussion

The first step in the formation of cross-linked layered polyelectrolytes is the desposition of PAH/PAA films. Optical ellipsometry indicates nonlinear bilayer growth for PAH/PAA films deposited in the absence of supporting electrolyte. The thickness increase for the first 1-5 bilayers ranges from 4 to 17 nm/bilayer, while for bilayers 6-9 the increase is 5.5 ± 1.1 nm/bilayer. The absence of supporting electrolyte contributes to the nonlinear thickness increases and the low individual layer thicknesses. The change in bilayer thickness is consistent with previous studies,^{5,6} which indicate that a precursor film is needed prior to regular film deposition.

After deposition of PAH/PAA films, cross-linking can be effected simply by heating the sample under N₂ as shown in Figure 3.1. FTIR-ERS spectra of 9-bilayer PAH/PAA films verify that cross-linking between ammonium groups of PAH and carboxylate groups of PAA occurs by formation of an amide bond (Figure 3.2). Before heating (Figure 3.2 A), the most notable peaks are due to the -COOH carbonyl and -COO⁻ asymmetric and symmetric stretches (1709, 1572, and 1399 cm⁻¹, respectively).^{7,8} Both carboxylate groups and a small fraction of protonated acid are present because the deposition was performed at pH 5.6. After heating the slide at 130 °C, the carboxylate peaks decrease, and amide peaks appear at ~1540 and 1670 cm⁻¹ as seen in Figure 3.2 B. Some protonated acid remains, but its absorbance peak shifts to higher wavenumbers

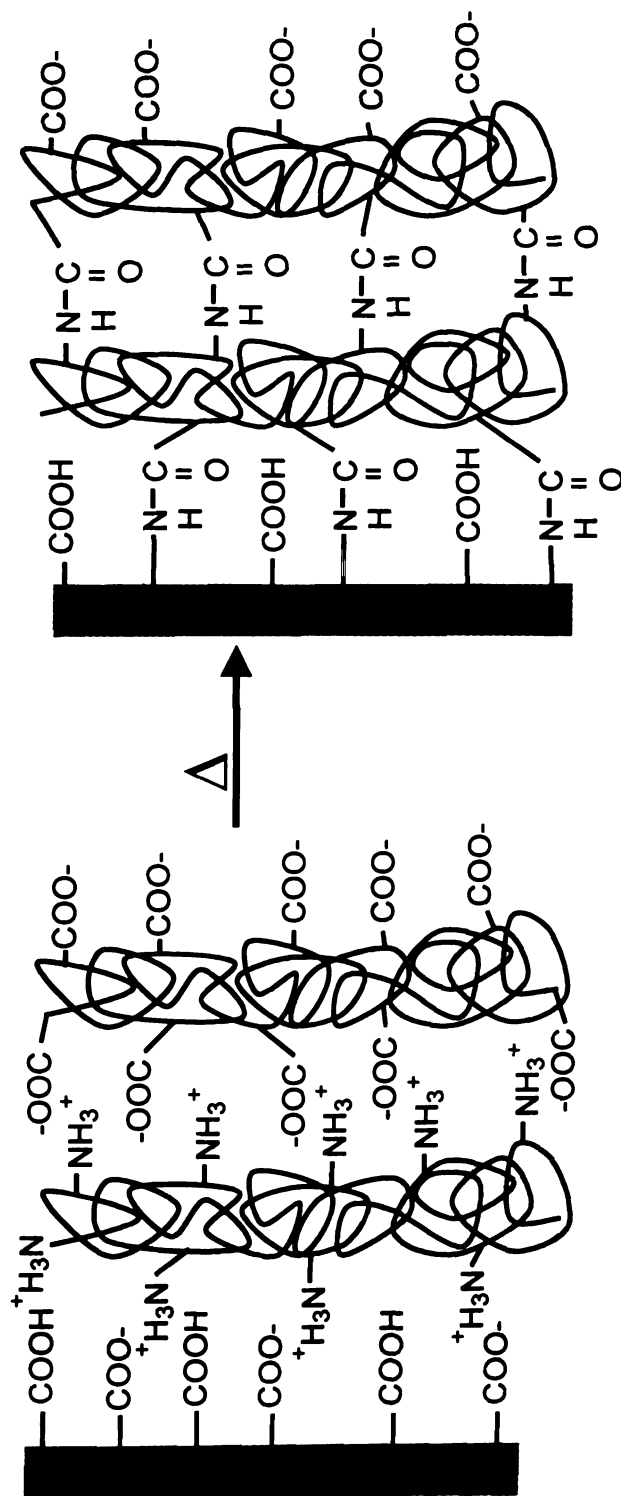


Figure 3.1: Schematic representation of cross-linking between PAA and PAH chains. The actual structure of these films is likely highly intermingled not discrete layers as shown in this representation.

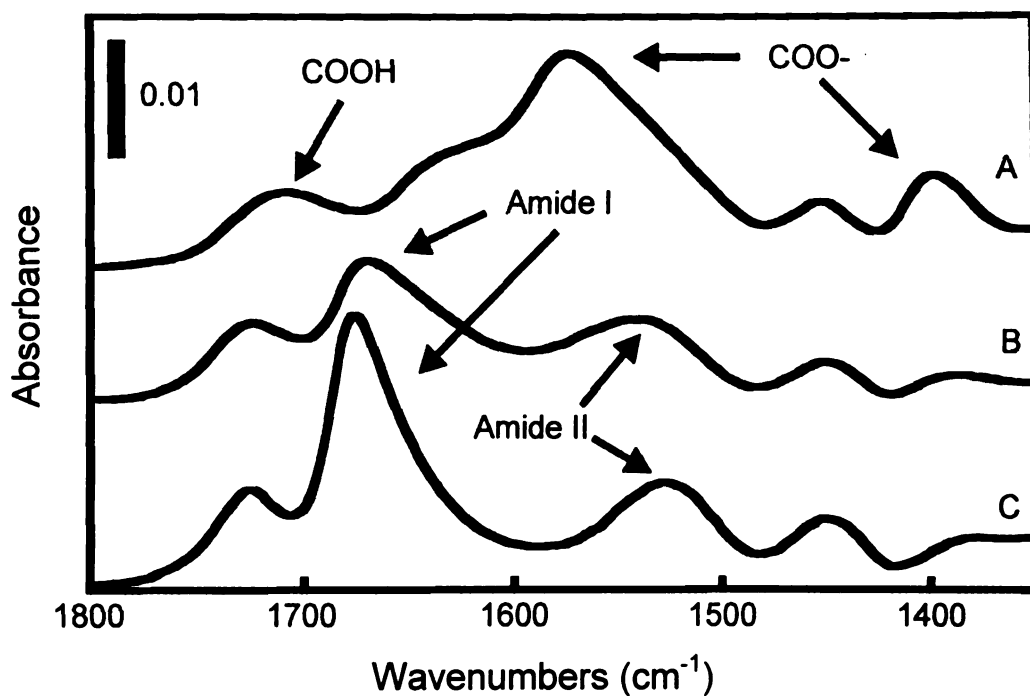


Figure 3.2: FTIR-ERS spectra of 9-bilayer PAH/PAA films before heating (A), after heating at 130 °C (B), or after heating at 215 °C (C).

indicating a change in hydrogen bonding or chemical environment. Similar spectral changes occur when a PAH/PAA film is heated at 215 °C (spectrum C), but the amide to acid peak-height ratio is larger suggesting more extensive cross-linking. Heating individual solvent-cast PAH and PAA films at 130 °C does not produce the amide peaks seen in Figure 3.2.

XPS also demonstrates the formation of amide bonds (N_{1s} spectrum) in heated PAH/PAA films. Figure 3.3A exhibits two peaks that we attribute to amino (398.8 eV) and ammonium (400.8 eV) nitrogens in PAH/PAA films⁹. After heating (215 °C for 2 hours), the XPS spectrum (Figure 3.3B) shows a single peak at 399.4 eV, which we assign to an amide nitrogen.⁹ The peak in Figure 3.3B probably also contains a small contribution from residual ammonium and amino nitrogens. XPS can also provide insight into whether counterions are included in the film structure. Consistent with previous studies,^{10,11} XPS (survey spectra) was unable to detect the inclusion of either Na^+ or Cl^- ions in the polyelectrolyte film.

Cyclic voltammetry demonstrates the dramatic decrease in film permeability that occurs upon cross-linking. Figure 3.4 shows cyclic voltammograms at a 9-bilayer PAH/PAA film-coated gold electrode before and after heating at 130 or 215 °C for 2 hours. Cross-linking at 130 °C reduces the peak current to about 1% of its initial value (Figure 3.4B). Heating at 215 °C has an even more dramatic effect on permeability. The voltammogram for this system shows an additional ~85% decrease in peak current from that of a film heated at 130 °C (Figure 3.4C). The decreased permeability shown by PAH/PAA films heated at 215 °C is probably due to the higher degree of cross-linking

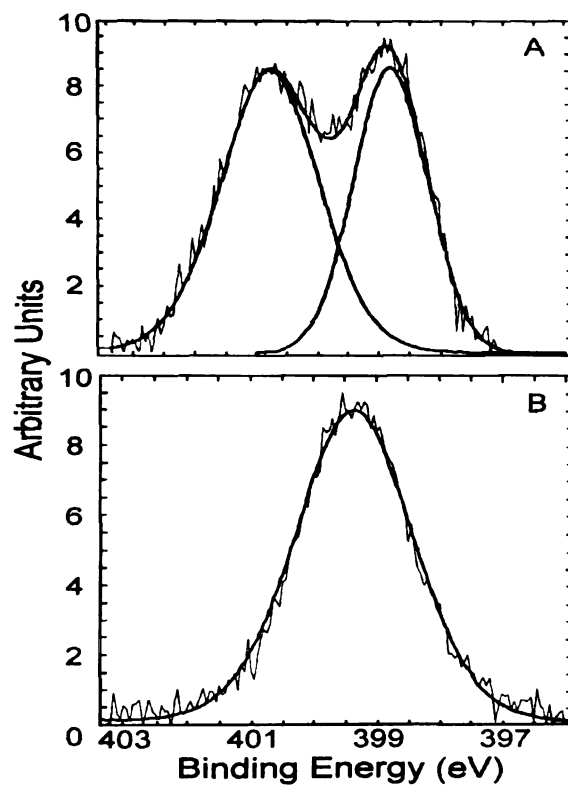


Figure 3.3: XPS spectra of the N_{1s} region of a 9-bilayer PAH/PAA film before (A) and after heating for 2 hours at 215 °C (B). Binding energy is referenced to the C_{1s} peak for hydrocarbons (284.6 eV).

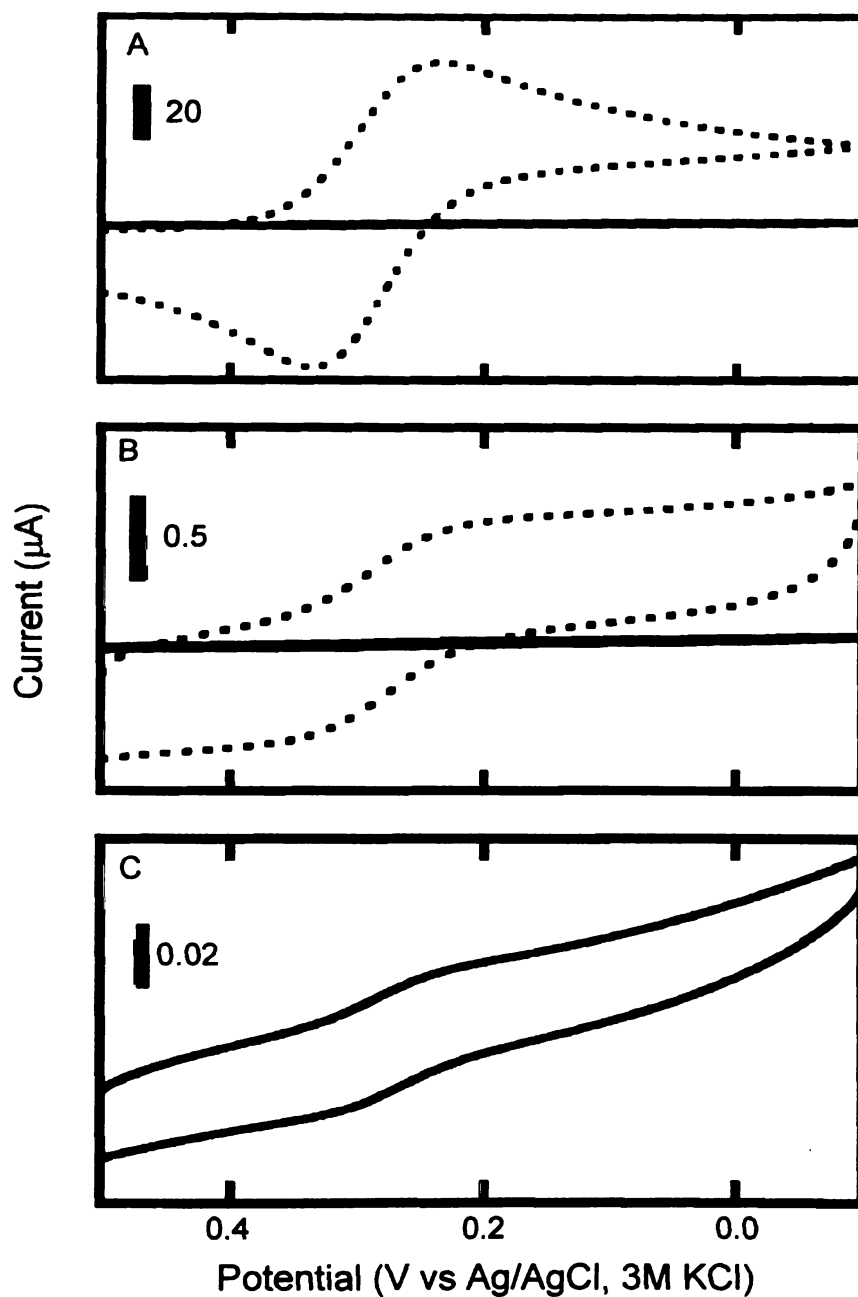


Figure 3.4: Cyclic voltammograms ($0.005 \text{ M Fe(CN)}_6^{3-}$ in $0.025 \text{ Na}_2\text{HPO}_4$, $0.025 \text{ NaH}_2\text{PO}_4$, $1 \text{ M Na}_2\text{SO}_4$, pH 6.3) at gold electrodes coated with 9 bilayers of PAH/PAA before (3A, dashed line), after heating a film at $130 \text{ }^\circ\text{C}$ for 2 hours (3A, solid line and 3B, dashed line), or after heating a film at $215 \text{ }^\circ\text{C}$ (3B and C, solid lines). Scan rate of 0.1 V/s and electrode area of 0.1 cm^2 . The electrode was immersed in the solution for 2 minutes prior to data acquisition.

suggested by FTIR-ERS, but there could also be some decrease due to annealing of the polyelectrolyte film or the underlying gold surface.

Impedance spectroscopy allows quantitative comparison of the permeability of films before and after cross-linking. Figure 3.5 shows typical plots of impedance for electrodes coated with 9-bilayers of PAH/PAA before and after heating at 130 °C or 215 °C. In the case of the unheated film (Figure 3.5A), we see a small semicircle at high frequencies and the beginnings of a straight line at low frequencies that is characteristic of semi-infinite linear diffusion.¹² The diameter of the semicircle is approximately equal to the charge transfer resistance, R_{ct} , which is indicative of the accessibility of the electrode. The impedance plot for a film after cross-linking at 215 °C (Figure 3.5C) contains only 1/8 of a circle showing that the reaction is completely kinetically controlled.¹² Using the modified Randle's equivalent circuit¹³ shown in Figure 3.6, we modeled the electrode-film interface and calculated values for R_{ct} , film resistance (R_f), film capacitance (C_f), double-layer capacitance (C_d) and the diffusion impedance (Z_w). The equivalent circuit provides an excellent fit to the experimental data. R_{ct} increases by a factor of 200 upon cross-linking at 130 °C ($8 \times 10^3 \Omega\text{-cm}^2$), and R_f values are $6.5 \times 10^3 \Omega\text{-cm}^2$. Heating of films at 215 °C has an even more dramatic effect on the electrode system. R_f and R_{ct} values for these systems ($8 \times 10^4 \Omega\text{-cm}^2$ and $1 \times 10^5 \Omega\text{-cm}^2$, respectively) are 1-2 orders of magnitude higher than for films heated at 130 °C. These results are in good agreement with cyclic voltammetry.

Cross-linking of PAH/PAA films dramatically increases their stability at high pH values. Prior to cross-linking, immersion of a PAH/PAA film in a pH 10-buffered solution (0.025 M Na_2CO_3 /0.025 M NaHCO_3 in 1 M Na_2SO_4) for 20 minutes results in

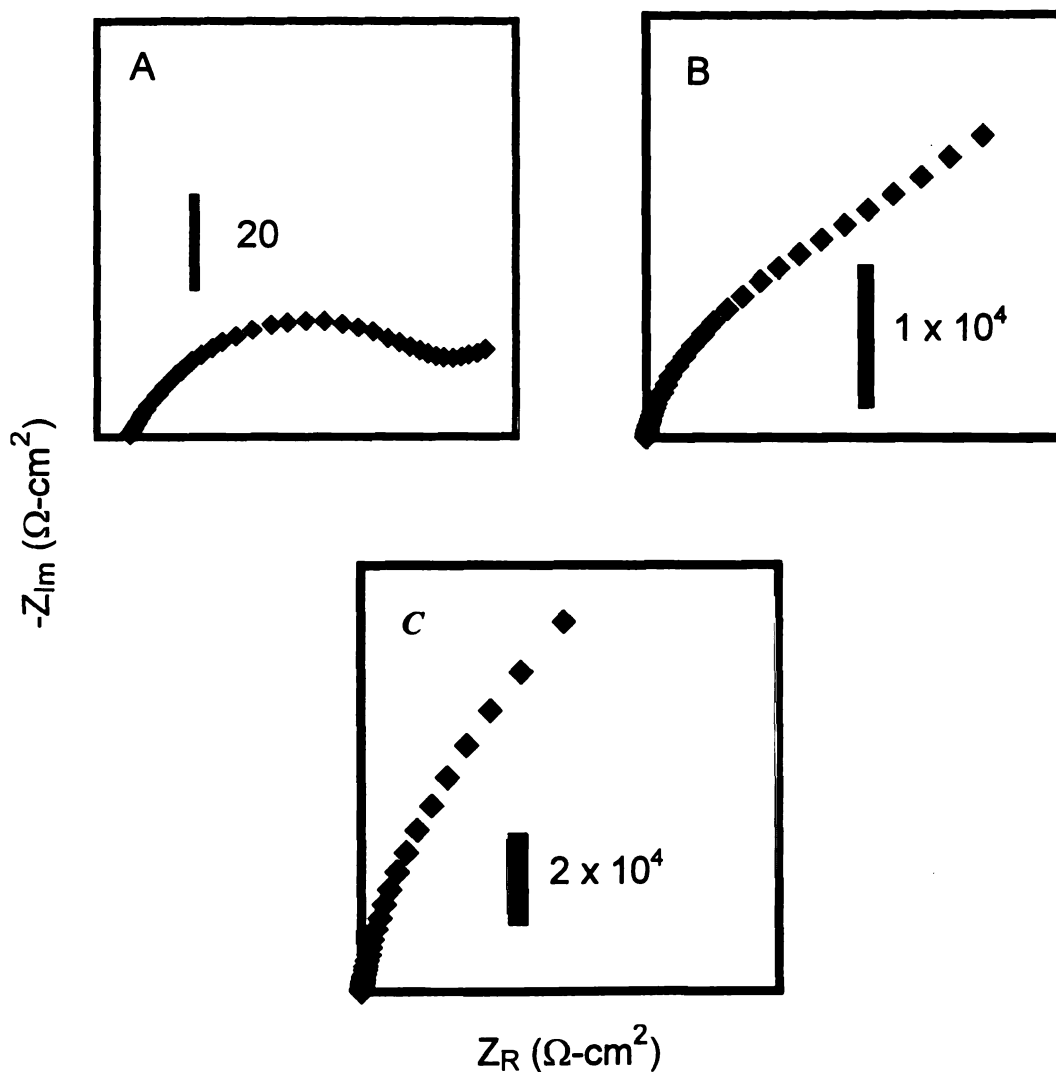


Figure 3.5: Impedance plots ($0.005 \text{ M Fe(CN)}_6^{3-/4-}$ in $0.025 \text{ Na}_2\text{HPO}_4$, $0.025 \text{ NaH}_2\text{PO}_4$, $1 \text{ M Na}_2\text{SO}_4$, pH 6.3) for gold electrodes coated with 9-bilayer PAH/PAA films before heating (A), after heating at 130°C (B), or after heating at 215°C (C). Scale bars apply to both x- and y-axes. Frequency range $1\text{-}10^5 \text{ Hz}$. Sinusoidal voltage: 5 mV about E° . The electrode was immersed in solution for 5 minutes prior to data acquisition. Scale bar is representative for both x- and y-axes.

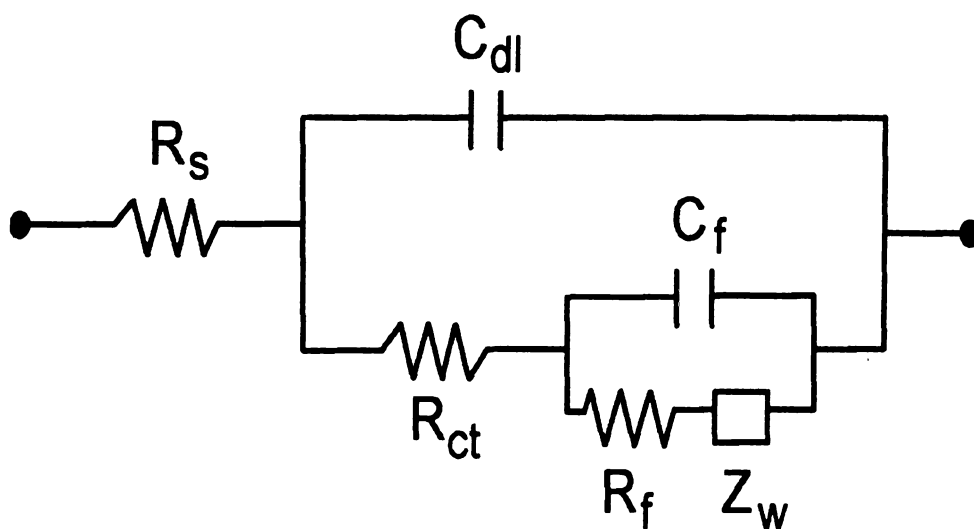


Figure 3.6: Modified Randles' equivalent circuit used to model impedance data from gold electrodes modified with cross-linked PAH/PAA films.

an ~30% decrease in ellipsometric thickness. We observe similar instability at high pH when working with PAH/PSS films. At pH 10, a large fraction of the amine groups in these films are deprotonated and many of the electrostatic bonds linking the layers are no longer present. In contrast, cross-linked PAH/PAA films show no decrease in film thickness after immersion in pH 10 buffer. As a control, we immersed PAH/PSS films, which were heated at 130 °C for 2 hours in pH 10 buffer for 20 minutes. These films still show an ~30% decrease in ellipsometric thickness.

In conclusion, heat-induced cross-linking between PAH and PAA occurs via formation of amide bonds and stabilizes these films over a wide pH range. Cyclic voltammetry and impedance spectroscopy show that film permeability decreases dramatically after cross-linking and depends upon heating conditions. We are investigating using these nylon-like, cross-linked films as ultrathin membranes or corrosion resistant coatings.¹⁴

IV. References

- 1) March, J. *Advanced Organic Chemistry*; 4th ed.; John Wiley: New York, 1992.
- 2) Beyer, D.; Bohanon, T. M.; Knoll, W.; Ringsdorf, H. *Langmuir* **1996**, *12*, 2514-2518.
- 3) Liu, Y.; Bruening, M. L.; Bergbreiter, D. E.; Crooks, R. M. *Angew. Chem. Int. Ed. Engl.* **1997**, *36*, 2114-2116.
- 4) Lee, B.-J.; Kunitake, T. *Langmuir* **1994**, *10*, 557-562.
- 5) Dubas, S. T.; Schlenoff, J. B. *Macromolecules* **1999**, *32*, 8153-8160.
- 6) Caruso, F.; Niikura, K.; Furlong, D. N.; Okahata, Y. *Langmuir* **1997**, *13*, 3422-3426.
- 7) Yoo, D.; Shiratori, S. S.; Rubner, M. F. *Macromolecules* **1998**, *31*, 4309-4318.
- 8) Socrates, G. *Infrared Characteristic Group Frequencies*; John Wiley & Sons: New York, 1980.
- 9) Wagner, C. D.; Riggs, W. M.; Davis, L. E.; Moulder, J. F.; Muilenberg, G. E. *Handbook of X-Ray Photoelectron Spectroscopy*; Wagner, C. D.; Riggs, W. M.; Davis, L. E.; Moulder, J. F.; Muilenberg, G. E., Ed.; Perkin Elmer: Eden Prairie, MN, 1979, pp 40-41.
- 10) Schlenoff, J. B.; Ly, H.; Li, M. *J. Am. Chem. Soc.* **1998**, *120*, 7626-7634.
- 11) Sukhorukov, G. B.; Schmitt, J.; Decher, G. *Ber. Bunsenges. Phys. Chem.* **1996**, *100*, 948-953.
- 12) Bard, A. J.; Faulkner, L. R. *Electrochemical Methods: Fundamentals and Applications*; John Wiley & Sons: New York, 1980.
- 13) Rubinstein, I.; Sabatani, E.; Rishpon, J. *J. Electrochem. Soc.* **1987**, *134*, 3078.
- 14) Dai, J.; Jensen, A. W.; Mohanty, D. K.; Erndt, J.; Bruening, M. L. *Langmuir* **2001**, *17*, 931-937.

CHAPTER 4

Layered Polyelectrolyte Films as Selective, Ultrathin Membranes for Anion Separations

I. Introduction

Ultrathin membranes are attractive for separation processes because they can simultaneously allow both high flux and high permselectivity.¹⁻³ Typically, such membranes consist of polymer “skins” (<50 nm thick) on a highly permeable support.² The support provides mechanical stability, but its high permeability presents minimal mass-transfer resistance. Martin and coworkers used ultrathin polymer membranes deposited on porous alumina substrates in the development of anion-permselective sensors as well as gas-separation membranes.¹⁻⁵ Regen showed that even Langmuir-Blodgett films offer permselectivity in some gas separations.⁶⁻⁹ Deposition of highly selective, stable, ultrathin membranes remains a challenge, however, because of the difficulty of fully covering a porous substrate without filling the pores.

Synthesis of high-flux composite membranes requires methods for deposition of ultrathin, defect-free films on highly permeable supports. Layer-by-layer deposition of polyelectrolytes on porous alumina (0.02 μm pore diameter) provides a convenient and versatile way to produce such membranes. Electron microscopy shows that 5-bilayers (~25 nm) of poly(allylamine hydrochloride) (PAH)/poly(styrene sulfonate) (PSS) are sufficient to cover porous alumina and that underlying pores are not clogged during the deposition process. The selectivity of anion transport through these membranes increases

with the number of bilayers until the substrate is fully covered. 5-bilayer PAH/PSS membranes have $\text{Cl}^-/\text{SO}_4^{2-}$ and $\text{Cl}^-/\text{Fe}(\text{CN})_6^{3-}$ selectivity values of 5 and 1000, respectively. PAH/poly(acrylic acid) (PAA) membranes show selectivity values similar to those of PAH/PSS membranes but with a 3-fold decrease in anion flux. Selectivity in both of these systems likely results from Donnan exclusion. By combining the properties of both PAH/PAA and PAH/PSS membranes it is possible to achieve increased $\text{Cl}^-/\text{SO}_4^{2-}$ values while maintaining high flux.

II. Experimental

A. Materials

Poly(allylamine hydrochloride) (PAH) (Aldrich, $M_w=70,000$), poly(styrene sulfonate) (PSS) (Aldrich, $M_w=70,000$), poly(acrylic acid) (PAA) ($M_w=90,000$, 25 wt% solution, Alfa Aesar), MnCl_2 (Mallinckrodt), NaBr (Aldrich), NaCl (Mallinckrodt), $\text{K}_2\text{Ni}(\text{CN})_4$ (Aldrich), KCl (Baker), KNO_3 (CCI), K_2SO_4 (CCI), $\text{K}_3\text{Fe}(\text{CN})_6$ (Mallinckrodt), and salicylic acid (Spectrum) were used as received. Prior to film deposition, the porous alumina support (Whatman[®] Anodisc[™] 0.02 μm membrane filters) was UV/ O_3 cleaned for 15 minutes (Boekel UV-Clean[™] model 135500). Polyelectrolyte deposition then began by immersing the alumina support in a solution of PAH (0.02 M with respect to the monomer unit, pH 2.3 for PAH/PSS films or pH 4.5 for PAH/PAA films) for 5-minutes. PAH solutions also contained either 0.5 M NaBr (PAH/PSS deposition) or 0.5 M NaCl (PAH/PAA deposition). Supporting electrolytes were chosen based on literature preparations of polyelectrolyte films.^{31,47,48} The alumina membrane has two distinct sides: the filtrate side has a skin layer of 0.02 μm diameter

pores and the permeate side has 0.2 μm diameter pores. We used a holder to limit polyelectrolyte deposition to the filtrate side. A 1-minute rinse with water (Milli-Q, 18 M Ω -cm) followed PAH deposition and all other polyelectrolyte deposition steps. To deposit the polyanion, the PAH-coated alumina support was immersed in either a solution of PSS or PAA. After the deposition of the desired number of polyelectrolyte layers, the membrane was dried with N₂. Polyelectrolyte deposition began with the polycation but the alumina substrate is also positively charged. Ellipsometry experiments on Al coated Si substrates shows that a layer of polyelectrolyte is deposited regardless of charge. A Hitachi S-4700 field-emission scanning electron microscope (FESEM) operating with accelerating voltages of between 6 and 8 kV was used to image polyelectrolyte films deposited on alumina membranes. The use of low voltages with the FESEM allows imaging of polymer films while reducing charging artifacts and specimen damage.^{10,11} Samples were coated with 5 nm of Au for FESEM imaging.

B. Transport Studies

The dialysis apparatus consists of two glass cells (volumes of 100 mL) connected by a 2.5 cm-long neck in which the membrane separates the feed and permeate sides (Figure 4.1). The exposed area of the membrane was 2.0 cm². The permeate cell contained Milli-Q water and the feed cell contained the appropriate 0.1 F salt solution (KCl, KNO₃, K₂SO₄, K₂Ni(CN)₄, or K₃Fe(CN)₆). The measured pH values of the unbuffered 0.1 F salt solutions were 4.8 (KCl), 5.3 (KNO₃), 5.5 (K₂SO₄), 6.4 (K₂Ni(CN)₄), and 6.2 (K₃Fe(CN)₆). These pH values are well below the pK value for ammonium groups and well above the pK value of styrene sulfonic acid. Thus, pH

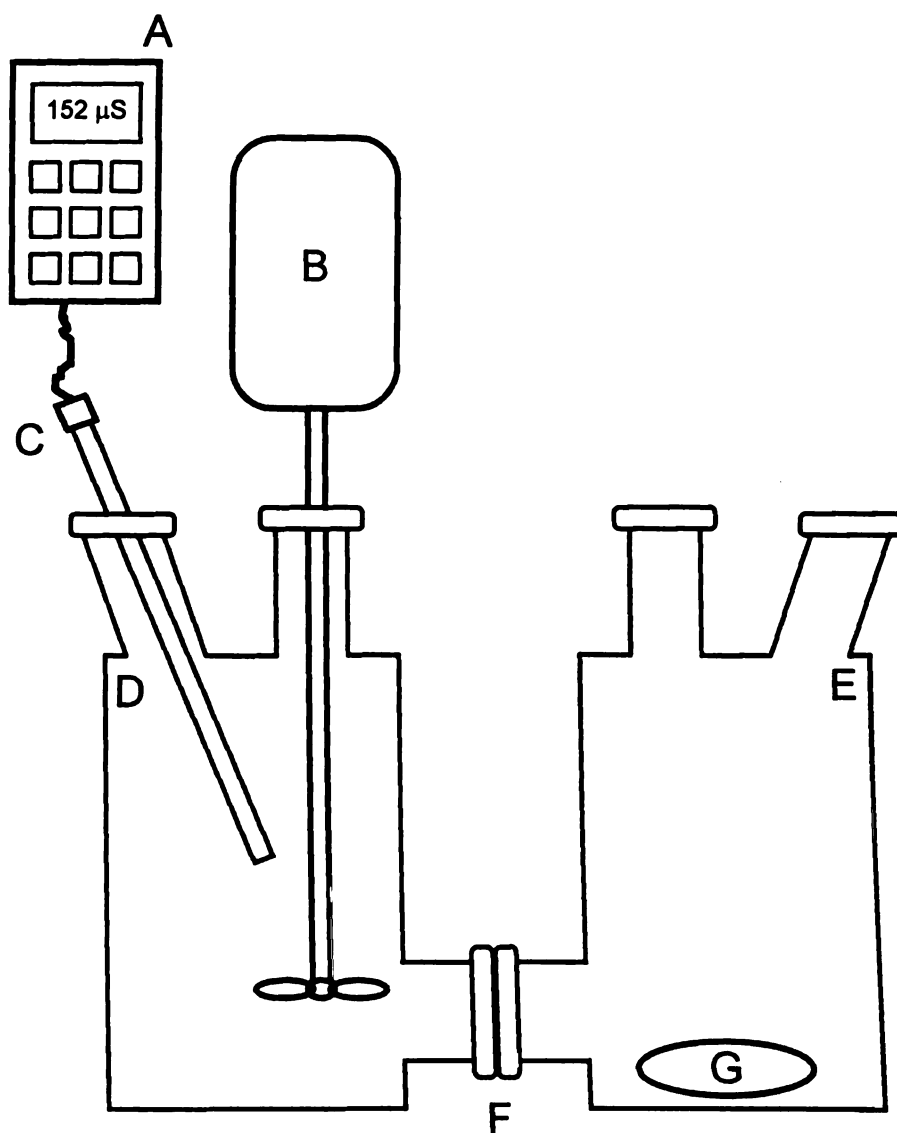


Figure 4.1: Dialysis cell used to measure ion-permeability of polyelectrolyte membranes: conductivity meter (A), electric stirrer (B), conductivity electrode (C), receiving phase (D), source phase (E), membrane (F), and magnetic stir bar (G).

should have little effect on transport in this system. However, in the case of PAH/PAA membranes, there is a possibility that pH may affect transport. As the selectivities in the PAH/PAA system were similar to those of PAH/PSS, we assume that the pH differences in these unbuffered solutions have little effect on transport. Salicylic acid (SA) was also used as a probe anion. Solutions of salicylic acid were adjusted to a pH of 6 with KOH to deprotonate the acid. The concentration of salt in the permeate cell was monitored at 10 minute intervals for 90 minutes using conductivity measurements (Orion Model 115 conductivity meter). To normalize receiving phase conductivity values, we divide by the conductivity of the source phase. Both feed and permeate solutions were stirred vigorously to minimize concentration polarization at the membrane surface. Permeability measurements made with different stirring speeds showed no significant change in flux. The order in which the anions were investigated was Cl^- , NO_3^- , SO_4^{2-} , $\text{Ni}(\text{CN})_4^{2-}$, and $\text{Fe}(\text{CN})_6^{3-}$. After determining the flux of each anion, the membrane was immersed in Milli-Q water for 15 minutes.

The integrity of the film during the permeability experiments was tested with a second Cl^- run performed after the experiment with $\text{Fe}(\text{CN})_6^{3-}$. The Cl^- flux changed less than 10% for PAH/PSS membranes, but PAH/PAA membranes showed an ~50% decrease. Three or more different membranes were tested for each type of polyelectrolyte film.

III. Results and Discussion

To synthesize ultrathin polyelectrolyte membranes, the layered film must cover the substrate without filling underlying pores. Although a few reports describe the layer-

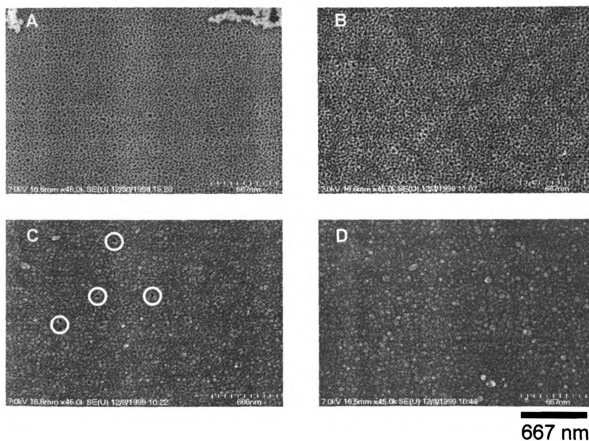


Figure 4.2: FESEM images of the filtrate side of a porous alumina substrate (A), and alumina substrates coated with 2 (B), 4 (C), or 5 PAH/PSS bilayers (D). The circles in image C are likely defects in the film structure. Samples were coated with ~5 nm Au for imaging.

by-layer deposition of polyelectrolyte films on highly porous substrates,¹²⁻²⁰ they do not emphasize surface coverage or the likely possibility of polyelectrolyte deposition in substrate pores. FESEM images (Figure 4.2) of PAH/PSS films on porous alumina show that coverage of the filtrate side of the membrane gradually increases with the deposition of each subsequent bilayer. Complete pore coverage occurs after the addition of about 5 PAH/PSS bilayers. Micrographs of the alumina permeate side (Figure 4.3) show that this surface remains polyelectrolyte free even after deposition of 10-bilayers on the filtrate side. This demonstrates that deposition of the polyelectrolyte does not occur throughout the membrane. FESEM micrographs of 5-bilayer PAH/PAA membranes also show a defect free film, but complete pore coverage occurs with fewer depositions as the bilayer thickness of PAH/PAA films is greater than that of PAH/PSS films.

Cross-sectional FESEM images show that the pores of the membrane are unblocked after film deposition. Figure 4.4 shows a 10-bilayer PAH/PSS film deposited on the membrane surface (filtrate side), with little polyelectrolyte in the alumina pores. There appears to be some polyelectrolyte in the upper part of the pores as the appearance of small cracks is likely due to a small amount of polyelectrolyte deposition. However, the majority of film deposition occurs at the support surface and the pores remain open, even if they contain a bilayer or two of polyelectrolyte. Figure 4.5 shows the interior pore structure of an alumina support that was coated with a 10-bilayer PAH/PSS film. The absence of polyelectrolyte in this image shows that polyelectrolytes are unable to penetrate much past the skin layer on the filtrate side of the support. The cross-sectional micrograph of the 10-bilayer PAH/PSS membrane (Figure 4.4) indicates a film thickness

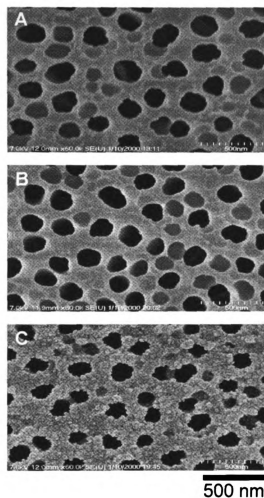


Figure 4.3: FESEM images of the permeate side of a bare alumina substrate before film deposition (A), after restricting deposition to the filtrate side (B), or following complete alumina immersion in polyelectrolyte solutions (C).

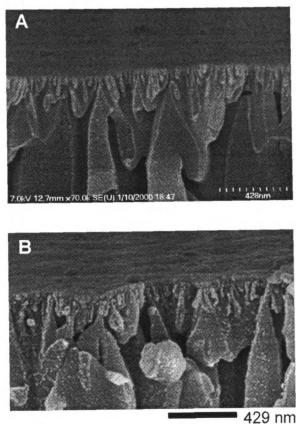


Figure 4.4: Cross-sectional FESEM images of the filtrate side of a bare alumina substrate (A) and an alumina substrate coated with 5-bilayers of PAH/PAA (B). Film thickness \cong 40 nm.

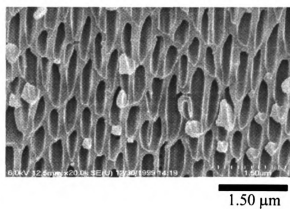


Figure 4.5: Cross-sectional FESEM image showing the lack of polyelectrolyte deposition in the inner pores of an alumina substrate where the filtrate side is coated with a 10-bilayer PAH/PSS film.

of ~35 nm, which is comparable to ellipsometric thicknesses for 10-bilayer films deposited on solid substrates.²¹ Images in Figures 4.2, 4.3, 4.4, and 4.5 show collectively that deposition of layered polyelectrolyte films is a simple means of creating ultrathin membranes on porous supports.

Because pore coverage depends on the number of polyelectrolyte bilayers, selectivity and flux through these membranes also vary with the number of PAH/PSS bilayers. Chloride flux shows little change with the number of PAH/PSS bilayers, while SO_4^{2-} transport decreases 5-fold with the addition of 10 bilayers (Table 4.1). Under the same conditions, $\text{Fe}(\text{CN})_6^{3-}$ flux decreases 330-fold. Figure 4.6, which shows receiving phase conductivity as a function of time, illustrates the effect of each additional PAH/PSS bilayer on SO_4^{2-} flux. The selectivity ratio for Cl^- to SO_4^{2-} , which is determined by dividing anion flux values, reaches its maximum value of 5 after the deposition of 5-bilayers.²² This is consistent with the FESEM images that show complete surface coverage with few defects after the deposition of 5-bilayers (Figure 4.2). Prior to complete pore coverage, most sulfate transport likely occurs through membrane defects. Upon full coverage, however, sulfate must enter and diffuse through the membrane causing a decrease in flux. Resistance to mass transfer of Cl^- through the polyelectrolyte film must be minimal because flux is hardly affected by full coverage of the support.

Figure 4.7 compares the fluxes of various anions through a 5-bilayer PAH/PSS membrane. The smallest measured fluxes for PAH/PSS membranes occur with $\text{Fe}(\text{CN})_6^{3-}$, because its high charge produces the largest electrostatic repulsion between anion and membrane. The linearity of the conductivity values with time, which occurs with each membrane tested, demonstrates steady-state anion transport where receiving-

Table 4.1: Anion flux values (moles $\text{cm}^{-2} \text{s}^{-1}$) through bare alumina and alumina substrates coated with between 1-5.5- or 10-bilayers of PAH/PSS.

Number of Bilayers	Cl^- Flux	NO_3^- Flux	SO_4^{2-} Flux	$\text{Ni}(\text{CN})_4^{2-}$ Flux	$\text{Fe}(\text{CN})_6^{3-}$ Flux
alumina	$6.7 \times 10^{-8} \pm 3\%$	$6.7 \times 10^{-8} \pm 6\%$	$5.1 \times 10^{-8} \pm 4\%$	$4.8 \times 10^{-8} \pm 1\%$	$5.0 \times 10^{-8} \pm 7\%$
1	$6.6 \times 10^{-8} \pm 4\%$		$4.8 \times 10^{-8} \pm 6\%$		$4.4 \times 10^{-8} \pm 10\%$
2	$5.7 \times 10^{-8} \pm 7\%$		$4.5 \times 10^{-8} \pm 3\%$		$4.1 \times 10^{-8} \pm 7\%$
3	$5.9 \times 10^{-8} \pm 5\%$		$2.9 \times 10^{-8} \pm 8\%$		$1.3 \times 10^{-8} \pm 40\%$
4	$5.1 \times 10^{-8} \pm 13\%$		$1.5 \times 10^{-8} \pm 14\%$		$2.7 \times 10^{-9} \pm 10\%$
5	$6.5 \times 10^{-8} \pm 25\%$	$6.1 \times 10^{-8} \pm 20\%$	$9.9 \times 10^{-9} \pm 8\%$	$4.7 \times 10^{-9} \pm 10\%$	$2.1 \times 10^{-10} \pm 30\%$
5.5	$4.6 \times 10^{-8} \pm 6\%$	$5.0 \times 10^{-8} \pm 4\%$	$2.2 \times 10^{-8} \pm 20\%$	$8.6 \times 10^{-9} \pm 30\%$	$1.9 \times 10^{-10} \pm 20\%$
10	$4.5 \times 10^{-8} \pm 1\%$	$5.1 \times 10^{-8} \pm 4\%$	$8.9 \times 10^{-9} \pm 1\%$	$3.6 \times 10^{-9} \pm 3\%$	$1.4 \times 10^{-10} \pm 20\%$

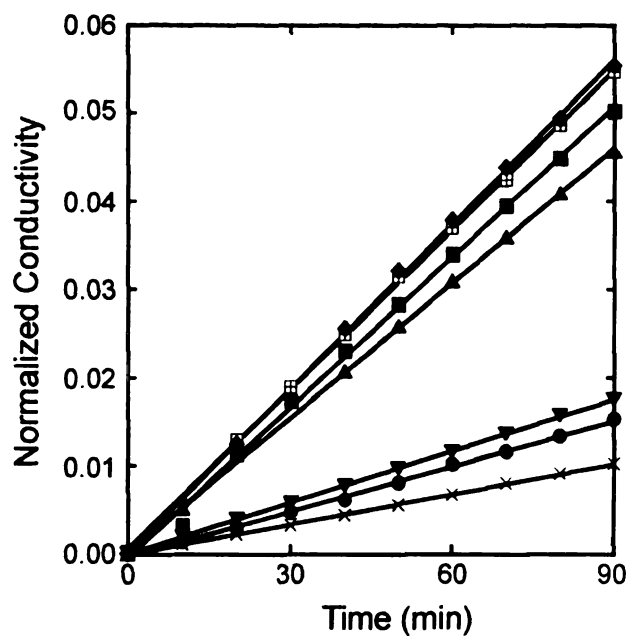


Figure 4.6: Plot of normalized receiving-phase conductivity (K_2SO_4) as a function of time when the source phase was separated from the receiving phase by a bare alumina substrate (open squares), or a 1- (diamonds), 2- (squares), 3- (triangles), 4- (inverted triangles), 5- (circles), or 10-bilayer (X's) PAH/PSS film.

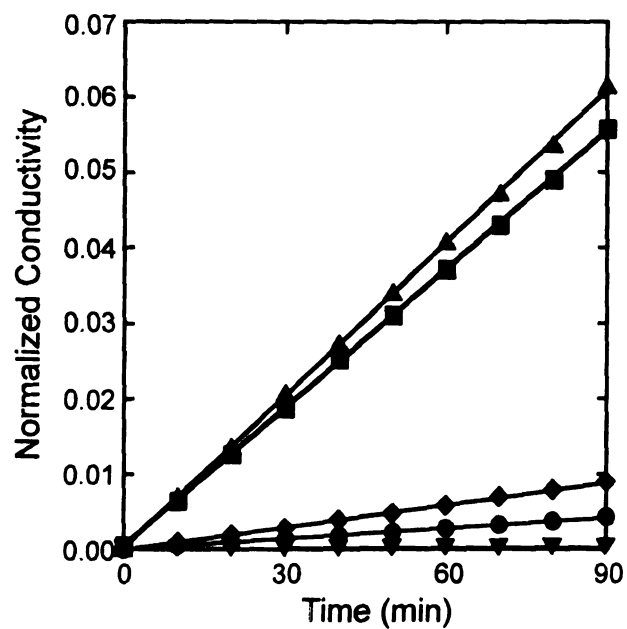


Figure 4.7: Plot of normalized receiving-phase conductivity as a function of time when the source phase was separated from the receiving phase by a 5-bilayer PAH/PSS film. Different symbols represent different salts: KCl (triangles), KNO₃ (squares), K₂SO₄ (diamonds), K₂Ni(CN)₄ (circles), and K₃Fe(CN)₆ (inverted triangles).

phase concentration is negligible compared to that in the source phase. Five-bilayer PAH/PSS membranes show selectivity ratios of 300, 50, and 20 for $\text{Cl}^-/\text{Fe}(\text{CN})_6^{3-}$, $\text{SO}_4^{2-}/\text{Fe}(\text{CN})_6^{3-}$, and $\text{Ni}(\text{CN})_4^{2-}/\text{Fe}(\text{CN})_6^{3-}$, respectively (Table 4.1 and Figure 4.7). The ability of PAH/PSS membranes to nearly eliminate $\text{Fe}(\text{CN})_6^{3-}$ flux suggests that these membranes could be useful for the dialytic purification of large, highly charged molecules.²³⁻²⁵

Once complete pore coverage occurs, the presence of additional polyelectrolyte bilayers decreases anion flux, but has little impact on selectivity. The $\text{Cl}^-/\text{SO}_4^{2-}$, $\text{Cl}^-/\text{Fe}(\text{CN})_6^{3-}$, $\text{Cl}^-/\text{Ni}(\text{CN})_4^{2-}$, and $\text{SO}_4^{2-}/\text{Ni}(\text{CN})_4^{2-}$ selectivity are nearly the same for 5 and 10-bilayer PAH/PSS membranes. On going from 5 to 10 PAH/PSS bilayers, anion flux decreases only between 10 and 30% (Table 4.1). Kraseman and Tieke report that transport selectivity does depend on the number of PAH/PSS bilayers.²⁶ However, the films in that study were deposited under different conditions and on different substrates.

The minimal decrease in the flux of highly charged anions on going from 5- to 10-bilayer membranes suggests that the major selectivity factor is Donnan exclusion near the surface.²⁶ Hindered diffusion would yield a significant decrease in anion flux with increasing membrane thickness, while Donnan exclusion due to uncompensated charge at the membrane surface should be relatively constant once full coverage is achieved.^{27,28} The large decreases in SO_4^{2-} , $\text{Ni}(\text{CN})_4^{2-}$, and $\text{Fe}(\text{CN})_6^{3-}$ fluxes upon addition of the first 5 PAH/PSS bilayers likely result from increased Donnan exclusion as surface coverage increases. Also consistent with a Donnan exclusion model is the minimal reduction in Cl^- and NO_3^- flux (Table 4.1) due to the much smaller repulsive forces generated by the monovalent anions.²⁷ One advantage of an electrostatic exclusion mechanism in

PAH/PSS membranes is that it provides monovalent/divalent and monovalent/trivalent selectivity with little inhibition of the monovalent anion flux (Table 4.1).

The majority of uncompensated charge in layered polyelectrolyte films lies near the film/solution interface^{29,30} so one should expect a change in anion flux if the outer layer is a polycation rather than a polyanion. We tested this possibility by depositing an additional PAH layer on a 5-bilayer film. This yields a membrane with a positive surface charge, while providing a minimal change in membrane thickness. The additional PAH layer has little effect on Cl^- and NO_3^- transport (Table 4.1) as the flux of these anions is already close to that of bare alumina. However, there is a 2-fold increase in SO_4^{2-} and $\text{Ni}(\text{CN})_4^{2-}$ flux when the outermost charge is positive (Table 4.1). This suggests that the outer layer charge does have a major effect on flux. In contrast, however, there is little change in $\text{Fe}(\text{CN})_6^{3-}$ flux when the outer layer charge is positive. Apparently, large repulsive forces between internal regions of the membrane and trivalent $\text{Fe}(\text{CN})_6^{3-}$ are dominant for decreasing $\text{Fe}(\text{CN})_6^{3-}$ flux. This is somewhat surprising as Schlenoff showed that strongly dissociated polyelectrolytes provide complete intrinsic charge compensation.²⁹ However, charge compensation appears to depend on deposition conditions and the polyelectrolyte used.³¹ For PAH/PSS films Lowack and Helm suggest significant extrinsic charge compensation, which could result in Donnan exclusion within the polyelectrolyte membrane.²⁸

Flux of the potassium salt of salicylic acid through PAH/PSS films supports the hypothesis that Donnan exclusion (rather than hindered diffusion) is the dominant factor governing transport selectivity. We chose to work with salicylate because it is a large monovalent anion with a diffusion coefficient 15% smaller than that of $\text{Fe}(\text{CN})_6^{3-}$.³² The

large size of salicylate is manifested by the fact that its flux through bare alumina (3.2×10^{-8} moles $\text{cm}^{-2} \text{ s}^{-1}$) is the lowest of any anion tested. The presence of 5 PAH/PSS bilayers on alumina reduces salicylate flux two-fold while reducing Cl^- flux by <30%. This suggests some size selectivity between monovalent anions. However, most selectivity among anions occurs as a result of Donnan exclusion as shown by the fact that 5 PAH/PSS bilayers reduce $\text{Fe}(\text{CN})_6^{3-}$ flux 220-fold and SO_4^{2-} flux 5-fold. This occurs in spite of the fact that salicylate, SO_4^{2-} , and $\text{Fe}(\text{CN})_6^{3-}$ have similar diffusion coefficients.^{32,33} These results show that Donnan exclusion is the major factor affecting anion transport, but there may be some effect of size for larger anions.

Transport selectivity is similar in PAH/PAA and PAH/PSS membranes, although fluxes are considerably lower through PAH/PAA membranes. Five-bilayer PAH/PAA membranes show between a 2- and 10-fold reduction in anion flux compared to 10-bilayer PAH/PSS membranes (Table 4.1), which have similar thicknesses as seen with FESEM. The $\text{Cl}^-/\text{SO}_4^{2-}$ and $\text{Cl}^-/\text{Fe}(\text{CN})_6^{3-}$ selectivity values for PAH/PAA films, 4 and 230, respectively, are similar to 10-bilayer PAH/PSS selectivity values. The decreases in anion flux are likely due to a tighter structure in PAH/PAA membranes than in PAH/PSS membranes. If the effect was due to higher charge densities, we would expect to see higher $\text{Cl}^-/\text{SO}_4^{2-}$ selectivities but this is not the case.

Decreased flux through PAH/PAA membranes is in contrast to our previous work with PAH/PAA films deposited on gold electrodes (Chapter 1). In those studies, cyclic voltammetry of $\text{Fe}(\text{CN})_6^{3-}$ was hardly affected by the presence of 5-bilayers of PAH/PAA, suggesting rapid $\text{Fe}(\text{CN})_6^{3-}$ flux through these films. We speculate that in the present case, PAH/PAA swelling is constricted at the surface of the alumina substrate.

Swelling of films on solid gold electrodes is uninhibited and may result in an open and highly permeable film. $\text{Fe}(\text{CN})_6^{3-}$ absorption may also play a role in the contrasting results. In the electrochemistry, absorption would result in higher peak currents indicating a higher permeability due to the higher concentration at the electrode surface. But, in the membrane studies ion absorption would have the effect of increasing the effective charge of the membrane therefore increasing the repulsive effects and decreasing the observed permeability.

In an attempt to utilize properties of both PAH/PSS and PAH/PAA membranes, composite membranes consisting of a thin PAH/PAA film deposited on a PAH/PSS precursor film show increased $\text{Cl}^-/\text{SO}_4^{2-}$ selectivity.³⁴ The PAH/PSS film allows for high flux while the PAH/PAA film dramatically decreases SO_4^{2-} transport. Composite membranes consisting of 2.5 bilayers of PAA/PAH deposited on 5-bilayers of PSS/PAH show $\text{Cl}^-/\text{SO}_4^{2-}$ selectivity of 150 and cross-linking of this membrane at 115 °C (as described in Chapter 3) increases selectivity 4-fold. FESEM images show changes in surface morphology when PAA/PAH films are deposited on the precursor PSS/PAH film (Figure 4.8). As observed in previous experiments the outer layer charge of the film dramatically affects membrane transport. In one case, $\text{Cl}^-/\text{SO}_4^{2-}$ selectivity decreases from 360 to 2 upon deposition of one layer of PAH.³⁴ Construction of composite membranes provides for additional means to easily tailor the transport of layered polyelectrolyte membranes.

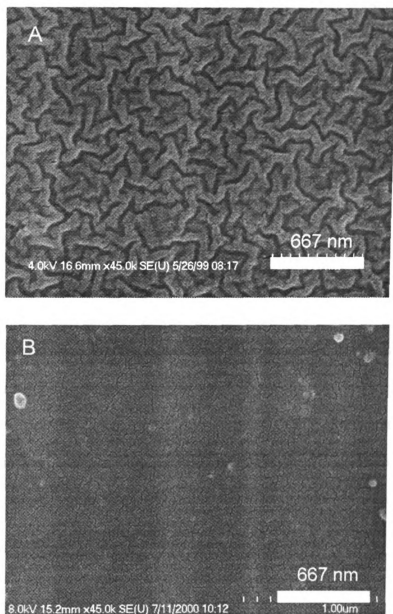


Figure 4.8: FESEM images of the top of an alumina substrate coated with either a 4.5-bilayer PAA/PAH film heated at 115 C (A) or a 5-bilayer PSS/PAH film coated with 1.5-bilayers of PAA/PAH (B). Samples were coated with 5 nm Au for imaging.

IV. Conclusions

Ultrathin polyelectrolyte films on porous supports show selectivities typical of anion exchange membranes. Using 5-bilayer PAH/PSS membranes on Celgard™ supports Krasemann and Tieke report a $\text{Cl}^-/\text{SO}_4^{2-}$ selectivity value of 17, which is somewhat higher than our value of 7.²⁶ This higher value may be a result of a different film structure due to a difference in preparation conditions or substrate topography. Our $\text{Cl}^-/\text{SO}_4^{2-}$ selectivity value of 7 is two-fold higher than a previous dialysis study using interpolymer type carboxylic ion-exchange membranes.³⁵ Electrodialysis studies with copolymer membranes show selectivity values between one and 100, where higher values usually result from cross-linked surfaces.³⁶⁻⁴⁰ Composite membranes show higher selectivity values without the need for cross-linking but upon cross-linking selectivity can be greatly enhanced. Ultrathin, polyelectrolyte membranes show a wide range of selectivity values depending on film composition and charge. These properties should provide easy means for the tailoring of specific properties in anion separation membranes.

V. References

- 1) Liu, C.; Espenscheid, M. W.; Chen, W.-J.; Martin, C. R. *J. Am. Chem. Soc.* **1990**, *112*.
- 2) Liu, C.; Martin, C. R. *Nature* **1991**, *352*, 50-52.
- 3) Liang, W.; Martin, C. R. *Chem. Mater.* **1991**, *3*, 390-391.
- 4) Ugo, P.; Moretto, L. M.; Mazzocchin, G. A.; Guerriero, P.; Martin, C. R. *Electroanalysis* **1998**, *10*, 1168-1173.
- 5) Liu, C.; Chen, W. J.; Martin, C. R. *J. Membr. Sci.* **1992**, *65*, 113-128.
- 6) Conner, M. D.; Janout, V.; Kudelka, I.; Dedek, P.; Zhu, J.; Regen, S. L. *Langmuir* **1993**, *9*, 2389-2397.
- 7) Albrecht, O.; Laschewsky, A.; Ringsdorf, H. *Macromolecules* **1984**, *17*, 937-940.
- 8) Hendel, R. A.; Nomura, E.; Janout, V.; Regen, S. L. *J. Am. Chem. Soc.* **1997**, *119*, 6909-6918.
- 9) Dedek, P.; Webber, A. S.; Janout, V.; Hendel, R. A.; Regen, S. L. *Langmuir* **1994**, *10*, 3943-3945.
- 10) Kim, K. Y.; Dickson, M. R.; Chen, V.; Fane, A. G. *Micron Microscopia Acta* **1992**, *23*, 259-271.
- 11) Kim, K. J.; Fane, A. G. *J. Membr. Sci.* **1994**, *88*, 103-114.
- 12) Nam, S. Y.; Lee, Y. M. *J. Membr. Sci.* **1997**, 161-171.
- 13) Ackern, F. v.; Krasemann, L.; Tieke, B. *Thin Solid Films* **1998**, 327-329, 762-766.
- 14) Kotov, N. A.; Magonov, S.; Tropsha, E. *Chem. Mater.* **1998**, *10*, 886-895.
- 15) Stroeve, P.; Vasquez, V.; Coelho, M. A. N.; Rabolt, J. F. *Thin Solid Films* **1996**, 708-712.
- 16) Leväsalmi, J.-M.; McCarthy, T. J. *Macromolecules* **1997**, *30*, 1752-1757.
- 17) Dauginet, L.; Duwez, A.-S.; Legras, R.; Demoustier-Champagne, S. *Langmuir* **2001**, *17*, 3952-3957.
- 18) Krasemann, L.; Toutianoush, A.; Tieke, B. *J. Membr. Sci.* **2001**, *181*, 221-228.
- 19) Tieke, B.; Ackern, F. v.; Krasemann, L. *Eur. Phys. E* **2001**, *5*, 29-39.

- 20) Meier-Haack, J.; Lenk, W.; Lehmann, D.; Lunkwitz, K. *J. Membr. Sci.* **2001**, *184*, 233-243.
- 21) Harris, J. J.; Stair, J. L.; Bruening, M. L. *Chem. Mater.* **2000**, *12*, 1941-1946.
- 22) Selectivity values can be calculated directly from flux ratios because source- phase concentrations were always 0.1 F.
- 23) Chen, D.-H.; Wang, S.-S.; Huang, T.-C. *J. Chem. Tech. Biotechnol.* **1995**, *64*, 284-292.
- 24) Åkerman, S.; Viinikka, P.; Svarfvar, B.; Järvinen, K.; Kontturi, K.; Näsman, J.; Urtti, A.; Paronen, P. *J. Controlled Release* **1998**, *50*, 153-166.
- 25) Saimoto, H.; Shigemasa, Y. *Polym. Adv. Technol.* **1999**, *10*, 39-42.
- 26) Krasemann, L.; Tieke, B. *Langmuir* **2000**, *16*, 287-290.
- 27) Peeters, J. M. M.; Boom, J. P.; Mulder, M. H. V.; Strathmann, H. *J. Membr. Sci.* **1998**, *145*, 199-209.
- 28) Lowack, K.; Helm, C. A. *Macromolecules* **1998**, *31*, 823-833.
- 29) Schlenoff, J. B.; Ly, H.; Li, M. *J. Am. Chem. Soc.* **1998**, *120*, 7626-7634.
- 30) Dubas, S. T.; Schlenoff, J. B. *Macromolecules* **1999**, *32*, 8153-8160.
- 31) Hoogeveen, N. G.; Cohen Stuart, M. A.; Fleer, G. J. *Langmuir* **1996**, *12*, 3675-3681.
- 32) Stojek, Z.; Ciszowska, M.; Osteryoung, J. G. *Anal. Chem.* **1994**, *66*, 1507-1512.
- 33) Bard, A. J.; Faulkner, L. R. *Electrochemical Methods: Fundamentals and Applications*; John Wiley & Sons: New York, 1980.
- 34) Stair, J. L.; Harris, J. J.; Bruening, M. L. *Chem. Mater.* **in press**.
- 35) Wycisk, R.; Trochimczuk, W. M. *J. Membr. Sci.* **1992**, *65*, 141-146.
- 36) Sata, T. *J. Membr. Sci.* **1994**, *93*, 117-135.
- 37) Sata, T.; Yamaguchi, T.; Kawamura, K.; Matsusaki, K. *J. Chem. Soc., Faraday Trans.* **1997**, *93*, 457-462.
- 38) Sata, T.; Yamaguchi, T.; Matsusaki, K. *J. Phys. Chem.* **1995**, *99*, 12875-12882.

- 39) Sata, T.; Tagami, Y.; Matsusaki, K. *J. Phys. Chem. B* **1998**, *102*, 8473-8479.
- 40) Sata, T.; Mine, K.; Higa, M. *J. Membr. Sci.* **1998**, *141*, 137-144.

CHAPTER 5

Development of Polyelectrolyte Films as Nanofiltration Membranes

I. Introduction

Nanofiltration (NF) membranes are used widely in the areas of water softening and purification, wastewater reclamation, and dye-salt separations.¹⁻⁶ The majority of NF membranes consist of a dense, thin active layer deposited on a thick support material, e.g. an ultra or microfiltration membrane. The composition of the thin active layer determines the separation characteristics of the membrane while the support material provides mechanical rigidity to the system. Typically, solute transport through a NF membrane is a function of the membrane charge and pore size.⁷⁻¹⁰

Nanofiltration represents a relatively new area of research in the membrane field and has separation characteristics between those of microfiltration and reverse osmosis. The technique is often referred to as “soft” reverse osmosis, and typical operating pressures are < 200 psi.^{2,10} The goal of nanofiltration is high water flux with moderate to high rejection of ions at low operating pressures. This differs from reverse osmosis, which typically requires NaCl rejections in the range of 99-100%. The separation mechanism in nanofiltration relies on both the size and charge of the analyte. For separating ions, the thin active layer in these membranes is highly charged and the effective pore size is generally between 1 and 5 nm.^{7-9,11-13}

Deposition of layered polyelectrolyte films provides one means of creating highly charged, ultrathin membranes and provides some control over both charge density and

membrane composition.¹⁴ Chapters 2 and 4 illustrate the high degree of multivalent ion rejection that is possible with polyelectrolyte films. The cross-linking strategy described in Chapter 3 should provide a means for decreasing the effective pore size of polyelectrolyte membranes, which should further increase ion rejections. Another possible means for modifying the separation properties of polyelectrolyte membranes is the derivatization of PAA layers in composite membranes to incorporate various moieties into the film structure. As described in Chapter 4 there are numerous means to tailor the ion-permeability of polyelectrolyte membranes.

This chapter discusses the use of layered polyelectrolyte films as nanofiltration membranes. The high degree of multivalent ion rejection shown by these films (Chapter 4) supports the proposition of using polyelectrolyte films for nanofiltration applications. Rejection and flux values should depend on the outer layer charge of the membrane and the concentration of the feed solutions. Along with high rejection values these ultrathin membranes should allow for high water flux. Performance of composite membranes and membranes derivatized with hydrophobic groups will also be discussed.

II. Experimental

A. Chemicals

Polyelectrolytes and salts were used as described in previous chapters. Ethyl chloroformate (Aldrich), N-methylmorpholine (Aldrich), dimethyl formamide (Aldrich), 1H-1H-perfluorooctylamine (Lancaster), ethanol (Aldrich), and ethyl acetate (Aldrich) were used as received.

B. Polyelectrolyte Deposition and Derivatization on Porous Alumina Supports

Polyelectrolyte membrane deposition followed the procedure described in Chapter 4 except that polyelectrolyte deposition began with the polyanion. In Chapter 4 polyelectrolyte deposition began with the polycation even though the alumina membrane has a positive charge below pH values of 8.¹⁵ Ellipsometric studies on Al coated Si wafers suggest that a layer of polyelectrolyte absorbs irrespective of the polyelectrolyte charge. Regardless, the initial layer should have little if any effect on the transport characteristics of the membrane. Composite membranes used for subsequent derivatization consist of a 1.5-bilayer PAA/PAH film deposited on a precursor 5-bilayer PSS/PAH film. For the PAA/PAH films, the deposition solutions contained 0.02 M polyelectrolyte and 0.5 M NaCl and were adjusted to a pH of 4.5.

The presence of –COOH groups in composite membranes allows for the derivatization of these films with perfluorooctylamine (PFOA).¹⁶ The derivatization of procedure begins with activation of the COOH groups in the PAA layer via a 10 min immersion in an ethyl chloroformate solution (100 μ L in 10 mL DMF/100 μ L N-methylmorpholine). After rinsing with ethyl acetate, the membrane was immersed in a solution of 0.01 N PFOA for one hour. Upon removal from the PFOA solution, the membrane was rinsed with ethanol and dried with N₂. The extent of derivatization was monitored using films of similar composition deposited on Au substrates. In that case, Au substrates were first coated with MPA followed by polyelectrolyte deposition, which followed the procedure described in Chapters 2 and 3.

C. Nanofiltration

Nanofiltration experiments were conducted in the home built cross-flow system described schematically in Figure 5.1. The system was pressurized to 70 psi with Ar. The feed tank was used to store the various brine solutions (~3 L), which consisted of 50 or 1000 ppm solutions of NaCl, Na₂SO₄, or CaCl₂. The concentrations were calculated with respect to the ion of interest (i.e. Na⁺, SO₄²⁻, or Ca²⁺). 2000 ppm MgSO₄ solutions were also used. An AcetatePlus™ (0.45 μm pore size) membrane (Osmonics) was used as a prefilter to remove any rust or particulate matter from the feed stream. The flow meter was set to 18 mL/min, which is at least 100-fold greater than the membrane flux. This flowrate is high enough to minimize concentration polarization and low enough to minimize delamination of the polyelectrolyte film. Increasing the flowrate to 40 mL/min has little if any effect on ion-rejection or permeate flux. The membranes were housed in a home built stainless steel cell as shown in Figure 5.2.¹⁷ The active area of the membrane contained within the o-ring was 1.6 cm². Pressure gauges were used to monitor possible pressure gradients that might arise from a fouled membrane cell. Graduated cylinders were used to collect the permeate stream from the membrane cells.

Once the system was pressurized, the membranes were allowed to equilibrate with the flowing solution for between 30 and 60 min. Upon equilibration permeate aliquots were collected every 30 min. The run was terminated upon the collection of 3 aliquots, that showed similar (within 20%) flux and rejection values. The membranes were tested first with the 50 ppm solution and then with the 1000 ppm solution. New membranes were used when salt solutions were changed and 3 membranes were tested for each salt solution.

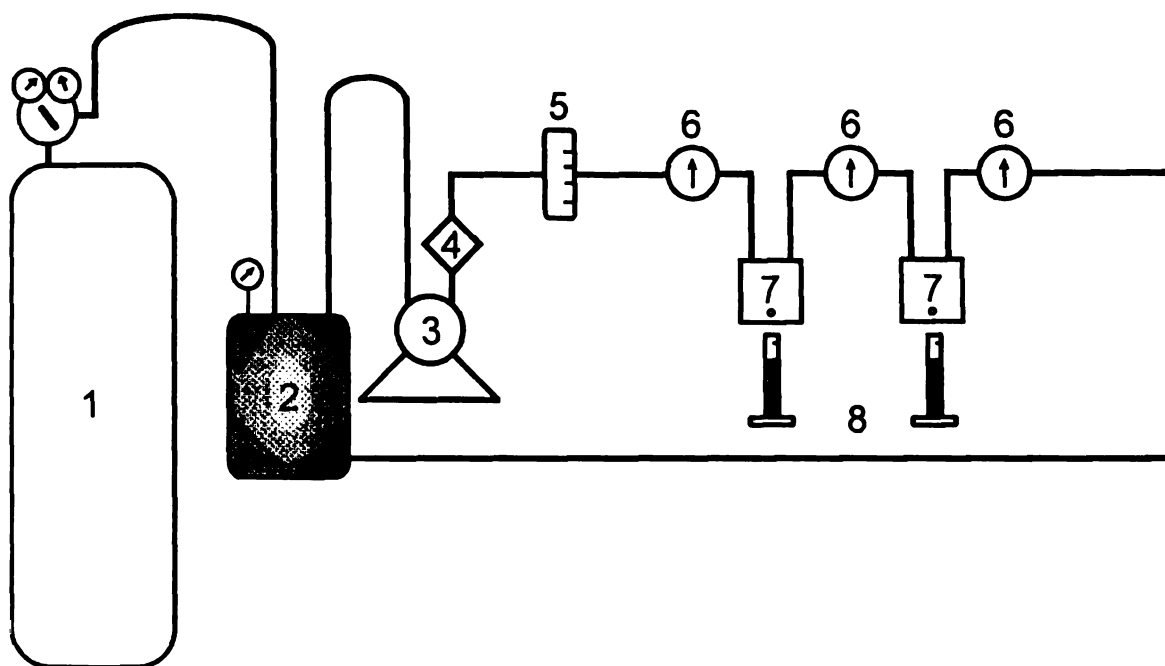


Figure 5.1: Experimental setup for nanofiltration experiments: Ar tank (1), stainless steel feed tank (2), centrifugal pump (3), prefilter (4), flowmeter (5), pressure gauges (6), membrane cells (7), and graduated cylinders (8). System pressure was 70 psi and flowrate was 18 mL/min.¹⁷

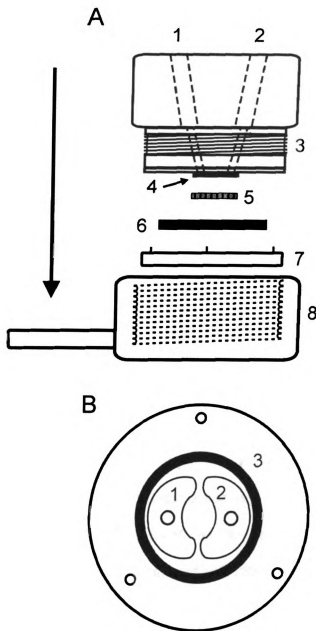


Figure 5.2: Schematic diagram of the nanofiltration membrane cell. (A) shows how the cell is placed together: inlet/outlet ports (1&2), threads (3), rubber o-ring (4), alumina membrane (5), porous stainless steel frit (6), cap that frit fits in and presses the membrane tight against O-ring (7), and threaded bottom part of cell that top part screws into (8). The cell is assembled in the direction of the arrow. (B) shows a bottom view of the upper portion of cell: recessed inlet/outlet channels (1&2) and o-ring (3).¹⁷

III. Results and Discussion

A. Nanofiltration Performance of PSS/PAH Membranes

As seen in Chapter 4, only 4.5-bilayers of PSS/PAH are needed to completely coat the porous structure of the alumina support. Nanofiltration experiments with PSS/PAH membranes focused on films consisting of 4.5 or 5 bilayers of PSS/PAH. Under 70 psi of pressure, the bare alumina membrane shows little if any resistance to pure water transport (flowrate through the membrane of >10 mL/min). Upon deposition of 4.5 bilayers of PSS/PAH, however, pure water flux decreases to 11 mL/hr. This dramatic decrease in flux occurs with a film that is only 20 nm thick.

PSS/PAH membranes show impressive ion-rejection values that vary with the outer layer charge of the membrane. As seen in Table 5.1, ion-rejection values increase when the outer layer charge matches the charge of the ion of interest. Ca^{2+} rejection values for 50 and 1000 ppm solutions, for example, increase from 92 to $>95\%$ upon deposition of a polycation layer. The same trend is also seen with SO_4^{2-} , whose rejection increases from 47 and 55% to 54 and 65%, for 50 and 1000 ppm solutions, respectively, when the outer layer of the membrane is terminated with PSS as opposed to PAH. Na^+ rejection values increase dramatically (2-to 3-fold) upon deposition of a polycation layer for both 50 and 1000 ppm brine solutions. This trend in rejection values is consistent with a Donnan repulsion model, which is discussed further in Section B. The performance of polyelectrolyte membranes also depends on the concentration of brine in solution. If rejection in polyelectrolyte membranes is represented by a Donnan

Table 5.1: Rejection and flux values (listed in parentheses) in $\text{m}^3 \text{m}^{-2} \text{d}^{-1}$ for various polyelectrolyte films used as nanofiltration membranes. Rejection values listed represent % decrease in permeate ion concentration relative to the feed concentration in the collected permeate. The fluorinated film was heated at 180 °C for 2 hrs. The salt solutions were NaCl, Na_2SO_4 , and CaCl_2 .

Membrane	50 ppm Na^+	1000 ppm Na^+	50 ppm SO_4^{2-}	1000 ppm SO_4^{2-}	50 ppm Ca^{2+}	1000 ppm Ca^{2+}
(PSS/PAH)4.5	47 ± 6 (1.3 \pm 0.08)	16 ± 6 (1.4 \pm 0.1)	54 ± 9 (1.3 \pm 0.2)	65 ± 7 (1.2 \pm 0.08)	92 ± 3 (1.6 \pm 0.1)	92 ± 3 (1.3 \pm 0.04)
(PSS/PAH)5	84 ± 0 (0.86 \pm 0)	48 ± 0 (0.82 \pm 0)	47 ± 0 (1.1 \pm 0)	55 ± 0 (1.3 \pm 0)	95 ± 0 (0.94 \pm 0)	98 ± 0 (1.2 \pm 0)
(PSS/PAH)5 + (PAA/PAH)1.5	43 (0.21)	32 (0.35)	77 (0.35)	96 (0.32)	85 (0.35)	96 (0.21)
(PSS/PAH)5+ (PAH/PAA)1+ 1-PAA/PAH	63 (0.21)	66 (0.14)	94 (0.20)	99.5 (0.17)	85 (0.21)	N/A

repulsion model, as suggested earlier, then rejection should decrease at higher concentrations due to increased charge screening by the electrolyte solution. Na^+ rejection does follow this trend (Table 5.1) as rejection decreases by 66 and 43% for 4.5- and 5-bilayer PSS/PAH films, respectively, as the feed concentration increases from 50 to 1000 ppm. However upon increasing salt concentration, SO_4^{2-} rejection values actually increases by ~20% for both 4.5- and 5-bilayer PSS/PAH membranes while Ca^{2+} rejections show little if any change due to feed concentration.

One possible explanation for increased SO_4^{2-} rejections at higher feed concentrations is that ion adsorption increases the amount of charge at the surface of polyelectrolyte films.¹⁸ The increased rejection values at high feed concentrations would seem to indicate an increase in the effective charge of the polyelectrolyte membrane, which would be consistent with a higher degree of ion adsorption at higher ion concentrations. The high Ca^{2+} rejection values (>90%) for 4.5-bilayer PSS/PAH membranes also suggest ion adsorption, as one would expect rejection to be low for this negatively capped membrane.

The rejection values for PSS/PAH membranes are similar to values obtained with commercially available membranes as shown in Table 5.2.¹⁹ One advantage of these membranes is their high water flux, which is on average $1.3 \text{ m}^3 \text{ m}^{-2} \text{ d}^{-1}$ (Table 5.1), a value greater than the majority of industrial nanofiltration membranes. The combination of a high degree of surface charge and the minimal thickness of polyelectrolyte membranes leads to high water fluxes while maintaining high ion rejections. In most cases the flux is unaffected by the concentration of salt in the feed stream. This is unexpected, as the flux should decrease at higher feed concentrations due to increased osmotic pressure. The

Table 5.2: Flux and rejection values for several commercially available nanofiltration membranes and PSS/PAH membranes. Feed solutions were NaCl, MgSO₄, and CaCl₂.

Membrane	Pressure (psi)	Flux (m ³ m ⁻² d ⁻¹)	Na ⁺ Rejection	SO ₄ ²⁻ Rejection	Ca ²⁺ Rejection
NF-200 [*]	70	0.82		>95% ⁴	35-50% ⁵
NF-90 [*]	70	0.91	85-95% ¹	>95% ⁴	
Desal 51 ⁺	50	0.94	41% ²		81% ⁶
Hydro 7540 [§]	50	0.34	33% ²		68% ⁶
(PSS/PAH)4.5	70	>1.2	16% ³	94% ⁴	92% ³
(PSS/PAH)5	70	>0.82	48% ³	95% ⁴	98% ³

Dow FilmTec Membranes^{*}

Osmonics⁺

Hydranautics[§]

¹ 2000 ppm NaCl

² 60 ppm NaCl

³ 1000 ppm solutions

⁴ 2000 ppm MgSO₄

⁵ 500 ppm CaCl₂

⁶ 34 ppm CaCl₂

increase in osmotic pressure decreases the effective pressure applied to the membrane and should affect the results of both 1000 ppm Na⁺ and Ca²⁺ solutions as their osmotic pressures are 31 and 27 psi, respectively. As seen in Table 5.1 there is little change in permeate flux at the higher feed concentrations. In addition to high permeate flux, the ease of tailoring the properties of the membrane by changing the outer layer charge is highly advantageous. This provides one with the ability to tune the quality of the permeate stream depending on the final application of the purified water.

B. Modeling of Ion Transport Through Polyelectrolyte Membranes

Modeling of the experimental data should provide a better understanding of the possible mechanisms involved in ion transport through polyelectrolyte membranes. Since charge interactions between the membrane and ions in solution appear to have a major effect on ion transport, Donnan theory may apply. This theory arises from the interfacial potential (Donnan Potential) that is created when a boundary separates two solutions of varying concentration. The potential is described by equation 5.1, where Φ is the Donnan potential, R is the gas constant, T is temperature, z_A is the charge of the ion, and C_A^{sol} and C_A^{mem} are the concentrations of ion A in the solution and membrane, respectively.

$$\Phi^{\text{don}} = \phi^{\text{mem}} - \phi^{\text{sol}} = \frac{RT}{z_A F} \ln \frac{C_A^{\text{mem}}}{C_A^{\text{sol}}} \quad 5.1$$

The distribution coefficient (Equation 5.2) can be derived from Equation 5.1 (Appendix 1 contains a detailed derivation) and this value correlates the concentration of ions in solution with that of ions in the membrane.²⁰ In this equation, z_x and C_x are the charge and concentration of fixed sites in the membrane. If flux through a membrane is sufficiently slow, equation 5.2 can be used to calculate ion rejection.

$$\frac{C_A^{mem}}{C_A^{sol}} = \left(\frac{|z_A|C_A^{sol}}{|z_A|C_A^{mem} + |z_X|C_X^{mem}} \right)^{|z_A|/|z_B|} \quad 5.2$$

To compare the performance of PSS/PAH membranes with this model, the concentration of fixed charge within the membrane, C_x , was calculated from rejection values using equation 5.2. These values (Table 5.3) were then compared to previously measured values of charge in polyelectrolyte films. Several studies determined the amount of charge present in polyelectrolyte films using various techniques.^{18,21,22} Using radiolabeled ions, Schlenoff determined that the amount of uncompensated charge at the film surface is $4.3 \times 10^{-10} \text{ mol cm}^{-2}$.¹⁸ Using Schlenoff's value of uncompensated charge,¹⁸ and assuming 1:1 charge compensation in the membrane bulk and a 2-4 nm thick charged outer layer, the concentration of fixed charge at the membrane surface would be between 1.1 and 2.2 M. This value of uncompensated charge is much greater than the charge required (Table 5.3) for the observed rejection values of PSS/PAH membranes. Theoretically, the rejection values for ions should be even higher in polyelectrolyte membranes, but flux may be high enough that ion concentrations in the membrane are greater than equilibrium values.

Table 5.3: Theoretical values for the concentration of fixed charge (M) in polyelectrolyte membranes calculated using Equation 5.2 and rejection values in Table 5.1.

50 ppm Na ⁺	1000 ppm Na ⁺	50 ppm SO ₄ ²⁻	1000 ppm SO ₄ ²⁻	50 ppm Ca ²⁺	1000 ppm Ca ²⁺
3.2×10^{-3}	2.0×10^{-2}	1.1×10^{-3}	2.8×10^{-2}	1.1×10^{-2}	2.2×10^{-2}

C. Performance of Composite and Derivatized Polyelectrolyte Membranes

In addition to control of ion transport through variation of surface charge, composite membranes can be derivatized or cross-linked to utilize size exclusion and hydrophobicity effects to alter ion transport. Previous studies show that ion-transport selectivity through polyelectrolyte membranes can be enhanced by using PSS/PAH+PAA/PAH composite membranes.²³ As seen in Table 5.1 Na^+ rejections for such membranes remain relatively low, but SO_4^{2-} rejections increase for these composite membranes compared to PSS/PAH membranes. Ca^{2+} rejections decrease for both 50 and 1000 ppm solutions with respect to PSS/PAH membranes. The trend of increasing SO_4^{2-} and Ca^{2+} rejection at higher feed concentrations, observed with PSS/PAH membranes, is also seen with the composite membranes.

Composite membranes that are derivatized with PFOA (Figure 5.3) and then cross-linked show even higher SO_4^{2-} rejections (99%) while maintaining moderate Ca^{2+} and Na^+ rejections. Increased SO_4^{2-} rejections are reasonable due to the increased hydrophobicity of the derivatized membrane. The SO_4^{2-} anion is highly hydrated and very hydrophilic.^{24,25} Post-deposition cross-linking and/or derivatization shows the versatility of polyelectrolyte membranes for ion separations. However, these modifications do decrease flux by a factor of about 3.

IV. Conclusions

Layered polyelectrolyte films provide a convenient means for the construction of nanofiltration membranes. The ion-rejection values of these membranes are competitive with commercially available membranes, while their water permeability is higher than

commercial systems. By changing the outer layer charge in PSS/PAH membranes or by using composite membranes, rejection and flux can be easily tailored to fit the needs of a desired applications. These attributes along with ease of synthesis makes layered polyelectrolyte films attractive for constructing ion-separation membranes.

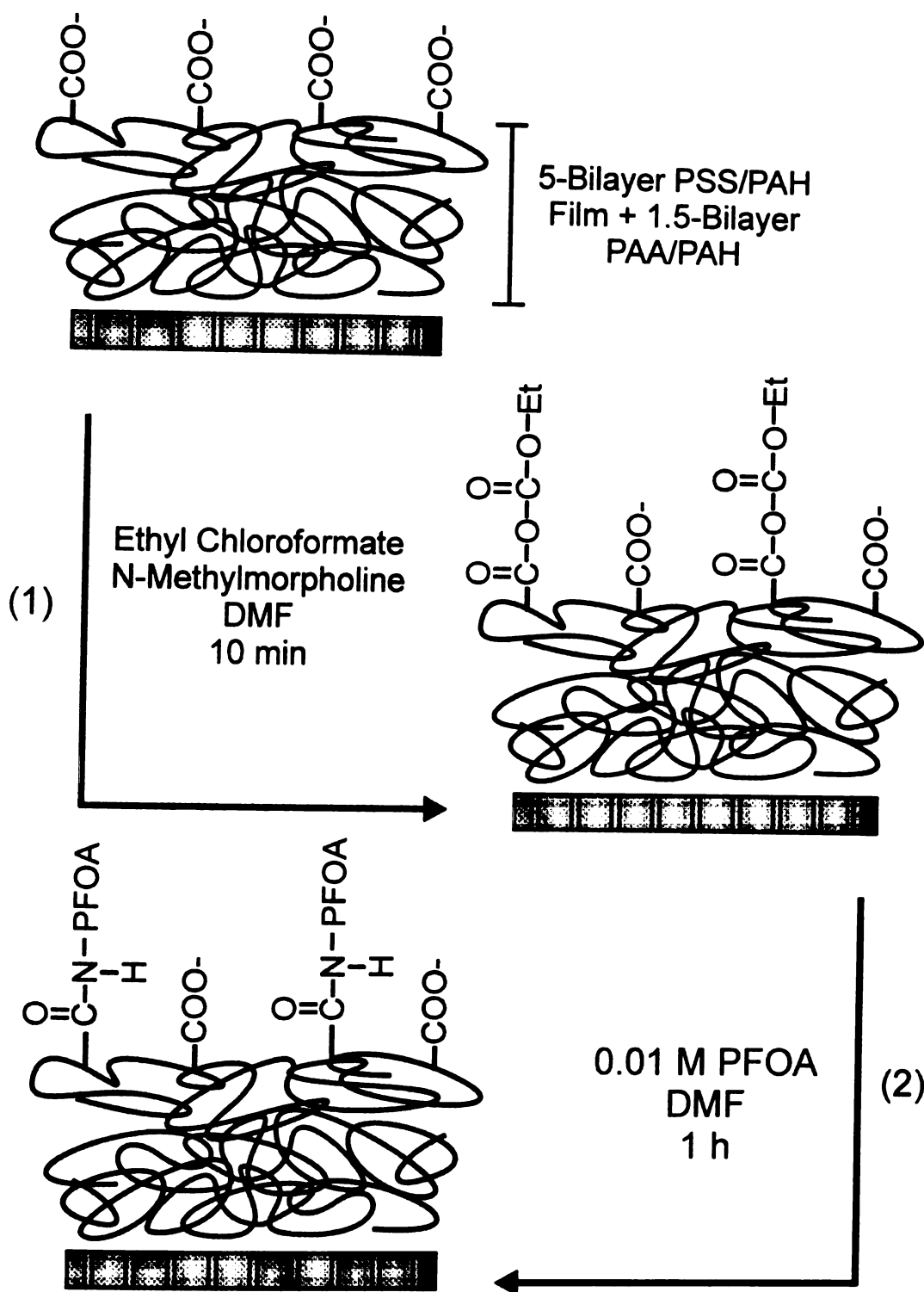


Figure 5.3: Reaction scheme for derivatization of composite membranes with 1H-1H-perfluorooctylamine (PFOA). In step 1 the acid groups of PAA are converted to a mixed anhydride. In step 2, the amine group of PFOA reacts with the anhydride resulting in attachment of PFOA to the composite film through an amide linkage.

V. References

- 1) Xu, X.; Spencer, G. *Desalination* **1997**, 114, 129-137.
- 2) Yaroshchuk, A.; Staude, E. *Desalination* **1992**, 86, 115-134.
- 3) Hofman, J. A. M. H.; Beerendonk, E. F.; Folmer, H. C.; Kruithof, J. C. *Desalination* **1997**, 113, 209-214.
- 4) Bohdziewicz, J.; Bodzek, M.; Wasik, E. *Desalination* **1999**, 121.
- 5) Berg, P.; Hagmeyer, G.; Gimbel, R. *Desalination* **1997**, 113, 205-208.
- 6) Rautenbach, R.; Linn, T.; Eilers, L. *J. Membr. Sci.* **2000**, 174, 231-241.
- 7) Childress, A. E.; Elimelech, M. *Environ. Sci. Technol.* **2000**, 34, 3710-3716.
- 8) Afonso, M. D.; Hagmeyer, G.; Gimbel, R. *Separation Purif. Technol.* **2001**, 22-23, 529-541.
- 9) Bowen, W. R.; Mohammad, A. W.; Hilal, N. *J. Membr. Sci.* **1997**, 126, 91-105.
- 10) Bhattacharyya, D.; Williams, M. E. *Membrane Handbook*; Bhattacharyya, D.; Williams, M. E., Ed.; Van Nostrand Reinhold: New York, 1992, pp 263-280.
- 11) Kim, C. K.; Kim, J. H.; Roh, I. J.; Kim, J. J. *J. Membr. Sci.* **2000**, 165, 189-199.
- 12) Košutic, K.; Kaštelan-Kunst, L.; Kunst, B. *J. Membr. Sci.* **2000**, 168, 101-108.
- 13) Shibata, M.; Kobayashi, T.; Fujii, N. *J. Appl. Polym. Sci.* **2000**, 75, 1546-1553.
- 14) Decher, G. *Science* **1997**, 277, 1232-1237.
- 15) Parks, G. A. *Chem. Rev.* **1965**, 65, 177-198.
- 16) Bruening, M. L.; Zhou, Y.; Aguilar, G.; Agee, R.; Bergbreiter, D. E.; Crooks, R. M. *Langmuir* **1997**, 13, 770-778.
- 17) The author would like to thank Keith Harris for the original design of the nanofiltration cell.
- 18) Schlenoff, J. B.; Ly, H.; Li, M. *J. Am. Chem. Soc.* **1998**, 120, 7626-7634.

- 19) Performance of commercially available membranes can be found at www.osmonics.com/products or www.dow.com/liquidseps/pc/product.htm.
- 20) Peeters, J. M. M.; Boom, J. P.; Mulder, M. H. V.; Strathmann, H. *J. Membr. Sci.* **1998**, 145, 199-209.
- 21) Hoogeveen, N. G.; Cohen Stuart, M. A.; Fleer, G. J. *Langmuir* **1996**, 12, 3675-3681.
- 22) Ruths, J.; Essler, F.; Decher, G.; Riegler, H. *Langmuir* **2000**, 16, 8871-8878.
- 23) Stair, J. L.; Harris, J. J.; Bruening, M. L. *Chem. Mater.* **in press**.
- 24) Collins, K. D.; Washabaugh, M. W. *Quar. Rev. Biophys.* **1985**, 18, 323-422.
- 25) Marcus, Y. *J. Chem. Soc. Faraday Trans.* **1991**, 87, 2995-2999.

CHAPTER 6

Conclusions and Future Work

I. Stability and Ion-Permeability of Layered Polyelectrolyte Films Deposited on Solid Supports

Chapter 2 shows that layered polyelectrolyte films offer a convenient means for surface modification. The deposition of PAH/PSS and PAH/PAA films follows a regular and controlled pattern, which allows for nanoscale control of film thickness and composition. Once deposited these films are stable in solutions at low and moderate pH values but delaminate and undergo irreversible structural changes in alkaline solutions. However, upon cross-linking, PAH/PAA films show increased stability at high pH due to the formation of covalent linkages between the individual polyelectrolyte layers as discussed in Chapter 3.

The permeability of polyelectrolyte films is related to the film stability and composition. At pH 3.2 and 6.3, the permeability of PAH/PSS films to $\text{Fe}(\text{CN})_6^{3-}$ is low and stable with time. Upon immersion in pH 10 solutions, the permeability of PAH/PSS films drastically increases at rates similar to those for film delamination. Even though a significant portion of polyelectrolyte film remains on the electrode, the structure is altered, allowing for a continued high ion-flux even upon reimmersion in a pH 3.2 solution. The permeability of PAH/PSS films also depends on film thickness. Decreases in permeability occur with increases in the number of bilayers up to 10-bilayers. Covalent cross-linking of PAH/PAA films increases film stability and dramatically decreases film permeability. By varying cross-linking temperature, the permeability of PAH/PAA films can be easily controlled due to the extent of amidation. Cross-linking

and varying the number of film bilayers provide two means for tailoring the permeability of polyelectrolyte films.

II. Polyelectrolyte Films as Anion-Separation Membranes

Polyelectrolyte films show promise as ion-separation membranes due to their high charge and wide tunability. Chapter 4 discusses the ion-permeability, as determined from dialysis measurements, of these films deposited on porous alumina supports. $\text{Cl}^-/\text{SO}_4^{2-}$ selectivity values for both PSS/PAH and PAA/PAH films are ~ 5 , but with PAA/PAH membranes there is a 70% decrease in ion flux. The use of composite membranes, which consist of a thin PAA/PAH film deposited on a precursor PSS/PAH film, results in $\text{Cl}^-/\text{SO}_4^{2-}$ selectivity values as high as 350. In these membranes the outer layer charge is the major factor in controlling the ion-permeability characteristics of the membrane. In most cases, anion selectivity values decrease upon deposition of a cationic layer at the membrane solution interface.

III. Characterization of Nanofiltration Membranes Made from Layered Polyelectrolyte Films

Chapter 5 shows that polyelectrolyte films are feasible candidates for nanofiltration membranes due to their high degree of charge and high multivalent ion rejection illustrated in Chapters 2 and 4. Polyelectrolyte membranes provide rejection values of 98 and 70% for Ca^{2+} and SO_4^{2-} , respectively, while maintaining moderate Na^+ rejection. As in Chapter 4, the ion rejection values are highly dependent on the charge of the outer layer of the polyelectrolyte film. Ion-rejections increase when the polyelectrolyte membrane is terminated with the same charge as the ion in solution. In

addition to high rejection values, these membranes show high water fluxes, which is critical for possible industrial applications. Further derivatization with hydrophobic groups and/or cross-linking increases certain rejection values, but fluxes decrease. Overall, polyelectrolyte films provide an easy means for membrane construction while providing a high level of membrane performance.

IV. Future Work

The primary drawback with polyelectrolyte membranes as described in this thesis is the porous alumina support material. While providing well-defined pores and a high pore density, the material is too fragile for practical applications. Work must be done to find a better support such as a polymeric membrane, which will provide mechanical stability but at the same time increased durability. Unfortunately, commercially available polymeric membranes suffer from low pore density, and therefore reduced fluxes. Another approach would be to use polyelectrolyte films to modify the separation properties of commercially available anion-exchange or nanofiltration membranes. This should provide an easy and practical means to tailor the properties of the membrane.

The derivatizable nature of PAH/PAA films provides several possible means for modifying separation characteristics of the membrane. Since the major separation mechanism in nanofiltration membranes is charge exclusion, the templating of metal ions in the film may provide a means for increasing the effective charge of the membrane upon removal of the ions. Also templating of molecules may provide for a means of creating well-defined pores in the membrane that would provide structure selective transport of molecules. The derivatization of polyelectrolyte membranes touched on in

Chapter 5 opens many opportunities for introducing new separation mechanisms (i.e. hydrophobicity) to the field of nanofiltration. In conclusion, this thesis presents the advantages and possibilities of using layered polyelectrolyte films as ion-separation membranes.

APPENDIX 1

Appendix 1 represents the derivazitation (page 115) of the distribution coefficient of anion (a) with respect to its concentration in solution (C_a^{sol}) and within the membrane (C_a^{mem}). Equation 1 and 2 equate the electrochemical and standard chemical potentials, respectively, between species (a) in the solution and membrane phase. This can also be done for the cation (equation 2a). The chemical potential between the membrane and solution phases (equation 4 and 4a) is solved by rearrangement of equation 2 and this represents the Donnan potential for species (a) and (c), respectively. Equation 5 represents the electroneutrality condition between species (a) and (c) in solution, while equation 5a describes the electroneutrality conditions between the species in solution and the fixed charge of the membrane. Since we are concerned with the anionic species equations 5 and 5a are solved for C_c^{sol} and C_c^{mem} resulting in equations 6 and 6a, respectively. Substituting equations 6 and 6a into equation 4 produces equation 7. Raising equation 7 to the $-z_a$ power produces equation 8. Inverting the left side of equation 8 (equation 9) followed by inserting absolute values for z_a and z_c results in equation 10.

APPENDIX 1

$$(1) \quad \bar{\mu}_a^{\text{mem}} = \bar{\mu}_a^{\text{sol}}$$

$$(2) \quad \mu_a^{\text{mem}} + RT \ln C_a^{\text{mem}} + z_a F \phi^{\text{mem}} = \mu_a^{\text{sol}} + RT \ln C_a^{\text{sol}} + z_a F \phi^{\text{sol}}$$

$$(2a) \quad \mu_c^{\text{mem}} + RT \ln C_c^{\text{mem}} + z_c F \phi^{\text{mem}} = \mu_c^{\text{sol}} + RT \ln C_c^{\text{sol}} + z_c F \phi^{\text{sol}}$$

$$(3) \quad \phi^{\text{mem}} - \phi^{\text{sol}} = \frac{RT}{z_a F} \ln \frac{C_a^{\text{sol}}}{C_a^{\text{mem}}} \quad (3a) \quad \phi^{\text{mem}} - \phi^{\text{sol}} = \frac{RT}{z_c F} \ln \frac{C_c^{\text{sol}}}{C_c^{\text{mem}}}$$

$$(4) \quad \left(\frac{C_a^{\text{mem}}}{C_a^{\text{sol}}} \right)^{-1/z_a} = \left(\frac{C_c^{\text{mem}}}{C_c^{\text{sol}}} \right)^{-1/z_c}$$

$$(5) \quad z_a C_a^{\text{sol}} + z_c C_c^{\text{sol}} = 0 \quad (5a) \quad z_a C_a^{\text{mem}} + z_c C_c^{\text{mem}} + z_x C_x^{\text{mem}} = 0$$

$$(6) \quad C_c^{\text{sol}} = \frac{-z_a C_a^{\text{sol}}}{z_c} \quad (6a) \quad C_c^{\text{mem}} = \frac{-z_x C_x^{\text{mem}} - z_a C_a^{\text{mem}}}{z_c}$$

$$(7) \quad \left[\frac{-(z_x C_x^{\text{mem}} + z_a C_a^{\text{mem}})}{z_c \left(\frac{-z_a C_a^{\text{sol}}}{z_c} \right)} \right]^{-1/z_c} = \left(\frac{C_a^{\text{mem}}}{C_a^{\text{sol}}} \right)^{-1/z_a}$$

$$(8) \quad \left[\frac{z_a C_a^{\text{mem}} + z_x C_x^{\text{mem}}}{z_a C_a^{\text{sol}}} \right]^{z_a/z_c} = \frac{C_a^{\text{mem}}}{C_a^{\text{sol}}}$$

$$(9) \quad \left[\frac{z_a C_a^{\text{sol}}}{z_a C_a^{\text{mem}} + z_x C_x^{\text{mem}}} \right]^{-z_a/z_c} = \frac{C_a^{\text{mem}}}{C_a^{\text{sol}}}$$

$$(10) \quad \left[\frac{|z_a| C_a^{\text{sol}}}{|z_a| C_a^{\text{mem}} + |z_x| C_x^{\text{mem}}} \right]^{|z_a|/|z_c|} = \frac{C_a^{\text{mem}}}{C_a^{\text{sol}}}$$

MICHIGAN STATE LIBRARIES



3 1293 02177 0726